Numerical Study on the Effect of Conduction in Mixed Convection Flow in a Rectangular Cavity with a Heat Conducting Horizontal Cylinder

Md. Mustafizur Rahman
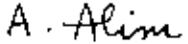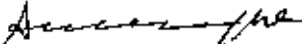Student No. P04050901P
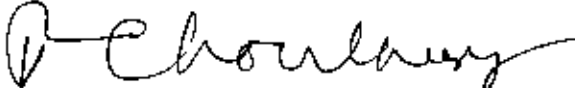Registration No. 0110645, Session: April-2005
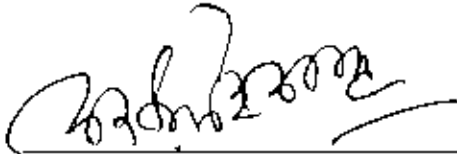
DOCTOR OF PHILOSOPHY
IN
MATHEMATICS

Department of Mathematics
BANGLADESH UNIVERSITY OF ENGINEERING AND
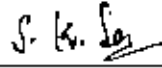TECHNOLOGY, DHAKA-1000
May- 2009

The thesis entitled **"Numerical Study on the Effect of Conduction in Mixed Convection Flow in a Rectangular Cavity with a Heat Conducting Horizontal Cylinder"**, submitted by **Md. Mustafizur Rahman**, Roll no P04050901P, Registration No. 0110645, Session April 2005 has been accepted as satisfactory in partial fulfillment of the requirement for the degree of Doctor of Philosophy in Mathematics on 02 May 2009.

Board of Examiners

1. A. Alim
   02/05/09

   Dr. Md. Abdul Alim   Chairman
   Associate Professor   (Supervisor)
   Department of Mathematics, BUET, Dhaka-1000

2.
   Head   Member
   Department of Mathematics   (Ex-Officio)
   BUET, Dhaka-1000

3.
   Dr. Md. Mustafa Kamal Chowdhury   Member
   Professor
   Department of Mathematics, BUET, Dhaka-1000

4.
   Dr. Md. Manirul Alam Sarker   Member
   Professor
   Department of Mathematics, BUET, Dhaka-1000

5.
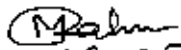
Dr. A. K. M. Sadrul Islam   Member
Professor
Department of Mechanical and Chemical Engineering
Islamic University of Technology (IUT)
Gazipur

6.

Dr. Md. Abdul Matin   Member
Professor
Department of Water Resources Engineering
BUET, Dhaka-1000

7.

Dr. Sujit Kumer Sen   Member
Professor   (External)
Research Centre for Mathematics & Physical Sciences (RCMPS)
University of Chittagong, Chittagong

iii

Candidate's Declaration

I am hereby declaring that no portion of the work considered in this thesis has been submitted in support of an application for another degree or qualification of this or any other University or Institute of learning either in home or abroad.

02-05-09

Md. Mustafizur Rahman

May 2009

Certificate of Research

This is to certify that the work presented in this thesis is carried out by the author under the supervision of Dr. Md. Abdul Alim, Associate Professor, Department of Mathematics, Bangladesh University of Engineering & Technology, Dhaka.

A. Alim
02-05-09

Dr. Md. Abdul Alim

02-05-09

Md. Mustafizur Rahman

Acknowledgement

Abstract

Fluid flow with heat transfer due to the combined effect of free and forced convection (mixed convection) are often encountered in engineering systems eg., in the design of building, air conditioning, cooling of electronic devices, nuclear reactors, chemical processing equipment, lubricating grooves and industrial process float glass manufacturing etc. The simplest configurations approximating some of these practical flow situations are the flow and heat transfer in a vented cavity, where the flow is induced by a shear force resulting from the external forced stream and in a lid-driven cavity where the flow is induced by a shear force resulting from the motion of a moving wall. In this thesis under the title "Numerical Study on the Effect of Conduction in Mixed Convection Flow in a Rectangular Cavity with a Heat Conducting Horizontal Cylinder", two problems have been studied. The study as well depending on various flow and geometrical conditions are abstracted below.

Firstly, the effect of conduction in mixed convection flow in a rectangular vented cavity with a heat conducting horizontal (circular/square) cylinder have been investigated. The right vertical wall of the cavity is kept at a uniform constant temperature, while the other walls (top, bottom and left vertical) are assumed adiabatic. A heat conducting horizontal cylinder is placed somewhere within the cavity. An external flow enters the cavity through an opening in the left vertical wall and exits to another opening in the opposite wall.

Finally, the effect of joule heating in the coupling of conduction with magnetohydrodynamics (MHD) mixed convection flow in a lid-driven cavity along with a heat conducting horizontal (circular/square) cylinder have been investigated. The cavity consists of adiabatic horizontal walls and differentially heated vertical walls, but it also contains a heat conducting horizontal cylinder located somewhere within the cavity. Temperature of the left moving wall, which has constant flow speed, is lower than that of the right vertical wall. A uniform magnetic field is applied in the horizontal direction normal to the moving wall

The physical problems are represented mathematically by different sets of governing equations along with the corresponding boundary conditions. Using a class of

appropriate transformations, the governing equations along with the boundary conditions are transformed into non-dimensional form, which are then solved by employing a finite-element scheme based on the Galerkin method of weighted residuals.

Results are presented in terms of streamlines, isotherms, average Nusselt number along the hot wall, average temperature of the fluid in the cavity and dimensionless temperature at the cylinder center for different combinations of the governing parameters namely Reynolds number Re, Prandtl number Pr, solid-fluid thermal conductivity ratio K, as well as the size, shape and locations of the inner cylinder, cavity aspect ratio AR, locations of the inlet and outlet port (for vented cavity), Hartmann number Ha, and Joule heating parameter J (for lid-driven cavity) at the three values of Richardson number Ri, varying from 0.0 to 5.0. This range of Ri are selected on the basis of calculation covering pure forced convection, pure mixed convection and free convection dominated regimes. Comparisons with previously published work are performed and the results are found to be in excellent agreement

The results indicate that both the flow and the thermal fields strongly depend on the parameters, Reynolds number Re, the size and locations of the inner cylinder, cavity aspect ratio AR, locations of the inlet and outlet port (for vented cavity), Hartmann number Ha, and Joule heating parameter J (for lid-driven cavity) at the three convective regimes. It is also observed that the parameters Prandtl number Pr, solid-fluid thermal conductivity ratio K, have insignificant effect on the flow fields and have significant effect on the thermal fields at the three convective regimes

The computational results also indicate that the average Nusselt number at the hot wall, average temperature of the fluid in the cavity and temperature at the cylinder center are depending on the aforementioned dimensionless parameters. For the purpose of comparison of the effect of cylinder shape on heat transfer, the results in terms of average Nusselt number are shown in tabular form. The obtained results reveal that the average Nusselt number at the hot wall for the case of square cylinder are generally higher than that of for the case of circular cylinder.

Table of Contents

Nomenclature

AR	cavity aspect ratio
B_0	magnetic induction (Wb/m^2)
c_p	specific heat at constant pressure ($J/kg.K$)
d	dimensional diameter of the cylinder (m)
D	dimensionless diameter of the cylinder
g	gravitational acceleration (ms^{-2})
Gr	Grashof number
h	convective heat transfer coefficient ($W/m^2.K$)
H	height of the cavity (m)
Ha	Hartmann number
H_λ	linear shape function
J	joule heating parameter
k	thermal conductivity of fluid ($Wm^{-1}K^{-1}$)
k_s	thermal conductivity of solid ($Wm^{-1}K^{-1}$)
K	Solid fluid thermal conductivity ratio
L	length of the cavity (m)
l_x	dimensional distance between y-axis and the cylinder center (m)
l_y	dimensional distance between x-axis and the cylinder center (m)
L_x	dimensionless distance between y-axis and the cylinder center
L_y	dimensionless distance between x-axis and the cylinder center
n	dimensional distance either along x or y direction (m)
N	non-dimensional distance either along X or Y direction
N_α	quadratic shape function
Nu_l	local Nusselt number
Nu	Average Nusselt number
p	pressure
P	non-dimensional pressure
Pr	Prandtl number
q_w	heat flux
Ra	Raleigh number
Re	Reynolds number
Ri	Richardson number
S_x	surface tractions along X-axis
S_y	surface tractions along Y-axis
T	dimensional fluid temperature (K)
T_s	dimensional solid temperature (K)
ΔT	dimensional temperature difference (K)
u	velocity in x-direction (m/s)

U	dimensionless horizontal velocity
U_0	lid velocity (m/s)
v	velocity in y-direction (m/s)
V	dimensionless vertical velocity
$\bar{V}$	cavity volume (m^3)
x, y	Cartesian coordinates (m)
X, Y	dimensionless Cartesian coordinates
$\bigcirc$	circular cylinder
$\square$	square cylinder

Greek symbols

α	thermal diffusivity ($m^2 s^{-1}$)
β	coefficient of thermal expansion (K^{-1})
θ	dimensionless fluid temperature
θ_s	dimensionless solid temperature
$\Delta\theta$	dimensionless temperature difference
μ	dynamic viscosity of the fluid ($m^2 s^{-1}$)
ν	kinematic viscosity of the fluid ($m^2 s^{-1}$)
ρ	density of the fluid ($kg m^{-3}$)
σ	fluid electrical conductivity ($\Omega^{-1} m^{-1}$)

Subscripts

av	average
h	heated wall
i	inlet state
c	cylinder center
s	solid
l	local

Abbreviation

CBC	convective boundary conditions
CFD	computational fluid dynamics
F D	finite difference
F V	finite volume
F E	finite element
BB	bottom inlet and bottom outlet
BT	bottom inlet and top outlet
TB	top inlet and bottom outlet
TT	top inlet and top outlet

List of Tables

List of Figures

Chapter 1

Introduction

Quite often we encounter fluid flow and heat transfer in cavities at different orientations. These classical problems have some analytical and huge numerical solutions. The effect of conduction in mixed convection flow in cavities or channels have been studied by many researchers and it has been a very popular research topic for many years. Conduction effects on mixed convection flows are important in the context of many engineering applications for predicting the performance, designing of many equipment, machine parts like small microchips to large nuclear reactor. But things used in practical purpose are much more complicated in design and prediction of their performance using results from simple geometry cause huge error. For this complexity, in recent years, attention has been given to study hydrodynamic and thermal characteristics of complex geometry. Among those the cavities incorporating solid bodies or partitions are given special attention due to their wide applications in computer hardware, heat exchangers, solar heat collector, some air conditioning equipment and furnaces etc. A study of the flow of electrically conducting fluid in presence of magnetic field is also important from the technical point of view and such types of problems have received much attention by many investigators. Mathematical models used to predict flow and thermal behavior are mainly of coupled non-linear partial differential equations and their analytical solution is impossible except some special cases.

The rest of this introductory chapter is as follows. Since the problems that we shall study in this thesis are conjugate effect of conduction and mixed convection flow in cavities, we begin with a brief description on mixed convection heat transfer in cavities in section 1.1. Then reviews on Magnetohydrodynamics (MHD) and Joule heating have given in sections 1.2 and 1.3 respectively. For convenience of present investigation, literature related to this study has been presented briefly in section 1.4. Then the motivation behind selection of the present problem, description of the present problem and objective of the current study are described in sections 1.5 to

1.7. Finally, in section 1.8, a brief outline of the remainder of the thesis has presented.

1.1 Mixed Convection Heat Transfer in Cavities

Mixed convection in cavities is a topic of contemporary importance, because cavities filled with fluid are central components in a long list of engineering and geophysical systems. The flow and heat transfer induced in a cavity differs fundamentally from the external mixed convection boundary layer. Mixed convection in a cavity unlike the external mixed convection boundary layer that is caused by the heat transfer interaction between a single wall and a very large fluid reservoir is the result of the complex interaction between finite size fluid systems in thermal communication with all the walls that confine it. The complexity of this internal interaction is responsible for the diversity of flows that can exist inside cavity.

The phenomenon of mixed convection in cavities is varied by the geometry and the orientation of the cavity. Judging by the potential engineering applications, the cavity phenomena can loosely be organized into two classes.

1 Vented cavity and 2. Lid-driven cavity

In a vented cavity, where the interaction between the external forced stream provided by the inlet and the buoyancy driven flows induced by the heat source leads to the possibility of complex flows. Therefore it is important to understand the fluid flow and heat transfer characteristics of mixed convection in a vented cavity. On the other hand, the fluid flow and heat transfer in a lid-driven cavity where the flow is induced by a shear force resulting from the motion of a lid combined with the buoyancy force due to non-homogeneous temperature of the cavity wall, provides another problem, studied extensively by researchers to understand the interaction between buoyancy and shearing forces in such flow situation. The interaction between buoyancy driven and shear driven flows inside a closed cavity in a mixed convection regime is quite complex. Therefore it is also important to understand the fluid flow and heat transfer characteristics of mixed convection in a lid-driven cavity.

1.2 Magnetohydrodynamics

Magnetohydrodynamics (MHD) is that branch of science, which deals with the flow of electrically conducting fluids in electric and magnetic fields. The motion of the conducting fluid across the magnetic field generates electric currents which change the magnetic field and the action of the magnetic field on these currents give rise to mechanical forces, which modify the fluid. However, MHD is usually regarded as a very contemporary subject. Probably the largest advance towards an understanding of such phenomena comes from the fields of astrophysics and geophysics. It has long been assumed that most of the matter in the universe is in the plasma or highly ionized state and much of the basic knowledge in the area of electromagnetic fluid dynamics evolved from these studies. Moreover MHD explains certain natural phenomena. The motions of the sea induce magnetic field that perturb the earth's magnetic field. Alternatively the electromagnetic force due to the interaction of currents and earth's magnetic field propels ocean movements. The MHD was originally applied to astrophysical and geophysical problems, where it is still very important. Engineers employ MHD principles in the design of heat exchanger, pumps and flow meters, in space vehicle propulsion, control and re-entry in creating novel power generating systems and developing confinement schemes for controlled fusion. Other potential applications for MHD include electromagnets with fluid conductors, various energy conversion or storage devices, and magnetically controlled lubrication by conducting fluids etc. Detailed discussion of the Magnetohydrodynamics (MHD) can be found in Shercliff (1965).

1.3 Joule Heating

When current flows in a wire, the resistance of the wire causes a voltage drop along the wire; as a result electrical energy is lost. This lost electrical energy is converted into thermal energy called Joule heating. The detail of discussion of the topic is available in Hagen (1999).

1.4 Literature Review

Combined free and forced (mixed) convective flow in which neither the free convection nor the forced convection effects are dominant and both modes are in a

comparable level arise in many natural and technological process. Various researchers investigated the effects of mixed convective flows in cavities, channels by using analytical, experimental and numerical methods. Some important works are presented below.

Mixed convection in Vented Cavity/ Channel without Obstacle

The study of mixed convection in vented cavities are important from both theoretical and practical points of view. In addition, the vented geometry has been widely studied in heat transfer because of its fundamental importance and its many applications, including electronic cooling and thermal environmental control of dwellings. The existing literature in this domain has focused considerable attention on mixed convection in vented cavities or channels.

Papanicolaou and Jaluria (1990, 1992, 1993 and 1994) carried out a series of numerical studies to investigate the combined forced and natural convective cooling of heat dissipating electronic components, located in rectangular enclosure and cooled by an external through flow of air. Moreover, Raji and Hasnaoui (1998a, 1998b) obtained numerical results by using a finite difference procedure for opposing flows mixed (forced and natural) convection flow in a rectangular cavity heated from the side with a constant heat flux and submitted to a laminar cold jet from the bottom of its heated wall. The fluid leaves the cavity via the top or the bottom of the opposite vertical wall. Later on, the same authors i.e. Raji and Hasnaoui (2000) investigated the mixed convection in ventilated cavities where the horizontal top wall and the vertical left wall were prescribed with equal heat fluxes. At the same time, Angirasa (2000) numerically studied and explained the complex interaction between buoyancy and forced flow in a square enclosure with an inlet and a vent situated respectively, at the bottom and top edges of the vertical isothermal surface, where the other three walls are adiabatic. Also, Omri and Nasrallah (1999) performed numerical analysis by a control volume finite element method on mixed convection in a rectangular enclosure with differentially heated vertical sidewalls. Later on, Singh and Sharif (2003) extended their works by considering six placement configurations of the inlet and outlet of a differentially heated rectangular enclosure whereas the previous work was limited to only two different configurations of inlet

and outlet. Hsu and Wang (2000) investigated the mixed convective heat transfer where the heat source was embedded on a board mounted vertically on the bottom wall at the middle in the enclosure. The cooling airflow enters and exits the enclosure through the openings near the top of the vertical sidewalls. Gau et al. (2000) performed experiments on mixed convection in a horizontal rectangular channel with side heating. A numerical study of mixed convection heat transfer in two dimensional open-ended enclosures were investigated by Khanafer et al. (2002) for three different forced flow angle of attack. Wang and Jaluria (2002) numerically investigated the characteristics of the instability and the resulting effect on the heat transfer in mixed convection flow in a horizontal duct with discrete heat sources. A numerical analysis of laminar mixed convection in a channel with an open cavity and a heated wall bounded by a horizontally insulted plate was presented in Manca et al. (2003), where they considered three heating modes: assisting flow, opposing flow and heating from below. Later on, similar problem for the case of assisting forced flow configuration was tested experimentally by Manca et al. (2006) The flow and temperature field for a two-dimensional confined slot jet impinging on an isothermal hot surface computed by Sahoo and Sharif (2004). A finite-volume based computational study of steady laminar forced convection inside a square cavity with inlet and outlet ports was presented in Saeidi and Khodadadi (2006). Recently Rahman et al. (2007) studied numerically the opposing mixed convection in a vented enclosure. They found that with the increase of Reynolds and Richardson numbers the convective heat transfer becomes predominant over the conduction heat transfer and the rate of heat transfer from the heated wall is significantly depended on the position of the inlet port.

Mixed convection in Vented Cavity/ Channel with Obstacle

Heat transfers are needed in modern technology and are very important in many industrial areas. Hence it is necessary to study and simulate heat transfer phenomena. Modification of heat transfer in cavities due to introduction of obstacles, partitions and fins attached to the wall (s) has received some consideration in recent years. Many authors have recently studied heat transfer with obstacles, partitions and fins, thereby altering the convection flow phenomenon.

In mixed convection, structures of laminar wakes and heat transfer in a horizontal channel with a built-in square cylinder were studied numerically by Biswas et al. (1990). In their study, they found that the channel walls and the surface of the bluff body have higher temperatures than the incoming flow and the mixed convection initiate periodicity and asymmetry in the wake at a lower Re than forced convection alone. They also found that the mixed convection can enhance the heating of the fluid within the channel up to a certain Gr and further increase in Gr leads to the deterioration in the heat transfer rate. Later, the laminar flow of an incompressible fluid in a channel past a single heated normal flat plate as well as cascades of heated normal plates were studied numerically by Lin and sharif (1997). They showed that both Re and blockage ratio have significant effects on the flow and the temperature field, especially in the wake region. At the same time, Gowda et al. (1997) studied numerically the heat transfer and fluid flow over a row of in-line cylinders placed between two parallel plates. They concluded that there are considerable effects of buoyancy and the blockage on the flow heat transfer over the cylinders. Unsteady mixed convection flows over a circular cylinder placed inside an insulted vertical channel have studied by Singh et al. (1998).

Three related studies of mixed convection in a partially divided rectangular enclosure were respectively carried out by Hsu et al. (1997), How and Hsu (1998) and Calmidi and Mahajan (1998). The simulation was conducted for wide range of Reynolds and Grashof numbers. They indicated that the average Nusselt number and the dimensionless surface temperature depended on the location and height of the divider. Combined free and forced convection in a square enclosure with heat conducting body and a finite-size heat source was simulated numerically by Hsu and How (1999). They concluded that both the heat transfer coefficient and the dimensionless temperature in the body center strongly depend on the configurations of the system. Shuja et al. (2000) examined numerically the natural convection in a square cavity with a heat generating body. Air and water are considered as the fluid in the cavity while steel substrate is considered as the heat generating body. They found that the heat transfer from the solid body surfaces increases where the surfaces facing the inlet and the exit of the cavity and the solid body losses more heat in the air than in water. Shuja et al (2000a) numerically studied mixed convection in a

square cavity due to heat generating rectangular body and investigated the effect of exit port locations on the heat transfer characteristics and irreversibility generation in the cavity. They showed that the normalized irreversibility increases as the exit port location number increases and the heat transfer from the solid body enhanced while the irreversibility reduces. The same authors (2000b) considered heat transfer enhancement due to flow over a two-dimensional rectangular protruding bluff body. Hung and Fu (1999) studied the passive enhancement of mixed convection heat transfer in a horizontal channel with inner rectangular blocks by geometric modification. Unsteady mixed convection in a horizontal channel containing heated blocks on its lower wall was studied numerically by Najam et al. (2003). Tsay et al. (2003) rigorously investigated the thermal and hydrodynamic interactions among the surface-mounted heated blocks and baffles in a duct flow mixed convection They focused particularly on the effects of the height of baffle, distance between the heated blocks, baffle and number of baffles on the flow structure and heat transfer characteristics for the system at various Re and Gr/Re^2. Turki et al. (2003) conducted a numerical investigation to analyze the unsteady flow field and heat transfer characteristics in a horizontal channel with a built-in heated square cylinder. They examined the effects of the blockage ratio, the Reynolds number and Richardson numbers on aerodynamic and heat transfer characteristics. Chang and Shiau (2005) numerically investigated the effects of a horizontal baffle on the heat transfer characteristics of pulsating opposing mixed convection in a parallel vertical open channel. Bhoite et al. (2005) studied numerically the problem of mixed convection flow and heat transfer in a shallow enclosure with a series of block-like heat generating component for a range of Reynolds and Grashof numbers and block-to-fluid thermal conductivity ratios. They showed that higher Reynolds number tend to create a recirculation region of increasing strength at the core region and the effect of buoyancy becomes insignificant beyond a Reynolds number of typically 600, and the thermal conductivity ratio has a negligible effect on the velocity fields. Recently Rahman et al. (2008a) studied of mixed convection in a square cavity with a heat conducting square cylinder at different locations. At the same time Rahman et al. (2008b) studied mixed convection in a vented square cavity with a heat conducting horizontal solid circular cylinder. Very recently Rahman et al. (2009) analyzed

mixed convection in a rectangular cavity with a heat conducting horizontal circular cylinder by using finite element method.

Mixed convection in Lid-driven Cavity without Obstacle

The fundamental problem of combined forced and free convection heat transfer in a closed cavity has received considerable attention from researchers. Such a problem is usually grouped under lid-driven cavity problems. This problem is often encountered in industrial process and in nature. The modeling and simulation of crystal growth, glass production, nuclear reactors and food processing are common examples of current industrial applications, while convective thermal currents associated with the flow structure occurring in the lakes and reservoirs are classically cited as a natural phenomenon.

Aydin (1999) conducted a numerical study to investigate the transport mechanism of laminar mixed convection in a shear- and buoyancy- driven cavity. Two orientations of thermal boundary conditions at the cavity walls were considered to simulate the aiding and opposing buoyancy mechanisms Aydin and Yang (2000) numerically studied mixed convection heat transfer in a two-dimensional square cavity having an aspect ratio of 1. In their configuration the isothermal sidewalls of the cavity were moving downwards with uniform velocity while the top wall was adiabatic. A symmetrical isothermal heat source was placed at the other adiabatic bottom wall. Mixed convection heat transfer in a two-dimensional rectangular cavity with constant heat flux from partially heated bottom wall while the isothermal sidewalls are moving in the vertical direction was numerically studied by Gau and Sharif (2004). Steady state two-dimensional mixed convection problem in a vertical two-sided lid-driven differentially heated square cavity investigated numerically by Oztop and Dagtekin (2004b). Hossain and Gorla (2006) investigated the effects of viscous dissipation on unsteady combined convective heat transfer to water near its density maximum in a rectangular cavity with isothermal wall. Two-dimensional flow in a two-sided lid-driven cavity containing a temperature gradient was investigated numerically by Luo and Yang (2007).

Conjugate heat transfer in Closed Cavity with Obstacle

Conjugate heat transfer in closed cavity with obstacle has received a great deal of attention by the research community due to its importance in many engineering devices. Heat exchangers, underground spread of pollutants, environmental control, food processing and nuclear reactor safety are just some applications of heat transfer phenomena.

Convection in enclosures containing blocks has gained recent research significance as a means of heat transfer enhancement. One of the systematic numerical investigations of this problem was conducted by House et al (1990), who considered natural convection in a vertical square cavity with heat conducting body, placed on center in order to understand the effect of the heat conducting body on the heat transfer process in the cavity. They found that the heat transfer across the enclosure enhanced by a body with thermal conductivity ratio less than unity. Lacroix (1992) performed a numerical study of natural convection heat transfer from two vertically separated heated cylinder to a rectangular cavity cooled from above. Later on, Lacroix and Joyeux (1995) conducted a numerical study of natural convection heat transfer from two horizontal heated cylinders confined to a rectangular enclosure having finite wall conductance's. They indicated that wall heat conduction reduces . the average temperature differences across the cavity, partially stabilizes the flow and decreases natural convection heat transfer around the cylinders. Sun and Emery (1997) investigated experimentally and numerically the conjugate heat transfer with internal heat source and internal baffle. They used finite difference method with SIMPLE algorithm for numerical analysis. They found that for an enclosure with a conductive baffle, heat transfer is strongly influenced by the coupling effect among baffle conduction, fluid convection and the strength of internal heating when the baffle is located near walls. Yedder and Bilgen (1997) has been studied laminar natural convection in enclosures bounded by a solid wall with its outer boundary at constant temperature while the opposing side has a constant heat flux. Oh et al (1997) studied the steady natural convection processes when a temperature difference exists across the enclosure and at the same time, a conducting body generates heat within the enclosure. They investigated the effects of Rayleigh numbers and temperature difference ratio on variations of streamlines, isotherms,

9

heat lines and the average Nusselt numbers on the hot and cold walls. Misra and Sarkar (1997) conducted a finite element analysis of conjugate natural convection in a square enclosure with a conducting vertical wall. The natural convection heat transfer in vertical slender cavities with conducting fins attached to the cold wall was numerically analyzed by Yucel and Turkoglu (1998). Sasaguchi et at. (1998) Performed numerical calculations to examine the effect of the position of a cooled cylinder in a rectangular cavity on the transient cooling of pure water around the cylinder. Ha et al. (1999) conducted a comprehensive numerical study to investigate the transient heat transfer and flow characteristics of the natural convection of three different fluids in a vertical square enclosure within which a centered, square, heat conducting body generates heat. Later on, Ha and Jung (2000) conducted a comprehensive numerical study to investigate three dimensional steady conjugate heat transfers of natural convection and conduction in a differentially heated in a vertical cubic enclosure within which a centered, cubic, heat-generating cubic conducting body. They concluded that for the presence of a conducting body in the enclosure, a larger variation of the local Nusselt number at the hot and cold walls in the z-direction is seen. Kimura et al. (2001) studied heat transfer in an inclined enclosure with an inner rotating plate. The effect of an internal volumetric heat generating and conducting solid body on the mixed convection in a square cavity was investigated by Yilbas et al. (2002). The numerical visualization of mass and heat transport for conjugate heat transfer by streamlines and heat lines were comprehensively studied by Deng and Tang (2002). Roychowdhury et al. (2002) analyzed the natural convective flow and heat transfer features for a heated cylinder kept in a square enclosure with different thermal boundary conditions. Natural convection heat transfer in a square cavity with a heated plate built-in vertically and horizontally was investigated by Oztop and Dagtekin (2004a) They addressed the effect of the position and aspect ratio of heated plate on heat transfer and fluid flow and it was found that mean Nusselt numbers at both vertical and horizontal location increased as Rayleigh number increased Dong and Li (2004) studied conjugate of natural convection and conduction in a complicated enclosure. They investigated the influences of material character, geometrical shape and Rayleigh number on the heat transfer in overall concerned region and concluded that the flow and heat transfer

increase with the increase of thermal conductivity in the solid region; both geometric shape and Rayleigh number affect the overall flow and heat transfer greatly. Buoyancy induced flow and heat transfer inside a square cavity due to a thin baffle on the hot wall was analyzed numerically in Tasnim and Collins (2004). They investigated the effects of baffle height, length and Rayleigh number on heat transfer performance. It was found that adding baffle on the hot wall increased the rate of heat transfer. Bilgen and Yamane (2004) examined numerically the conjugate heat transfer by laminar natural convection and conduction in two-dimensional rectangular enclosures with openings. A chimney inside the enclosure was simulated as a vertical rectangular body with a uniform heat flux on one side and insulation on the other. They investigated the effects of the various geometrical parameters and the thickness of the insulation layer on the fluid flow rate and heat transfer characteristics. Later, Bilgen (2005) numerically studied heat transfer by natural convection in differentially heated square cavities with horizontal thin fin. He concluded that normalized Nusselt number is an increasing function of Rayleigh number, and decreasing function of fin length and relative conductivity ratio. Merrikh and Lage (2005) studied numerically natural convection within a differentially heated heterogeneous square enclosure consisting of several disconnected and conducting solid blocks within a saturated fluid. Braga and Lemos (2005) numerically studied steady laminar natural convection within a square cavity filled with a fixed amount of conducting solid material consisting of either circular or square obstacles. They showed that the average Nusselt number for cylindrical rods is slightly lower than those for square rods. The problem of laminar natural convection heat transfer in a square cavity with an adiabatic arc shaped baffle was numerically analyzed by Tasnim and Collins (2005). They were identified that flow and thermal fields are modified by the blockage effect of the baffle and increasing the shape parameter of the baffle enhances the degree of flow modification due to blockage. Lee and Ha (2005) investigated natural convection in a horizontal layer of fluid with a conducting body in the interior, using an accurate and efficient Chebyshev spectral collocation approach. Later on, the same authors Lee and Ha (2006) also studied natural convection in horizontal layer of fluid with heat generating conducting body in the interior. Bhave et al. (2006) were investigated the

11

effect on the steady-state natural convection heat transfer enhancement of a centrally-placed adiabatic block within a differentially heated square cavity with a fixed temperature drop between the vertical walls. Kumar and Dalal (2006) studied natural convection around a tilted heated square cylinder kept in an enclosure in the range of $10^3 \leq Ra \leq 10^6$. They reported detailed flow and heat transfer features for two different thermal boundary conditions and found that the uniform wall temperature heating is quantitatively different from the uniform wall heat flux heating. Oztop and Bilgen (2006) numerically studied a differentially heated, partitioned, square cavity containing a heat generating fluid. The vertical walls were isothermal while the horizontal walls were adiabatic and an isothermal cold partitioned was attached to the bottom wall. They considered external and internal Rayleigh numbers (Ra_E and Ra_I) ranged from 10^3 to 10^6, and concluded that the flow field was modified considerably with partial dividers and heat transfer was generally reduced particularly when the ratio of internal and external Rayleigh numbers was from 10^1 to 10^2. Xu et al. (2006) experimentally observed the thermal flow around a square obstruction on a vertical wall in a differentially heated cavity. Natural convection conjugate heat transfer inside an inclined square cavity with an internal conducting block was carried out in Das and Reddy (2006). Nakhi and Chamkha (2006) considered steady laminar natural convective flow of a viscous fluid in an inclined enclosure with partitions. They predicted that the wall heat transfer and the flow characteristics inside the partitioned enclosure depended strongly on the dimensionless partitioned height, Rayleigh number and the enclosure inclination. Later, Nakhi and Chamkha (2007) numerically studied steady, laminar, conjugate natural convection around a finned pipe placed in the center of a square enclosure with uniform internal heat generation. Jami et al (2007) numerically investigated the laminar natural convective flow in an enclosure with a heat-generating cylindrical conducting body.

Heat transfer in a Closed Cavity/ Channel with MHD Effect

A combined free and forced convection flow of an electrically conducting fluid in a lid-driven cavity or in a channel in the presence of a magnetic field is of special technical significance because of its frequent occurrence in many industrial

applications such as geothermal reservoirs, cooling of nuclear reactors, thermal insulations and petroleum reservoirs. These types of problems also arise in electronic packages, micro electronic devices during their operations.

Oreper and Szekely (1983) studied the effect of an externally imposed magnetic field on buoyancy driven flow in a rectangular cavity. They found that the presence of a magnetic field can suppress natural convection currents and that the strength of the magnetic field is one of the important factors in determining the quality of the crystal. Ozoe and Maruo (1987) investigated magnetic and gravitational natural convection of melted silicon two-dimensional numerical computations for the rate of heat transfer. Garandet et al. (1992) studied natural convection heat transfer in a rectangular enclosure with a transverse magnetic field Rudraiah et al. (1995a) investigated the effect of surface tension on buoyancy driven flow of an electrically conducting fluid in a rectangular cavity in the presence of a vertical transverse magnetic field to see how this force damps hydrodynamic movements. At the same time, Rudraiah et al. (1995b) also studied the effect of a magnetic field on free convection in a rectangular enclosure. The problem of unsteady laminar combined forced and free convection flow and heat transfer of an electrically conducting and heat generating or absorbing fluid in a vertical lid-driven cavity in the presence of a magnetic field was formulated by Chamkha (2002). Mahmud et al. (2003) studied analytically a combined free and forced convection flow of an electrically conducting and heat-generating/ absorbing fluid a vertical channel made of two parallel plates under the action of transverse magnetic field. Sarris et al. (2005) presented a numerical study of unsteady two-dimensional natural convection of an electrically conducting fluid in a laterally and volumetrically heated square cavity under the influence of a magnetic field.

1.5 Motivation behind the Selection of Present Problem

From the literature review it is clear that very little numerical study on the effect of conduction in mixed convection heat transfer in vented cavities with inner obstacle have been carried out. The study of mixed convection in vented cavities with inner obstacle is important for numerous engineering applications. To apply a system as an effective heat transfer devices such as in designing nuclear reactors, solar collectors,

electrical, microelectronic equipments containers and in many other design problems mixed convection heat transfer is pronominent. Thus the analysis of the effect of mixed convection for different boundary conditions and shapes are necessary to ensure efficient performance of heat transfer equipments. On the other hand, the majority of the conjugate mixed convection studies were carried out in channel with inner obstacle and conjugate natural convection studies were carried out in closed cavities with inner obstacle. Thus far, none have conducted studies involving the effect of conduction in mixed convection flow in a lid-driven cavity containing an obstacle, although they are widely used. Numerical studies are therefore essential to observe the variation in fluid flow and heat transfer due to the above physical changes, which forms the basis of the motivation behind the present study

1.6 Present Problems

Previously no work has been reported for the actual heat transfer augmentation in vented as well as lid-driven cavities with inner obstacle. So the present study is a numerical investigation on the vented as well as lid-driven cavities with inner obstacle for the purpose of actual heat transfer augmentation In the present investigation, two different types of cavities are considered. One is rectangular vented cavity containing a fixed amount of conducting solid material in the form of circular as a case 1 and square cylinder as a case 2, where the right side wall is heated and the other sidewalls remain adiabatic. Another type is a vertical lid-driven cavity, where the top and bottom walls are assumed to be adiabatic while the left and the right walls are maintained at constant and different temperatures. The left wall of the cavity is allowed to move in its own plane at a constant velocity. A magnetic field is applied in the horizontal direction normal to the moving wall and Joule heating term is considered in the cavity. A conducting solid material is also considered inside the cavity. The solid phase is shaped into two different geometries, namely square and circular, which are horizontally or vertically displaced inside the cavity. The proposed studies are expected to reveal that the heat transfers in such arrangements are different from those studied in the above literature and it will therefore prove useful from the designer's point of view in choosing the best physical condition that suits him.

1.7 Objectives of the Present Study

The overall goal of this thesis is to numerically simulate fluid flow and heat transfer behaviors inside two different types of cavity configurations as stated in previous section. The investigations are to be carried out at different non-dimensional governing parameters such as Reynolds number, Richardson number, Prandtl number solid-fluid thermal conductivity ratio and different physical parameters such as cylinder size, shape, locations inside the cavity and cavity aspect ratio. In addition, the effect of inlet and outlet port locations is studied only for vented cavity where as the effect of Hartmann number and Joule heating parameter are studied for the case of lid-driven cavity. The effect of the non-dimensional parameters on overall heat transfer, velocity and temperature distribution will be examined both qualitatively and quantitatively. Results will be presented in terms of streamlines, isotherms. as well as the average Nusselt number, average temperature of the fluid and dimensionless temperature at the cylinder center for different values of the governing and the geometric parameters. However, the specific aims of the study are as follows:

- To modify a mathematical model regarding the conjugate effect of conduction and mixed convection flow around a horizontal cylinder (circular/square) placed in a rectangular vented cavity and hence to solve that model using finite element method.

- To modify a mathematical model for the effect of Joule heating on the coupling of conduction and magnetohydrodynamic mixed convection flow in a rectangular lid-driven cavity along with a heat conducting horizontal cylinder (circular/square) and hence to solve that model using finite element method.

- To carry out the validation of the present finite element model by investigating the effect of natural convection heat transfer in a square cavity with heat conducting body in its center and the effect of hydro magnetic combined convection flow in a vertical lid-driven cavity with internal heat generation or absorption.

- To find out the best location of the inlet and outlet port for which optimum heat transfer performance can be achieved in the case of vented cavity.

- To examine the effect of Reynolds number, Richardson number, Prandtl number, as well as the size, location, and thermal conductivity of the conducting cylinder

and aspect ratio of the cavity on the fluid flow and heat transfer characteristics in the vented cavity.

- To investigate the effect of Reynolds number, Richardson number, Prandtl number, Hartmann number, Joule heating parameter, as well as the size, location, and thermal conductivity of the conducting cylinder and aspect ratio of the cavity on the flow and thermal fields of the lid-driven cavity.

1.8 Outline of the Thesis

This dissertation contains five chapters. In this chapter a brief introduction is presented with aim and objective. There is nothing new to say about it. This chapter also consists a literature review of the past studies on fluid flow and heat transfer in cavities or channels. In this state-of-the art review, different aspects of the previous studies have been mentioned categorically. This is followed by the post-mortem of a recent historical event for the illustration of fluid flow and heat transfer effects in cavities or channels.

Chapter 2 presents the computational procedure of the problem for viscous incompressible flow.

In Chapter 3 a detailed parametric study on the conjugate effect of conduction and mixed convection flow in vented cavities with inner obstacle is conducted. Effect of the major parameters such as Reynolds number, Richardson number, Prandtl number solid-fluid thermal conductivity ratio and different physical parameters such as cylinder size, locations inside the cavity, inlet and outlet locations and cavity aspect ratio have been presented to better understand the heat transfer mechanisms in vented cavities.

In Chapter 4 the effect of joule heating in the coupling of conduction with magnetohydrodynamic mixed convection flow in a rectangular vertical lid-driven cavity along with a heat conducting horizontal cylinder are conducted. Parametric studies for the relevant parameters are also performed in this chapter.

Finally, in Chapter 5 the dissertation is rounded of with the conclusions and recommendations for further study of the present problem are outlined.

Chapter 2

Computational Details

Mathematical model of physical phenomena may be ordinary or partial differential equations, which have been the subject of analytical and numerical investigations. The partial differential equations of fluid mechanics and heat transfer are solvable for only a limited number of flows. To obtain an approximate solution numerically, we have to use a discretization method, which approximated the differential equations by a system of algebraic equations, which can then be solved on a computer. The approximations are applied to small domains in space and /or time so the numerical solution provides results at discrete locations in space and time. Much as the accuracy of experimental data depends on the quality of the tools used, the accuracy of numerical solutions depend on the quality of discretizations used

Computational fluid dynamics (CFD) computation involves the formation of a set numbers that constitutes a practical approximation of a real life system The outcome of computation process improves the understanding of the performance of a system. Thereby, engineers need CFD codes that can make physically realistic results with good quality accuracy in simulations with finite grids. Contained within the broad field of computational fluid dynamics are activities that cover the range from the automation of well established engineering design methods to the use of detailed solutions of the Navier-Stokes equations as substitutes for experimental research into the nature of complex flows. CFD have been used for solving wide range of fluid dynamics problem. It is more frequently used in fields of engineering where the geometry is complicated or some important feature that cannot be dealt with standard methods. More details are available in Ferziger & Perić (1997) and Patankar (1980).

2.1 Advantages of Numerical Investigation

The analysis of flow and heat transfer in thermodynamics can be performed either theoretically or experimentally. Experimental investigation of such problem could not gain that much popularity in the field of thermodynamics because of their limited

flexibility and applications. For every change of geometry body and boundary condition, it needs separate investigation, involving separate experimental requirement/ arrangement, which, in turn makes it unattractive, especially from the time involved as well as economical point of views. The theoretical investigation on the other hand, can be carried out either by analytical approach or by numerical approach. The analytical methods of solution are not of much help in solving the practical problems. This is mainly due to the very involvement of a large number of variables, complex geometrical bodies, boundary conditions and arbitrary boundary shapes. General closed form solutions can be obtained only for very ideal cases and the results obtained for a particular problem, usually with uniform boundary conditions. For two-dimensional thermodynamics problems, mathematical model involve partial differential equations are required to be solved simultaneously with some boundary conditions. Therefore, there no alternatives except the numerical methods for the solution of the problems of practical interest. The details are to be had in Fletcher (1991) and Patankar (1980).

2.2 Components of a Numerical Solution Methods

Several components of numerical solution methods are available in Ferziger and Perić (1997), here only the main steps will be demonstrate in the following.

2.2.1 Mathematical Model

The starting point of any numerical method is the mathematical model, i.e. the set of partial differential equations and boundary conditions. A solution method is usually designed for a particular set of equations. Trying to produce a general-purpose solution method, i.e. one which is applicable to all flows, is impractical, is not impossible and as with most general purpose tools, they are usually not optimum for any one application.

2.2.2 Discretization Method

After selecting the mathematical model, one has to choose a suitable discretization method, i.e. a method of approximating the differential equations by a system of

18

algebraic equations for the variable at some set of discrete locations in space and time.

2.2.3 Numerical Grid

The numerical grid defines the discrete locations, at which the variables are to be calculated, which is essentially a discrete representation of the geometric domain on which the problem is to be solved. It divided the solution domain into a finite number of sub-domains (elements, control volumes etc). Some of the options available are structural (regular) grid, block structured grid, unstructured grids etc.

2.2.4 Finite Approximations

Following the choice of grid type, one has to select the approximations to be used in the discretization process. In a finite difference method, approximations for the derivatives at the grid points have to be selected. In a finite volume method, one has to select the methods of approximating surface and volume integrals. In a finite element method, one has to choose the functions and weighting functions.

2.2.5 Solution Method

Discretization yields a large system of non-linear algebraic equations. The method of solution depends on the problem. For unsteady flows, methods based on those used for initial value problems for ordinary differential equation (marching in time) is used. At each time step an elliptic problem has to be solved. Pseudo-time marching or an equivalent iteration scheme usually solves steady flow problems. Since the equations are non-linear, an iteration scheme is used to solve them. These methods use successive linearization of the equations and the resulting linear systems are almost always solved by iterative techniques. The choice of solver depends on the grid type and the number of nodes involved in each algebraic equation.

2.3 Discretization Approaches

The first step to numerically solve a mathematical model of physical phenomena is its numerical discretization. This means that each component of the differential equations is transformed into a "numerical analogue" which can be represented in the

computer and then processed by a computer program, built on some algorithm. There are many different methodologies were devised for this purpose in the past and the development still continues. In order to short them, we can at first divide the spatial discretisation schemes into the following three main categories. finite difference (FD), finite volume (FV) finite element (FE) methods, Boundary element (BE) method and Boundary volume (BV) method.

In the present numerical computation, Galerkin finite element method (FEM) is used. Detailed discussion of this method is available in Chung (2002) and Dechaumphai (1999).

Finite Element Method

The finite element method (FEM) is a powerful computational method for solving problems, which are described by partial differential equations. The fundamental idea of the finite element method is to outlook a given domain as an assemblage of simple geometric shapes, called finite elements, for which it is possible to systematically generate the approximation functions needed in the solution of partial differential equations by the weighted residual method. The computational domains with irregular geometries by a collection of finite elements makes the method a valuable practical tool for the solution of boundary value problems arising in various fields of engineering. The approximation functions, which satisfy the governing equations and boundary conditions, are often constructed using ideas from interpolation theory. Approximating functions in finite elements are determined in terms of nodal values of a physical field, which is required. A continuous physical problem is transformed into a discretized finite element problem with unknown nodal values. For a linear problem, a system of linear algebraic equations should be solved. Values inside finite elements can be recovered using nodal values.

The finite element method is one of the numerical methods that have received popularity due to its capability for solving complex structural problems. The method has been extended to solve problems in several other fields such as in the field of heat transfer, computational fluid dynamics, electromagnetic, biomechanics etc. In spite of the great success of the method in these fields, its application to fluid mechanics, particularly to convective viscous flows, is still under intensive research.

The major steps involved in finite element analysis of a typical problem are:

1. Discretization of the domain into a set of finite elements (mesh generation).
2. Weighted-integral or weak formulation of the differential equation to be analyzed.
3. Development of the finite element model of the problem using its weighted-integral or weak form.
4. Assembly of finite elements to obtain the global system of algebraic equations.
5. Imposition of boundary conditions.
6. Solution of equations.
7. Post-computation of solution and quantities of interest.

2.3.1 Grid Generation

The area of numerical grid generation is relatively young in practice, although its roots in mathematics are old. The arrangement of discrete points throughout the flow field is simply called a grid. The determination of a proper grid for the flow through a given geometric shape is important. The way that such a grid is determined is called grid generation. The grid generation is a significant consideration in CFD Finite element method can be applied to unstructured grids. This is because the governing equations in this method are written in integral form and numerical integration can be carried out directly on the unstructured grid domain in which no coordinate transformation is required. A two-dimensional domain may be triangulated as shown in Figure 2.1. In finite element method, the mesh generation is the technique to subdivide a domain into a set of sub-domains, called finite elements. Figure 2.1 shows a domain, A is subdivided into a set of sub-domains, A^e with boundary Γ^e. Detailed discussion of this issue is available in Anderson (1995) and Chung (2002).
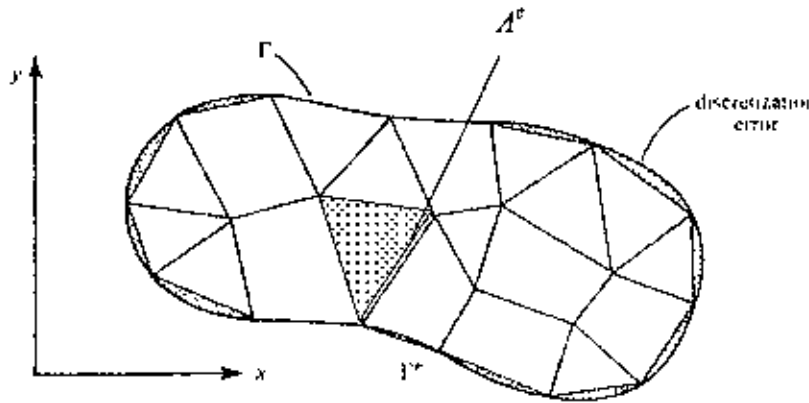
Figure 2.1: A typical FE discretization of a domain, Reddy & Gartling (1994)

2.3.2 Finite Element Formulation and Computational Procedure

Viscous incompressible thermal flows have been the subject of our investigation. The problem is relatively complex due to the coupling between the energy equation and the Navier-Stokes equations, which govern the fluid motion. These equations comprise a set of coupled nonlinear partial differential equations, which is difficult to solve especially with complicated geometries and boundary conditions. The finite element formulation and computational procedure for Navier-Stokes equations along with energy equations will be discuss in the chapter 3

2.3.3 Algorithm

The algorithm was originally put forward by the iterative Newton-Raphson algorithm; the discrete forms of the continuity, momentum and energy equations are solved to find out the value of the velocity and the temperature. It is essential to guess the initial values of the variables. Then the numerical solutions of the variables are obtained while the convergent criterion is fulfilled. The simple algorithm is shown by the flow chart below.
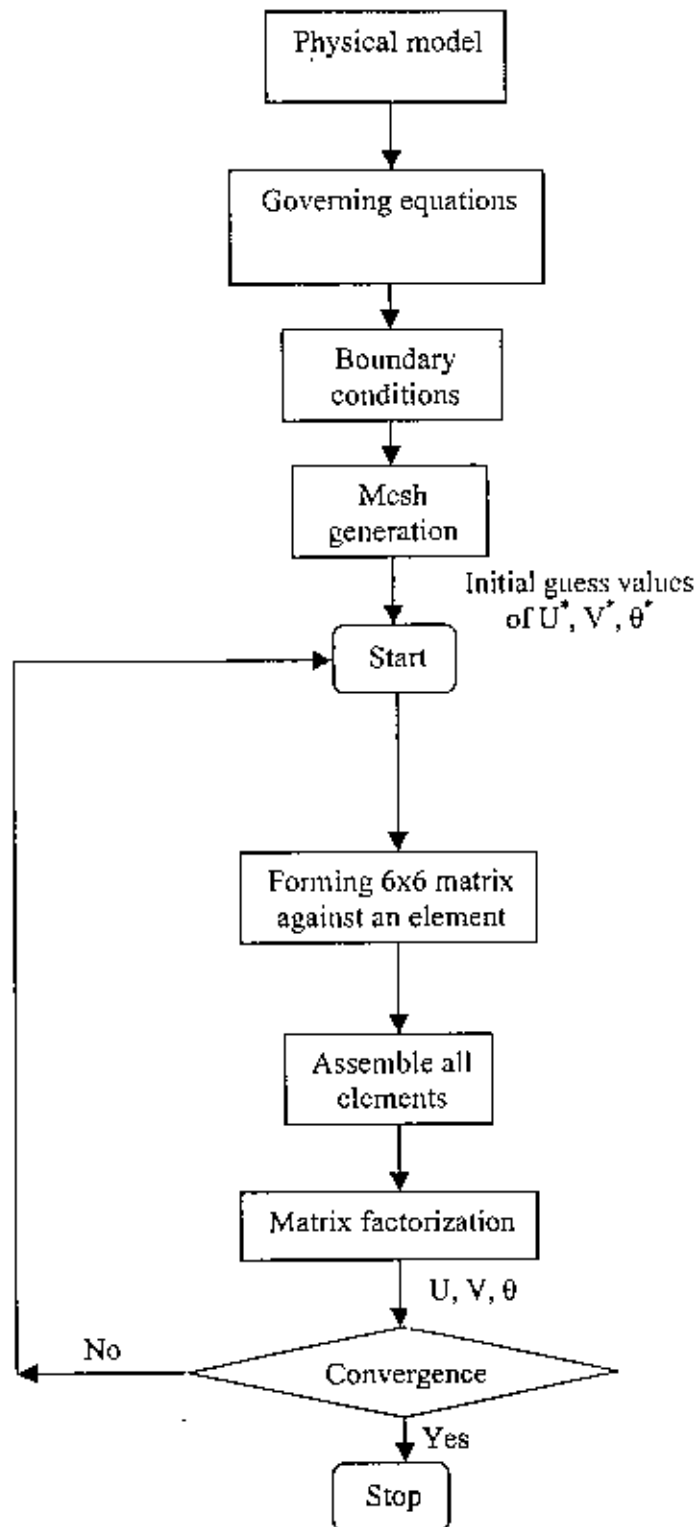
Figure 2.2: Flow chart of the computational procedure

2.3.4 Solution of System of Equations

A system of linear algebraic equations has been solved by the UMFPACK with MATLAB interface. UMFPACK is a set of routines for solving asymmetric sparse linear systems $Ax = b$, using the Asymmetric MultiFrontal method and direct sparse LU factorization. Five primary UMFPACK routines are required to factorize A or Ax = b:

1. Pre-orders the columns of A to reduce fill-in and performs a symbolic analysis.
2. Numerically scales and then factorizes a sparse matrix.
3. Solves a sparse linear system using the numeric factorization.
4. Frees the Symbolic object.
5. Frees the Numeric object.

Additional routines are:

1. Passing a different column ordering
2. Changing default parameters
3. Manipulating sparse matrices
4. Getting LU factors
5. Solving the LU factors
6. Computing determinant

UMFPACK factorizes PAQ, $PRAQ$, or $PR^{-1}AQ$ into the product LU, where L and U are lower and upper triangular, respectively, P and Q are permutation matrices, and R is a diagonal matrix of row scaling factors (or $R = I$ if row-scaling is not used). Both P and Q are chosen to reduce fill-in (new nonzeros in L and U that are not present in A). The permutation P has the dual role of reducing fill-in and maintaining numerical accuracy (via relaxed partial pivoting and row interchanges). The sparse matrix A can be square or rectangular, singular or non-singular, and real or complex (or any combination). Only square matrices A can be used to solve $Ax = b$ or related systems. Rectangular matrices can only be factorized. UMFPACK first finds a column pre-ordering that reduces fill-in, without regard to numerical values. It scales and analyzes the matrix, and then automatically selects one of three strategies for pre-ordering the rows and columns: asymmetric, 2-by-2 and symmetric. These strategies are described below.

One notable attribute of the UMFPACK is that whenever a matrix is factored, the factorization is stored as a part of the original matrix so that further operations on the matrix can reuse this factorization. Whenever a factorization or decomposition is calculated, it is preserved as a list (element) in the factor slot of the original object. In this way a sequence of operations, such as determining the condition number of a matrix and then solving a linear system based on the matrix, do not require multiple factorizations of the intermediate results.

Conceptually, the simplest representation of a sparse matrix is as a triplet of an integer vector i giving the row numbers, an integer vector j giving the column numbers, and a numeric vector x giving the non-zero values in the matrix. The triplet representation is row-oriented if elements in the same row were adjacent and column-oriented if elements in the same column were adjacent. The compressed sparse row (csr) or compressed sparse column (csc) representation is similar to row-oriented triplet or column-oriented triplet respectively. These compressed representations remove the redundant row or column in indices and provide faster access to a given location in the matrix.

2.4 Concluding Remarks

This chapter has presented a tutorial introduction to computational method with advantages of numerical investigation. Because numerical method has played a central role in this thesis. Various components of numerical method have been also explained. Finally, the major steps involved in finite element analysis of a typical problem have been discussed.

Chapter 3

Effect of Conduction in Mixed Convection Flow in a Rectangular Vented Cavity filled with a Heat Conducting Horizontal Cylinder

Mixed convection in vented cavities have received sustainable attention, due to the interest of the phenomenon in many technological processes, such as the design of solar collectors, thermal design of building, air conditioning and recently the cooling of electronic circuit boards. The details are available in Papanicolaou and Jaluria (1990, 1994), Omri and Nasrallah (1999) and Raji and Hasnaoui (1998a, 1998b, 2000). In vented cavities, the interaction between the external forced stream and the buoyancy driven flow induced by heat source could lead to complex flow structures. Analysis of the above phenomena incorporating a heat conducting solid cylinder extends its usability to many other practical situations such as any projections on a motherboard of a computer and a conductive material in an inert atmosphere inside a furnace with a constant flow of gas from outside constitute practical applications for the present problem. To have a clear understanding of heat transfer augmentation and fluid flow characteristics in an obstructed vented cavity a number of studies were carried out in the past by different researchers Papanicolaou and Jaluria (1993), Shuja et al. (2000a, 2000b) and Hsu and How (1999)

This chapter describes the effect of conduction in mixed convection flow in rectangular vented cavities filled with a heat conducting horizontal circular or square cylinder. Here buoyancy is generated because of the difference in temperatures between the hot wall and through stream. The interaction between the buoyancy and the forced flow is examined in detail. The governing equations along with appropriate boundary conditions for the present problem are first transformed into a non-dimensional form and the resulting non-linear system of partial differential equations are then solved numerically using a very efficient finite element method. Here numerical solutions are obtained over a wide range of non-dimensional parameters i.e. Reynolds number Re, Richardson number Ri, Prandtl number Pr,

solid-fluid thermal conductivity ratio K and various physical parameters i.e. the inlet and outlet position of the cavity, the sizes and locations of the inner cylinder and aspect ratio of the cavity. Parametric results are presented in terms of streamlines and isotherms. As the heat transfer at the heated wall depends upon a number of factors, a dimensional analysis is presented to show the important non-dimensional parameter (Nusselt number) that will influence the dimensionless heat transfer at the heated surface. Finally, the average Nusselt number at the hot wall, average temperature of the fluid in the cavity and temperature at the cylinder center, obtained from the cavity with circular cylinder and are compared with those calculated with square cylinder for several parameters.

The remainder of this chapter is as follows. In section 3.1, the physical configurations of the current research interest are shown. Then the appropriate mathematical model (both governing equations and boundary conditions) is considered in section 3.2. After that a numerical scheme that is employed in this study are described in the section 3.3. Next parametric results are presented in the section 3.4. Finally, section 3.5 gives a summary of our conclusions.

3.1 Physical Configurations

The schematic drawing of the system and the coordinates are shown in figures 3.1 and 3.2, which consider rectangular vented cavities filled with a heat conducting horizontal solid material in the form of circular cylinder as a case 1 (figure 3.1) and square cylinder as a case 2 (figure 3.2). In both cases, the quantity of solid material is the same. The cavity dimensions are defined by height H and length L. The cavities are heated from the right vertical wall, with a uniform constant temperature T_h while the remaining walls are considered perfectly insulated. In both of the cases, the inflow opening located on the left vertical adiabatic wall and the outflow opening on the opposite vertical heated wall is arranged as shown in the schematic figures and may vary in location either top or bottom position. The cavities presented in figures 3.1 (a) and 3.2 (a) are subjected to an external flow which enters via the bottom of the insulated vertical wall and leaves via the bottom of the opposite heated vertical wall.
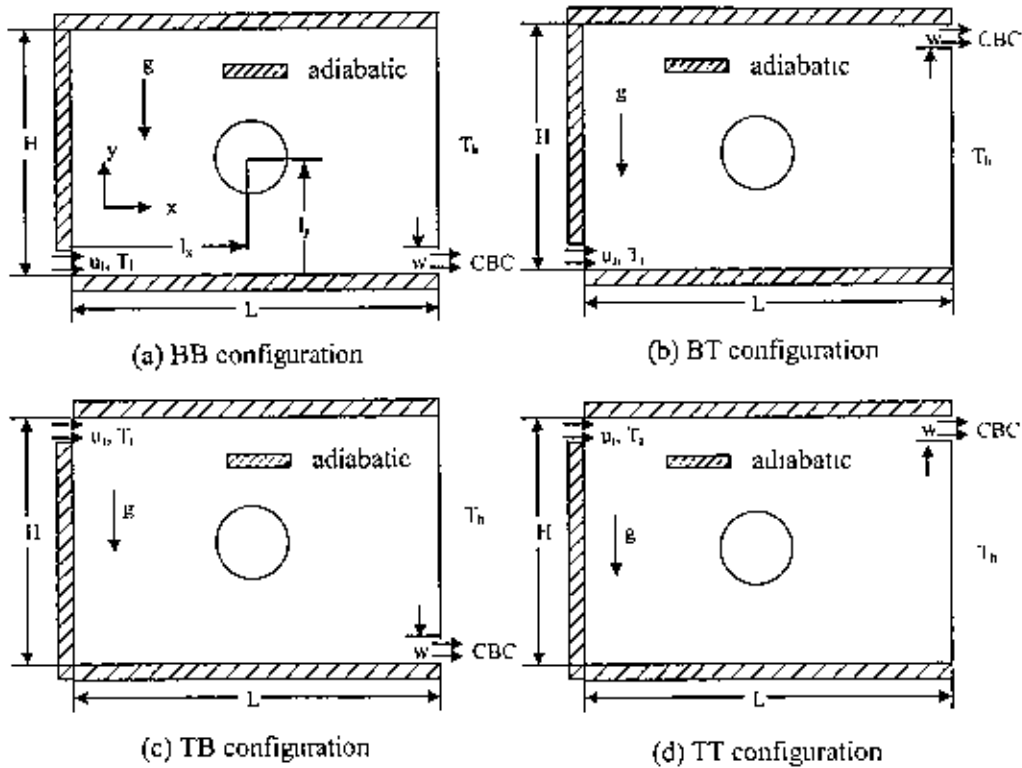
Figure 3.1: Four schematic diagrams of thermally driven ventilated cavity with a circular cylinder (case 1).

For reasons of brevity, this case will be referred to as BB configuration from now. When the horizontal cold fluid enters into the cavity from the bottom of insulated wall and leaves at the top of the other vertical one in figures 3.1 (b) and 3.2 (b), these case will be referred as BT configuration. Similarly, figures 3.1-3.2 (c) and 3.1-3.2 (d) are referred to as TB and TT configurations respectively. For simplicity, the heights of the two openings are set equal to the one-tenth of the enclosure height. It is assumed that the incoming fluid flow through the inlet at a uniform velocity u_i at the ambient temperature T_i and the outgoing flow are assumed to have zero diffusion flux for all variables i.e. convective boundary conditions (CBC). All solid boundaries are assumed to be rigid no-slip walls.

The mathematical model developed in the last section is used to investigate the mutual interaction conduction-mixed convection in an obstructed vented cavity.

(a) BB configuration

(b) BT configuration

(c) TB configuration
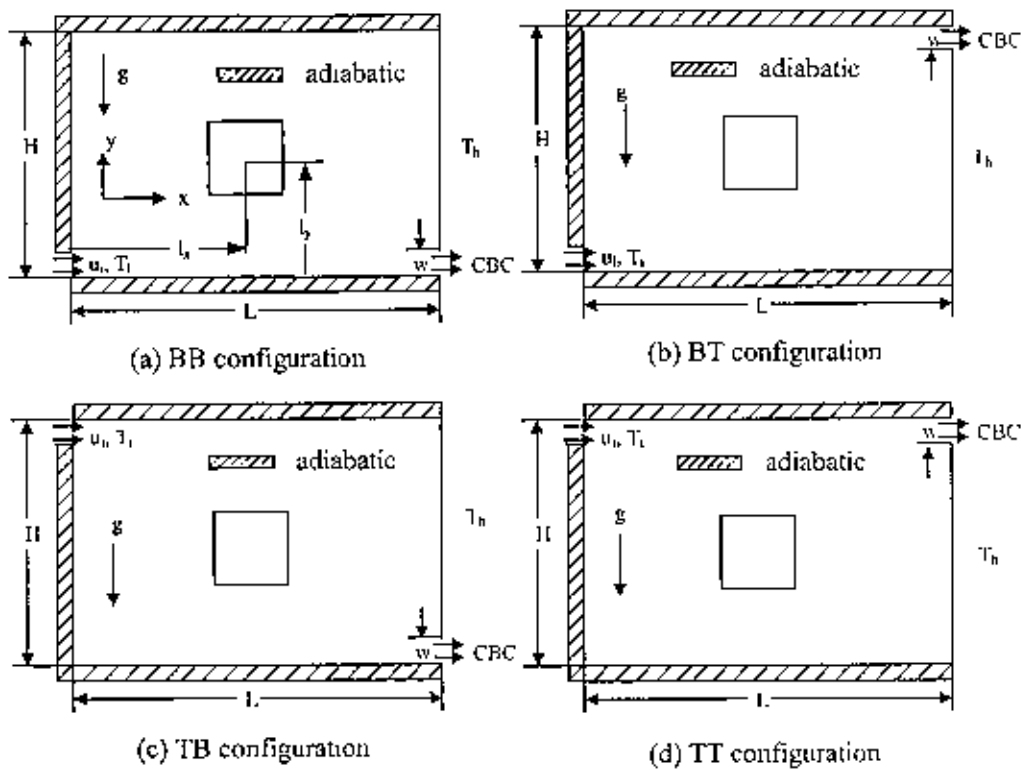
(d) TT configuration

Figure 3.2: Four schematic diagrams of thermally driven ventilated cavity with a square cylinder (case 2).

3.2 Mathematical Formulation

The several steps of the mathematical formulation for the above physical configurations are shown as follows

3.2.1 Governing Equations

The fundamental laws used to solve the fluid flow and heat transfer problems are the conservation of mass (continuity equations), conservation of momentums (momentum equations), and conservation of energy (energy equations), which constitute a set of coupled, nonlinear, partial differential equations. For laminar incompressible thermal flow, the buoyancy force is included here as a body force in the v-momentum equation. The governing equations for the two-dimensional steady flow after invoking the Boussinesq approximation and neglecting radiation and viscous dissipation can be expressed as

Continuity Equation

$$\frac{\partial u}{\partial x} + \frac{\partial v}{\partial y} = 0 \tag{3.1}$$

Momentum Equations

$$u\frac{\partial u}{\partial x} + v\frac{\partial u}{\partial y} = -\frac{1}{\rho}\frac{\partial p}{\partial x} + \upsilon\left(\frac{\partial^2 u}{\partial x^2} + \frac{\partial^2 u}{\partial y^2}\right) \tag{3.2}$$

$$u\frac{\partial v}{\partial x} + v\frac{\partial v}{\partial y} = -\frac{1}{\rho}\frac{\partial p}{\partial y} + \upsilon\left(\frac{\partial^2 v}{\partial x^2} + \frac{\partial^2 v}{\partial y^2}\right) + g\beta\left(T - T_r\right) \tag{3.3}$$

Energy Equations

$$u\frac{\partial T}{\partial x} + v\frac{\partial T}{\partial y} = \frac{k}{\rho c_p}\left(\frac{\partial^2 T}{\partial x^2} + \frac{\partial^2 T}{\partial y^2}\right) \tag{3.4}$$

For solid cylinder

$$0 = \frac{k_s}{\rho c_p}\left(\frac{\partial^2 T_s}{\partial x^2} + \frac{\partial^2 T_s}{\partial y^2}\right) \tag{3.5}$$

where x and y are the distances measured along the horizontal and vertical directions respectively; u and v are the velocity components in the x and y directions respectively; T and T_s denote the fluid and solid temperature respectively, T_r denotes the reference temperature for which buoyant force vanishes, p is the pressure and ρ is the fluid density, g is the gravitational constant, β is the volumetric coefficient of thermal expansion, c_p is the fluid specific heat, k and k_s are the thermal conductivity of fluid and solid respectively.

3.2.2 Boundary Conditions

The boundary conditions for the present problem are specified as follows:

At the inlet: $u = u_i, v = 0, T = T_i$

At the outlet: convective boundary condition (CBC), $p = 0$

At all solid boundaries: $u = 0, v = 0$

At the heated right vertical wall. $T = T_h$

At the left, top and bottom walls: $\dfrac{\partial T}{\partial n} = 0$

At the fluid-solid interface: $\left(\dfrac{\partial T}{\partial n}\right)_{fluid} = \dfrac{k_s}{k}\left(\dfrac{\partial T_s}{\partial n}\right)_{solid}$

Where n is the non-dimensional distances either along x or y direction acting normal to the surface and k and k_s are the thermal conductivity of the fluid and the solid cylinder respectively.

The local Nusselt number at the heated surface of the cavity which is defined by Cengel (2007) is calculated by the following expression.

$Nu_l = h(y)L/k$

Such local values have been further averaged over the entire heated surface to obtain the surface averaged or overall mean Nusselt number

$$Nu = \frac{1}{L_s}\int_0^{l_s} Nu_l \, dy$$

where L_s and $h(y)$ are the length and the local convection heat transfer coefficient of the heated wall respectively. The average Nusselt number can be used in process engineering design calculations to estimate the rate transfer from the heated surface.

3.2.3 Dimensional Analysis

Non-dimensional variables are used for making the governing equations (3.1–3.5) into dimensionless form are stated as follows:

$$X = \frac{x}{L}, \; Y = \frac{y}{L}, \; U = \frac{u}{u_l}, \; V = \frac{v}{u_l}, \; P = \frac{p}{\rho \, u_l^2}, D = \frac{d}{L}, L_x = \frac{l_x}{L}, L_y = \frac{l_y}{L},$$

$$\theta = \frac{(T - T_l)}{(T_h - T_l)}, \; \theta_s = \frac{(T_s - T_l)}{(T_h - T_l)}$$

Where X and Y are the coordinates varying along horizontal and vertical directions, respectively, U and V are the velocity components in the X and Y directions, respectively, θ is the dimensionless temperature and P is the dimensionless pressure.

After substitution the dimensionless variables into the equations (3.1-3.5), we get the following dimensionless equations as

Continuity Equation

$$\frac{\partial U}{\partial X} + \frac{\partial V}{\partial Y} = 0 \tag{3.6}$$

Momentum Equations

$$U\frac{\partial U}{\partial X} + V\frac{\partial U}{\partial Y} = -\frac{\partial P}{\partial X} + \frac{1}{Re}\left(\frac{\partial^2 U}{\partial X^2} + \frac{\partial^2 U}{\partial Y^2}\right) \tag{3.7}$$

$$U\frac{\partial V}{\partial X} + V\frac{\partial V}{\partial Y} = -\frac{\partial P}{\partial Y} + \frac{1}{Re}\left(\frac{\partial^2 V}{\partial X^2} + \frac{\partial^2 V}{\partial Y^2}\right) + Ri\theta \tag{3.8}$$

Energy Equations

$$U\frac{\partial \theta}{\partial X} + V\frac{\partial \theta}{\partial Y} = \frac{1}{Re\,Pr}\left(\frac{\partial^2 \theta}{\partial X^2} + \frac{\partial^2 \theta}{\partial Y^2}\right) \tag{3.9}$$

For solid .

$$0 = \frac{K}{Re\,Pr}\left(\frac{\partial^2 \theta_s}{\partial X^2} + \frac{\partial^2 \theta_s}{\partial Y^2}\right) \tag{3.10}$$

The dimensionless parameters appearing in the equations (3.6) through (3.10) are the Reynolds number Re, Grashof number Gr, Prandtl number Pr, Richardson number Ri, and solid fluid thermal conductivity ratio K. They are respectively defined as follows:

$$Re = UL/\upsilon, \; Gr = g\,\beta\,\Delta T\,L^3/\upsilon^2, \; Pr = \upsilon/\alpha, \; Ri = Gr/Re^2 \; and \; K = k_s/k$$

where $\Delta T = T_h - T_i \; and \; \alpha = k/\rho C_p$ are the temperature difference and thermal diffusivity of the fluid respectively.

The dimensionless boundary conditions under consideration can be written as·

At the inlet: $U = 1$, $V = 0$, $\theta = 0$

At the outlet: convective boundary condition (CBC), $P = 0$

At all solid boundaries: $U = 0, V = 0,$

At the heated right vertical wall: $\theta = 1$

At the left, top and bottom walls: $\dfrac{\partial \theta}{\partial N} = 0$

At the fluid-solid interface: $\left(\dfrac{\partial \theta}{\partial N}\right)_{fluid} = K\left(\dfrac{\partial \theta_s}{\partial N}\right)_{solid}$

Where N is the non-dimensional distances either along X or Y direction acting normal to the surface and K (k_s/k) is the dimensionless ratio of the thermal conductivity. According to Singh and Sharif (2003), the average Nusselt number at the heated wall of the cavity based on the no-dimensional variables may be expressed as $Nu = -\int_0^{t_h/L} \dfrac{\partial \theta}{\partial X}\, dY$ and the bulk average temperature defined as $\theta_m = \int \theta\, d\overline{V}/\overline{V}$,

where $\overline{V}$ is the cavity volume.

3.3 Numerical Analysis

The governing equations along with the boundary conditions are solved numerically, employing Galerkin weighted residual finite element techniques discussed below.

3.3.1 Finite Element Formulation and Computational Procedure

To derive the finite element equations, the method of weighted residuals Zienkiewicz (1991) is applied to the equations (3.6) – (3.10) as

$$\int_A N_\alpha\left(\frac{\partial U}{\partial X} + \frac{\partial V}{\partial Y}\right) dA = 0 \tag{3.11}$$

$$\int_A N_\alpha\left(U\frac{\partial U}{\partial X} + V\frac{\partial U}{\partial Y}\right) dA = -\int_A H_\lambda\left(\frac{\partial P}{\partial X}\right) dA + \frac{1}{Re}\int_A N_\alpha\left(\frac{\partial^2 U}{\partial X^2} + \frac{\partial^2 U}{\partial Y^2}\right) dA \tag{3.12}$$

$$\int_A N_\alpha\left(U\frac{\partial V}{\partial X} + V\frac{\partial V}{\partial Y}\right) dA = -\int_A H_\lambda\left(\frac{\partial P}{\partial Y}\right) dA + \frac{1}{Re}\int_A N_\alpha\left(\frac{\partial^2 V}{\partial X^2} + \frac{\partial^2 V}{\partial Y^2}\right) dA \tag{3.13}$$
$$+ Ri\int_A N_\alpha T\, dA$$

$$\int_A N_\alpha \left(U \frac{\partial \theta}{\partial X} + V \frac{\partial \theta}{\partial Y} \right) dA = \frac{1}{Re\,Pr} \int_A N_\alpha \left(\frac{\partial^2 \theta}{\partial X^2} + \frac{\partial^2 \theta}{\partial Y^2} \right) dA \qquad (3.14)$$

$$0 = \frac{K}{Re.Pr} \int_A N_\alpha \left(\frac{\partial^2 \theta_s}{\partial X^2} + \frac{\partial^2 \theta_s}{\partial Y^2} \right) dA \qquad (3.15)$$

where A is the element area, N_α ($\alpha = 1, 2, \ldots \ldots, 6$) are the element interpolation functions for the velocity components and the temperature, and H_λ ($\lambda = 1, 2, 3$) are the element interpolation functions for the pressure.

Gauss's theorem is then applied to equations (3.12)-(3.15) to generate the boundary integral terms associated with the surface tractions and heat flux. Then equations (3.12)-(3.15) become,

$$\int_A N_\alpha \left(U \frac{\partial U}{\partial X} + V \frac{\partial U}{\partial Y} \right) dA + \int_A H_\lambda \left(\frac{\partial P}{\partial X} \right) dA$$
$$+ \frac{1}{Re} \int_A \left(\frac{\partial N_\alpha}{\partial X} \frac{\partial U}{\partial X} + \frac{\partial N_\alpha}{\partial Y} \frac{\partial U}{\partial Y} \right) dA = \int_{S_0} N_\alpha S_x dS_0 \qquad (3.16)$$

$$\int_A N_\alpha \left(U \frac{\partial V}{\partial X} + V \frac{\partial V}{\partial Y} \right) dA + \int_A H_\lambda \left(\frac{\partial P}{\partial Y} \right) dA$$
$$+ \frac{1}{Re} \int_A \left(\frac{\partial N_\alpha}{\partial X} \frac{\partial V}{\partial X} + \frac{\partial N_\alpha}{\partial Y} \frac{\partial V}{\partial Y} \right) dA - Ri \int_A N_\alpha \theta\, dA = \int_{S_0} N_\alpha S_y dS_0 \qquad (3.17)$$

$$\int_A N_\alpha \left(U \frac{\partial T}{\partial X} + V \frac{\partial T}{\partial Y} \right) dA + \frac{1}{Re.Pr} \int_A \left(\frac{\partial N_\alpha}{\partial X} \frac{\partial T}{\partial X} + \frac{\partial N_\alpha}{\partial Y} \frac{\partial T}{\partial Y} \right) dA = \int_{S_w} N_\alpha\, q_{1w}\, dS_w. \quad (3.18)$$

$$\frac{K}{Re.Pr} \int_A \left(\frac{\partial N_\alpha}{\partial X} \frac{\partial T}{\partial X} + \frac{\partial N_\alpha}{\partial Y} \frac{\partial T}{\partial Y} \right) dA = \int_{S_w} N_\alpha\, q_{2w}\, dS_w \qquad (3.19)$$

Here (3.16)-(3.17) specifying surface tractions (S_x, S_y) along outflow boundary S_0 and (3.18)-(3.19) specifying velocity components and fluid temperature or heat flux (q_w) that flows into or out from domain along wall boundary S_w.

The basic unknowns for the above differential equations are the velocity components U, V the temperature, θ and the pressure, P. The six node triangular element is used in this work for the development of the finite element equations. All six nodes are associated with velocities as well as temperature; only the corner nodes are

associated with pressure. This means that a lower order polynomial is chosen for pressure and which is satisfied through continuity equation. The velocity component and the temperature distributions and linear interpolation for the pressure distribution according to their highest derivative orders in the differential equations (3.6)-(3.10) as

$$U(X,Y) = N_\beta U_\beta \tag{3.20}$$

$$V(X,Y) = N_\beta V_\beta \tag{3.21}$$

$$T(X,Y) = N_\beta T_\beta \tag{3.22}$$

$$T_s(X,Y) = N_\beta T_{s\,\beta} \tag{3.23}$$

$$P(X,Y) = H_\lambda P_\lambda \tag{3.24}$$

where $\beta = 1, 2, \dots \dots, 6;\ \lambda = 1, 2, 3$.

Substituting the element velocity component distributions, the temperature distribution, and the pressure distribution from equations (3.20)-(3.24), the finite element equations can be written in the form,

$$K_{\alpha\beta^x} U_\beta + K_{\alpha\beta^y} V_\beta = 0 \tag{3.25}$$

$$K_{\alpha\beta\gamma^x} U_\beta U_\gamma + K_{\alpha\beta\gamma^y} V_\gamma U_\gamma + M_{\alpha\mu^x} P_\mu + \frac{1}{Re}\left(S_{\alpha\beta^{xx}} + S_{\alpha\beta^{yy}}\right) U_\beta = Q_{\alpha^u} \tag{3.26}$$

$$\begin{aligned} K_{\alpha\beta\gamma^x} U_\beta V_\gamma + K_{\alpha\beta\gamma^y} V_\gamma V_\gamma + M_{\alpha\mu^y} P_\mu + \\ \frac{1}{Re}\left(S_{\alpha\beta^{xx}} + S_{\alpha\beta^{yy}}\right) V_\beta - Ri\, K_{\alpha\beta}\theta_\beta = Q_{\alpha^v} \end{aligned} \tag{3.27}$$

$$K_{\alpha\beta\gamma^x} U_\beta\theta_\gamma + K_{\alpha\beta\gamma^y} V_\beta\theta_\gamma + \frac{1}{Re.Pr}\left(S_{\alpha\beta^{xx}} + S_{\alpha\beta^{yy}}\right)\theta_\beta = Q_{\alpha^\theta} \tag{3.28}$$

$$\frac{K}{Re.Pr}\left(S_{\alpha\beta^{xx}} + S_{\alpha\beta^{yy}}\right)\theta_\beta = Q_{\alpha^{\theta_s}} \tag{3.29}$$

where the coefficients in element matrices are in the form of the integrals over the element area and along the element edges S_θ and S_w as

$$K_{\alpha\beta^x} = \int_A N_\alpha N_{\beta,x}\, dA \tag{3.30a}$$

35

$$K_{\alpha\beta^y} = \int_A N_\alpha N_{\beta,y} dA \tag{3 30b}$$

$$K_{\alpha\beta^x} = \int_A N_\alpha N_\beta N_{\gamma,\tau} dA \tag{3 30c}$$

$$K_{\alpha\beta\gamma^y} = \int_A N_\alpha N_\beta N_{\gamma,y} dA \tag{3.30d}$$

$$K_{\alpha\beta} = \int_A N_\alpha N_\beta dA \tag{3.30e}$$

$$S_{\alpha\beta^{xx}} = \int_A N_{\alpha,x} N_{\beta,\tau} dA \tag{3.30f}$$

$$S_{\alpha\beta^{yy}} = \int_A N_{\alpha,y} N_{\beta,y} dA \tag{3.30g}$$

$$M_{\alpha\mu^x} = \int_A H_\alpha H_{\mu,\tau} dA \tag{3.30h}$$

$$M_{\alpha\mu^y} = \int_A H_\alpha H_{\mu,y} dA \tag{3.30i}$$

$$Q_{\alpha^u} = \int_{S_0} N_\alpha S_x dS_0 \tag{3.30j}$$

$$Q_{\alpha^v} = \int_{S_0} N_\alpha S_y dS_0 \tag{3.30k}$$

$$Q_{\alpha\theta} = \int_{S_w} N_\alpha q_{1w} dS_w \tag{3.30l}$$

$$Q_{\alpha\theta s} = \int_{S_w} N_\alpha q_{2w} dS_w \tag{3.30m}$$

These element matrices are evaluated in closed form ready for numerical simulation. Details of the derivation for these element matrices are omitted herein.

The derived finite element equations (3.25)-(3.29) are nonlinear. These nonlinear algebraic equations are solved by applying the Newton-Raphson iteration technique by first writing the unbalanced values from the set of the finite element equations (3.25)-(3.29) as,

$$F_{\alpha^p} = K_{\alpha\beta^x} U_\beta + K_{\alpha\beta^y} V_\beta \tag{3.31a}$$

$$F_{\alpha^u} = K_{\alpha\beta\gamma^x} U_\beta U_\gamma + K_{\alpha\beta\gamma^y} V_\gamma U_\gamma + M_{\alpha\mu^x} P_\mu$$
$$+ \frac{1}{Re}(S_{\alpha\beta^{xx}} + S_{\alpha\beta^{yy}}) U_\beta - Q_{\alpha^u} \tag{3.31b}$$

$$F_{\alpha}{}^{v} = K_{\alpha\beta\gamma}{}^{x}U_{\beta}V_{\gamma} + K_{\alpha\beta\gamma}{}^{y}V_{\gamma}V_{\gamma} + M_{\alpha\mu}{}^{y}P_{\mu} +$$
$$\frac{1}{Re}(S_{\alpha\beta}{}^{xx} + S_{\alpha\beta}{}^{yy})V_{\beta} - Ri\,K_{\alpha\beta}\theta_{\beta} - Q_{\alpha}{}^{v} \tag{3.31c}$$

$$F_{\alpha}{}^{\theta} = K_{\alpha\beta\gamma}{}^{x}U_{\beta}\theta_{\gamma} + K_{\alpha\beta\gamma}{}^{y}V_{\beta}\theta_{\gamma} + \frac{1}{Re.Pr}\left(S_{\alpha\beta}{}^{xx} + S_{\alpha\beta}{}^{yy}\right)\theta_{\beta} - Q_{\alpha}{}^{\theta} \tag{3.31d}$$

$$F_{\alpha}{}^{\theta_s} = \frac{K}{Re.Pr}\left(S_{\alpha\beta}{}^{xx} + S_{\alpha\beta}{}^{yy}\right)\theta_{s\beta} - Q_{\alpha}{}^{\theta_s} \tag{3.31e}$$

This leads to a set of algebraic equations with the incremental unknowns of the element nodal velocity components, temperatures, and pressures in the form,

$$
\begin{bmatrix}
K_{pu} & K_{pv} & 0 & 0 & 0 \\
K_{uu} & K_{uv} & 0 & K_{up} & 0 \\
K_{\theta u} & K_{\theta v} & K_{\theta\theta} & 0 & 0 \\
K_{vu} & K_{vv} & K_{v\theta} & K_{vp} & 0 \\
0 & 0 & 0 & 0 & K_{\theta_s\theta_s}
\end{bmatrix}
\begin{Bmatrix}
\Delta p \\
\Delta u \\
\Delta \theta \\
\Delta v \\
\Delta \theta_s
\end{Bmatrix}
= -
\begin{Bmatrix}
F_{\alpha}{}^{p} \\
F_{\alpha}{}^{u} \\
F_{\alpha}{}^{\theta} \\
F_{\alpha}{}^{v} \\
F_{\alpha}{}^{\theta_s}
\end{Bmatrix}
\tag{3.32}
$$

where $K_{uu} = K_{\alpha\beta\gamma}{}^{x}U_{\beta} + K_{\alpha\gamma\beta}{}^{x}U_{\gamma} + K_{\alpha\beta\gamma}{}^{y}V_{\beta} + \frac{1}{Re}\left(S_{\alpha\beta}{}^{xx} + S_{\alpha\beta}{}^{yy}\right)$

$K_{uv} = K_{\alpha\beta\gamma}{}^{y}U_{\gamma}$

$K_{u\theta} = K_{u\theta_s} = 0$, $K_{up} = M_{\alpha\mu}{}^{x}$

$K_{vu} = K_{\alpha\beta\gamma}{}^{x}V_{\gamma}$

$K_{vv} = K_{\alpha\beta\gamma}{}^{x}U_{\beta} + K_{\alpha\gamma\beta}{}^{y}V_{\gamma} + K_{\alpha\beta\gamma}{}^{y}V_{\gamma} + \frac{1}{Re}\left(S_{\alpha\beta}{}^{xx} + S_{\alpha\beta}{}^{yy}\right)$

$K_{v\theta} = -Ri\,K_{\alpha\beta}$, $K_{vp} = M_{\alpha\mu}{}^{v}$

$K_{v\theta_s} = 0$, $K_{\theta u} = K_{\alpha\beta\gamma}{}^{x}\theta_{\gamma}$, $K_{\theta v} = K_{\alpha\beta\gamma}{}^{y}\theta_{\gamma}$

$K_{\theta\theta} = K_{\alpha\beta\gamma}{}^{x}U_{\beta} + K_{\alpha\beta\gamma}{}^{y}V_{\beta} + \frac{1}{Re.Pr}(S_{\alpha\beta}{}^{xx} + S_{\alpha\beta}{}^{yy})$

$K_{\theta p} = K_{\theta\theta_s} = 0$, $K_{\theta_s u} = K_{\theta_s v} = K_{\theta_s\theta} = K_{\theta_s p} = 0$

37

$$K_{\theta_s \theta_s} = \frac{K}{Re.Pr}(S_{\alpha\beta^{xx}} + S_{\alpha\beta^{yy}})$$

$$K_{pu} = K_{\alpha\beta^x}, \; K_{pv} = K_{\alpha\beta^y} \; \text{and} \; K_{p\theta} = 0 = K_{pp} = K_{p\theta_s}$$

The iteration process is terminated if the percentage of the overall change compared to the previous iteration is less than the specified value.

To solve the sets of the global nonlinear algebraic equations in the form of matrix, the Newton-Raphson iteration technique has been adapted through PDE solver with MATLAB interface. The convergence of solutions is assumed when the relative error for each variable between consecutive iterations is recorded below the convergence criterion ε such that $\left|\Psi^{n+1} - \Psi^n\right| < \varepsilon$, where n is number of iteration and $\Psi = U, V, \theta$. The convergence criterion was set to $\varepsilon = 10^{-4}$.

3.3.2 Grid Size Sensitivity Test

Geometry studied in this chapter is an obstructed vented cavity; therefore several grid size sensitivity tests are conducted in this geometry to determine the sufficiency of the mesh scheme and to ensure that the solutions are grid independent. This is obtained when numerical results of the average Nusselt number Nu, average temperature θ_{av} of the fluid and solution time become grid size independent, although we continue the refinement of the mesh grid. Five different non-uniform grids with the following number of nodes and elements were considered for the grid refinement tests: 24545 nodes, 3788 elements; 29321 nodes, 4556 elements, 37787 nodes, 5900 elements; 38163 nodes, 5962 elements and 48030 nodes, 7516 elements as shown in Table 3 1. Considering both the accuracy and the computational time, the values, 38163 nodes and 5962 elements can be chosen throughout the simulation to optimize the relation between the accuracy required and the computing time

The numerical grid defines the discrete locations, at which the variables are to be calculated, which is essentially a discrete representation of the geometry domain on which the problem is to be solved. It divides the solution domain into a finite number of sub domains are called elements. Unstructured triangular grids are used in the present finite element simulation. The mesh mode for the obstructed vented cavity

problem generated by Delaunay Triangular method. The Delaunay triangulation is a geometric structure that has enjoyed great popularity in mesh generation since the mesh generation was in its infancy. The mesh mode for the present numerical computation is shown in figure 3.3.

Table 3.1: Grid Sensitivity Check at $Re = 100$, $Ri = 1.0$, $K = 5.0$, $D = 0.2$, $L_x = L_y = 0.5$ and $Pr = 0.71$ for the case 1

Nodes (elements)	24545 (3788)	29321 (4556)	37787 (5900)	38163 (5962)	48030 (7516)
Nu	4.167817	4.168185	4.168376	4.168394	4.168461
θ_{av}	0.197191	0.197204	0.197233	0.197224	0.197227
Time (s)	323.610	408.859	563.203	588.390	793.125
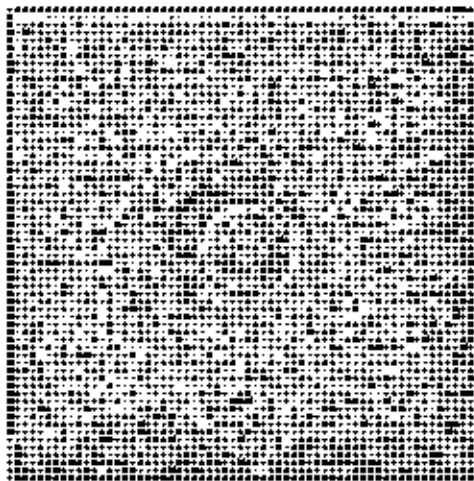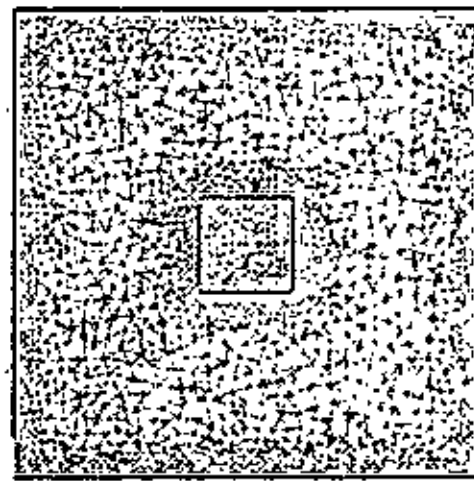
Case 1   Case 2

Figure 3.3: Grid used for numerical simulations at the case 1 and case 2.

3.3.3 Validation of the Numerical Scheme

In order to verify the accuracy of the numerical results and the validity of the numerical scheme obtained throughout the present study, comparisons with the previously published results are necessary. But due to the lack of availability of experimental data on the particular problems along with its associated boundary conditions investigated in this study, validation of the predictions could not be done against experiment. The present numerical scheme is validated for natural convection heat transfer in a square cavity with differentially heated sidewalls reported by House et al. (1990), which is based on finite volume scheme. However, we recall here some results obtained by our scheme in comparison with those reported in House et al. (1990) for $Ra = 0.0$, 10^5 and three values of $K = 0.2$, 1.0 and 5.0. The physical problem studied by House et al. (1990) was a vertical square enclosure with sides of length L. The vertical walls were isothermal and differentially heated, where as the bottom and top walls were adiabatic. A square heat conducting body with sides of length equal to $L/2$ was placed at the center of the enclosure. We have compared results for the average Nusselt number (at the hot wall) as shown in Table 3.2. The present results have an excellent agreement with the results obtained by House et al. (1990). Based on the above study, it was concluded the numerical scheme could be reliably applied to the considered problem.

Table 3.2: Comparison of Nusselt Number values with numerical data for Pr = 0.71

Ra	K	Nu		Error (%)
		Present work	House et al. (1990)	
0	0.2	0.7071	0.7063	0.11
0	1.0	1.0000	1.0000	0.00
0	5.0	1.4142	1.4125	0.12
10^5	0.2	4.6237	4.6239	0.00
10^5	1.0	4.5037	4.5061	0.05
10^5	5.0	4.3190	4.3249	0.14

3.4 Results and Discussion

Numerical results are presented in order to determine the effects of the presence of dimensionless parameters in rectangular vented cavities with a heat conducting horizontal cylinder (circular/square). The dimensionless parameters that must be specified for the system are Reynolds number Re, Richardson number Ri, Prandtl number Pr, ratio of the cylinder diameter and cavity length D, ratio of the solid and fluid thermal conductivity K, cavity aspect ratio AR, and physical parameters for the system are the location of the inlet and the out positions of the cavity and the location of the cylinder in the cavity. Since so many basic dimensionless parameters are required to characterize a system, an analysis of all combinations of these parameters is not practical. The numerical results will be aimed to explain the effect of several parameters at a small fraction of the possible situations by simplifying the configuration. The presentation of the results will begin with the streamline and isotherm patterns in the cavity. Representative distributions of average Nusselt number at the heated surface, average temperature of the fluid in the cavity and temperature at the cylinder center will then be presented. Finally, the effect of cylinder shape on fluid flow and heat transfer are compared in tabular form.

3.4.1 Effects of Inlet and Outlet Locations

The location of the inflow and outflow opening is one of the major parameters affecting the fluid flow and heat transfer in a vented cavity. Keeping the position of the centered cylinder unchanged results are obtained for various locations of the inflow and outflow opening at $AR = 1.0$, $Re = 100$, $D = 0.2$, $Pr = 0.71$, $K = 5.0$ and various values of Ri in terms of streamlines, isotherms, average Nusselt number at the heated wall, average temperature of the fluid in the cavity and dimensionless temperature at the cylinder center. Here four different cavity configurations namely BB, BT, TB and TT and three values of Ri i.e. $Ri = 0.0$ for pure forced convection, $Ri = 1.0$ for pure mixed convection and $Ri = 5.0$ for free convection dominated region are investigated in order to compare the fluid flow and heat transfer for different relative inlet and outlet locations at the three convective regimes.

41
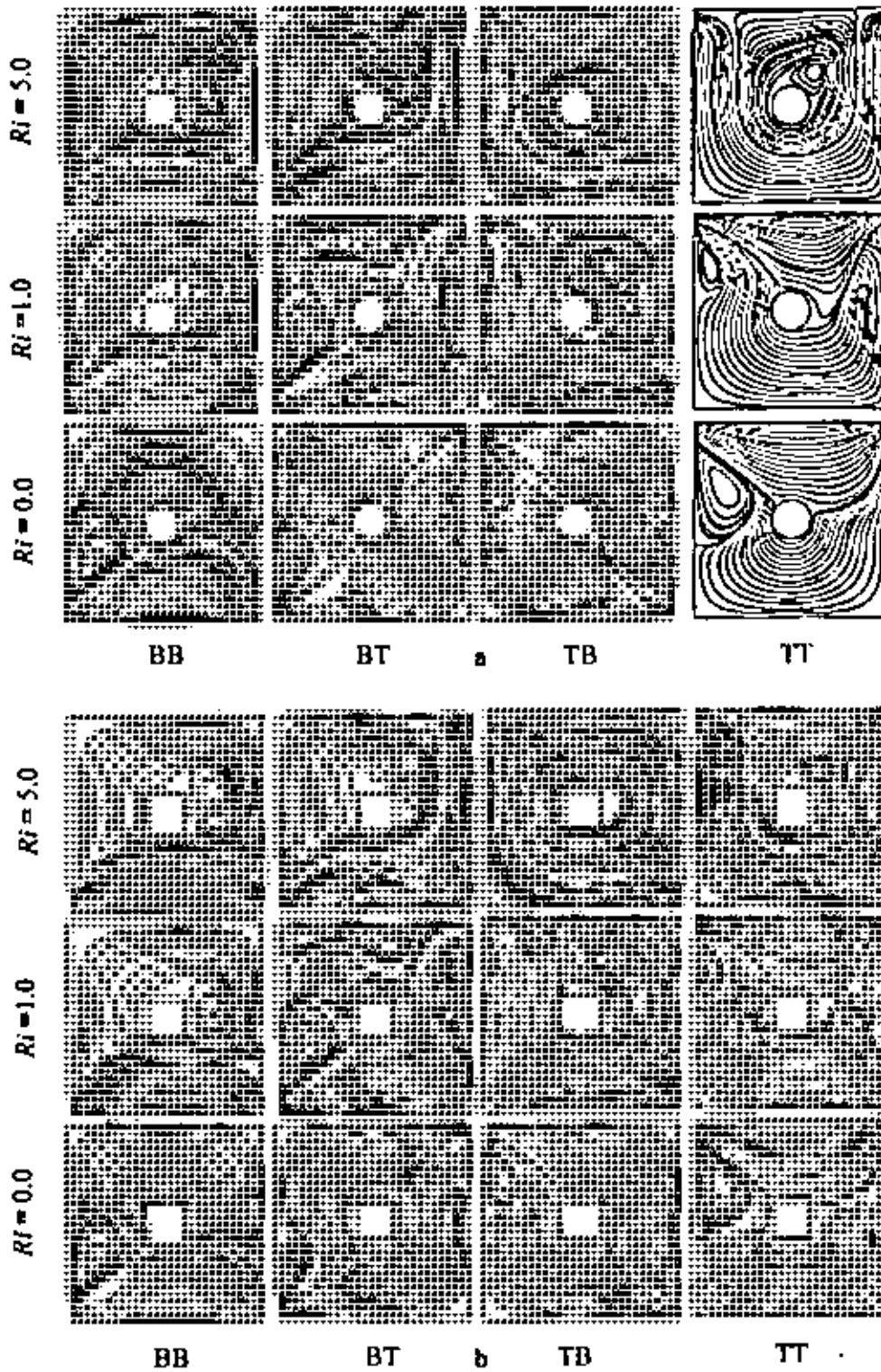
Figure 3.4: Streamlines for the (a) case 1 and (b) case 2 at different inlet and outlet locations and various values of Richardson number Ri, while $AR = 1.0$, $Re = 100$, $K = 5.0$, $Pr = 0.71$, $L_x = L_y = 0.5$ and $D = 0.2$.

42

The effect of inlet and outlet positions on streamlines for the case of circular cylinder (case 1) and the case of square cylinder (case 2) is shown in figure 3 4. The flow structure for the BB configuration at the three-convection regime is presented in the left column of the figure 3.4 in both of the cases. Now for the BB configuration and at $Ri = 0.0$, the induced flow enters into cavity through small inlet area and sudden expansion of the bulk fluid in the cavity is occurred due to pressure rise into the cavity. Thus the bulk fluid occupies most part of the cavity and a small recirculation cell appears just at the top of the inlet port near the left wall. Next for $Ri = 1.0$, it is seen that recirculation cell spreads significantly and thereby squeezes the induced flow path, which is due to the presence of natural convection effect in the cavity. As Ri increase further to 5.0, the recirculating cell further increases in size and leads to a large change in the streamlines structure, indicating a sign of supremacy of natural convection in the upper part of the cavity. As the outlet port is moved along the heated wall at the top corner and keeping every thing else fixed, (i.e. for BT configuration) the recirculation cell become shrinking in size and occupies the space just at the top of the inlet port adjacent to the left wall at $Ri = 0.0$. In this folder, as Ri increases to 1.0, the recirculation cell becomes large and two cellular. Further as Ri increases to 5.0, the two cellular cell merge into a large uni-cellular, due to the supremacy of the convective current in the cavity Next for TB configuration, the bulk induced fluid flows throughout the cavity and a small rotating cell is developed just at the below of the inlet port at low Ri. Further at $Ri = 1.0$, the existence of two cells indicates that natural convection effect is comparable with forced convection effect. Finally at $Ri = 5.0$, the two cells merge into a large one, this scenario indicates that the forced convection is overwhelmed by the natural convective current. Lastly for TT configuration the induced flow enters into cavity through small inlet area and sudden expansion of the bulk fluid in the cavity is occurred due to pressure rise into the cavity. Thus the bulk fluid occupies most part of the cavity and a small recirculation cell appears just at the below of the inlet port near the left wall at $Ri = 0.0$. Next at $Ri = 1.0$, it is seen that recirculation cell becomes small in size. As Ri increase further to 5.0, the recirculating cell becomes large and shifted at the upper mid section in the cavity. Thereby it squeezes the entrance stream to flow in it, indicating the dominant natural convection contribution in the mixed convection.
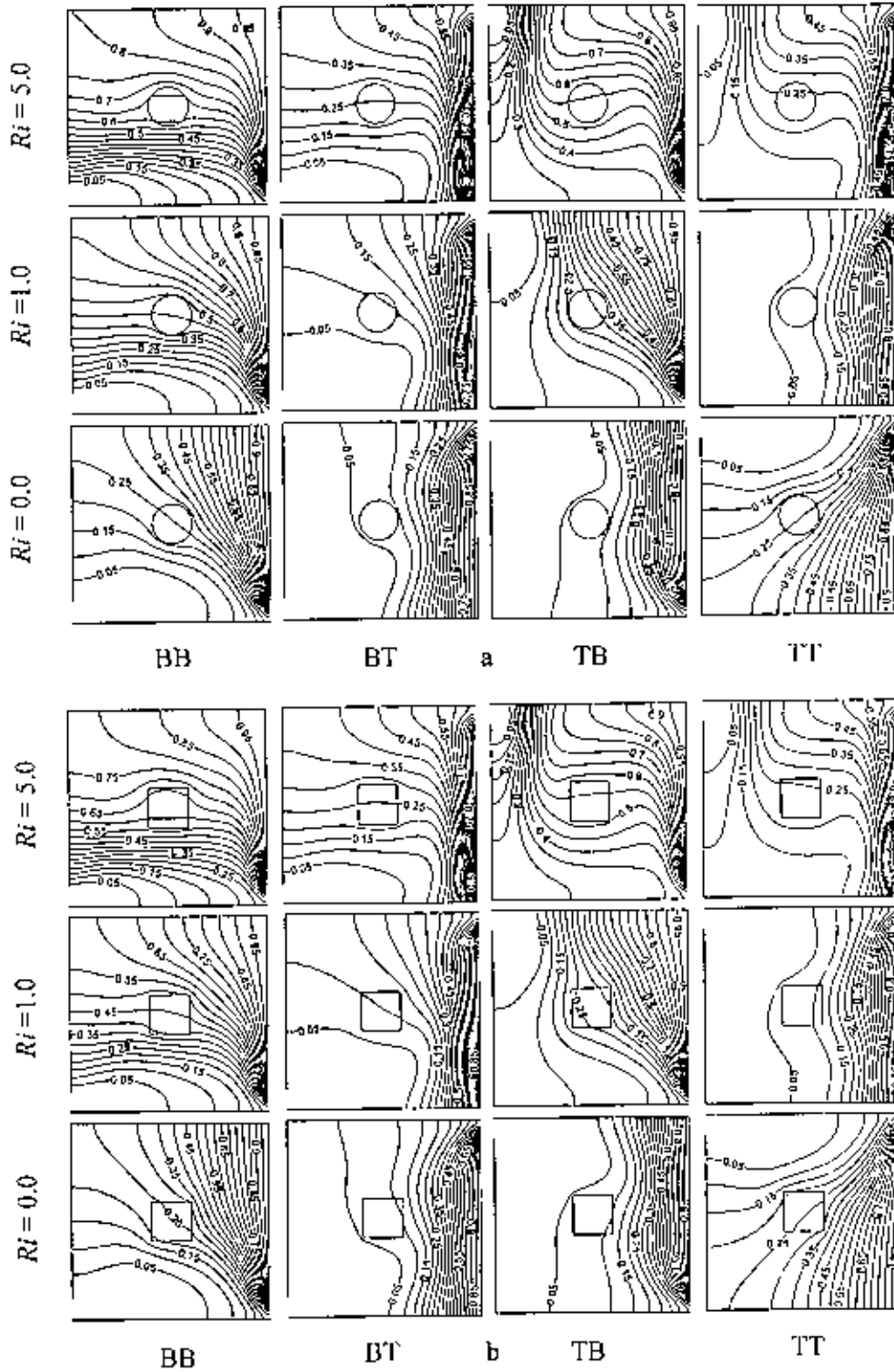
Figure 3.5: Isotherms for the (a) case 1 and (b) case 2 at different inlet and outlet locations and various values of Richardson number Ri, while $AR = 1.0$, $Re = 100$, $K = 5.0$, $Pr = 0.71$, $D = 0.2$ and $L_x = L_y = 0.5$.

44

The effect of inlet and outlet locations on isotherms for the aforementioned two cases is shown in figure 3.5. For BB configuration, it is seen that the thermally influenced region is bulky in the upper part of the cavity for all values of Ri. This is because, the fresh fluid entering at the lower part of the cavity and travels the shortest distance possible leaving at the lower part in the cavity, as a result the cold fluid cannot close with the hotter fluid. On the other hand, the inverse isotherm patterns are found for TT configuration at low Ri, which is due to, the entering fresh fluids travels the shortest distance possible leaving, but it come into intimate mixing with the hotter fluids before leaving the cavity. Next at $Ri = 1.0$ the isotherms become clustered near the heat source, indicating mixed convection dominated heat transfer in the cavity. Further as Ri increases to 5.0, the concentrated thin thermal layer is seen near the heated wall and nonlinearity of the isotherms is found. Moreover, the isotherms are clustered near the heat source for the BT and TB configurations at $Ri = 0.0$, which points to the forced convection and conduction-like heat transfer at the vicinity of the heat source. This is because, the fresh fluid entering the cavity travels the long possible distance before leaving the cavity and come into intimate mixing with the hotter fluids. As Ri increases to 1.0, nonlinearity in the isotherms are found for these cases. Further as Ri increases to 5.0, nonlinearity of the isotherms becomes higher and plume formation is philosophical for these cases, indicating well established natural convection heat transfer in the cavity.

If we compare the results of the distribution of streamlines and isotherms for the case 2 with those for case 1, the distribution of streamlines and isotherms for the case 2 (square cylinder) is generally similar to that for case 1 (circular cylinder) at each values of Richardson numbers considered, except some slight differences due to the variation in the cylinder shape.

The effect of inlet and outlet port locations on average Nusselt number (Nu) at the hot wall, average temperature (θ_{av}) of the fluid in the cavity and temperature at the cylinder center (θ_c) for both of the above cases is shown in figure 3.6. In both of the cases, as Ri increases average Nusselt number increases sharply for the BT and TT configurations. On the other hand, the values of Nu decreases sharply in the forced convection dominated region and increases mildly in the free convection dominated region with increasing Ri for TB configuration, while the values of Nu is independent
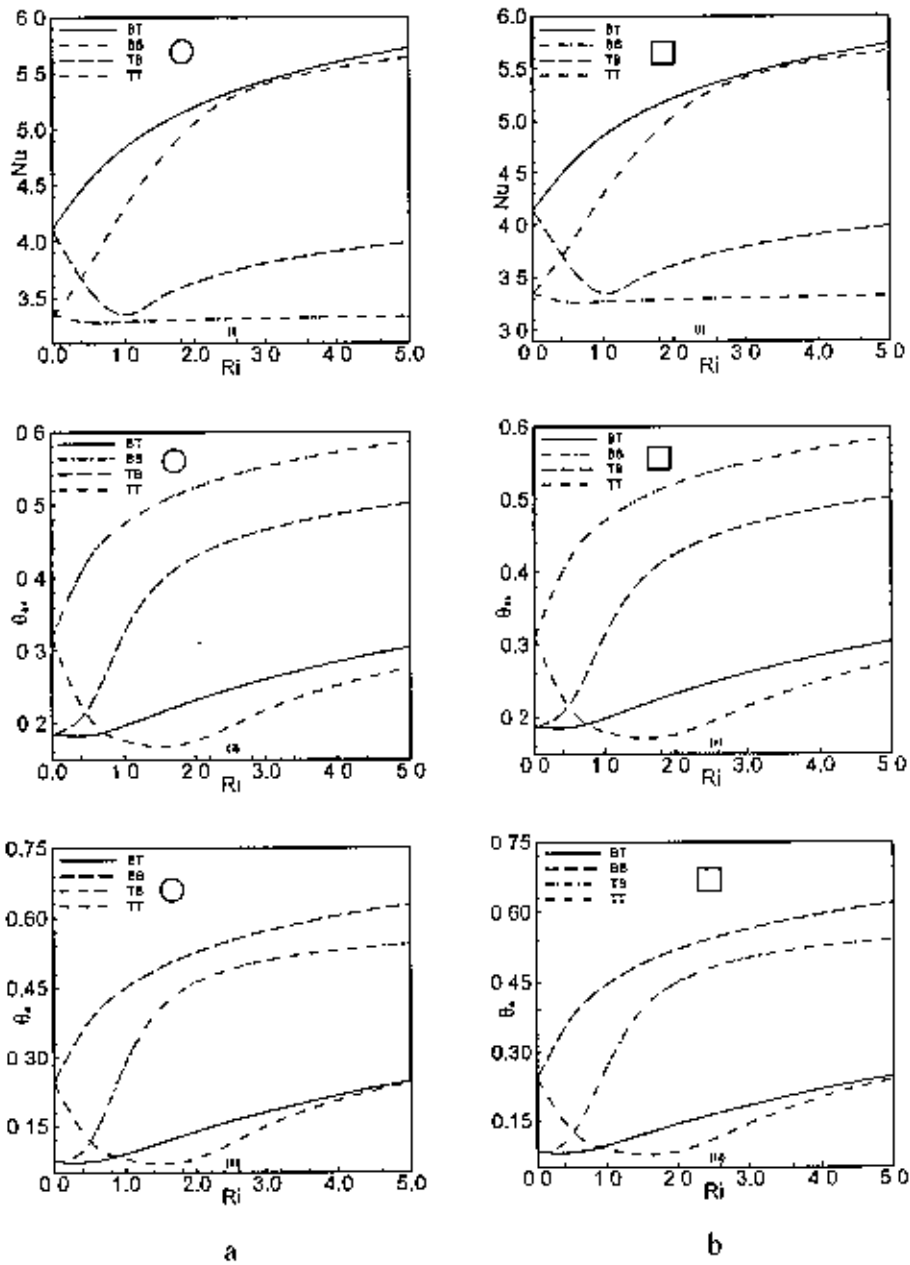
Figure 3.6: Effect of inlet and outlet locations on (i) average Nusselt number, (ii) average fluid temperature and (iii) temperature at the cylinder center in the cavity for (a) case 1 and (b) case 2, while $AR = 1.0$, $L_x = L_y = 0.5$, $Re = 100$, $Pr = 0.71$, $D = 0.2$ and $K = 5.0$.

Table 3.3 (a): Variation of average Nusselt number with inlet and outlet locations for the case 1

Ri	Nu			
	BB	BT	TB	TT
0.0	3.359446	4.112987	4.107176	3.326240
0.5	3.284949	4.532336	3.584707	3.774529
1.0	3.289600	4.832878	3.351737	4.293870
1.5	3.298392	5.044868	3.504415	4.726882
2.0	3.305957	5.203415	3.637501	5.060425
2.5	3.312125	5.329231	3.734022	5.277601
3.0	3.317211	5.433276	3.807227	5.404791
3.5	3.321498	5.521770	3.865441	5.487388
4.0	3.325194	5.598567	3.913473	5.548996
4.5	3.328443	5.666231	3.954230	5.599212
5.0	3.331350	5.726561	3.989574	5.642250

Table 3.3 (b): Variation of average Nusselt number with inlet and outlet locations for the case 2

Ri	Nu			
	BB	BT	TB	TT
0.0	3.354834	4.140904	4.149896	3.349152
0.5	3.268273	4.553558	3.638081	3.785130
1.0	3.274215	4.852818	3.353925	4.285956
1.5	3.285747	5.063939	3.483720	4.710881
2.0	3.295706	5.220678	3.619473	5.046088
2.5	3.303773	5.344344	3.721080	5.276631
3.0	3.310331	5.446298	3.798898	5.417247
3.5	3.315753	5.532912	3.860969	5.507134
4.0	3.320323	5.608074	3.912183	5.571996
4.5	3.324248	5.674337	3.955573	5.623495
5.0	3.327677	5.733475	3.993104	5.666875

of Ri for BB configuration. However, for particular values of Ri maximum average Nusselt number is found for BT configuration. The average temperature of the fluid in the cavity and temperature at the cylinder center are the lowest for the BT configuration in the forced convection dominated region and for the TT configuration in the free convection dominated region. Even though the overall trends of the plots of the average Nusselt number (Nu), average fluid temperature (θ_{av}) and temperature at the cylinder center (θ_c) are similar for both of the aforementioned cases, a slight difference can be noticed at the numerical values of these items. Finally, the numerical values of the average Nusselt number (Nu) for both of the cases are listed in Tables 3.3 (a) and 3.3 (b). It is observed from these tables that the values of Nu for the case 2 are slightly higher than those obtained for case 1 only for BT configuration.

Due to the better performance of the BT configuration in heat transfer, the computations will be done for the BT configuration in the following subsections.

3.4.2 Effects of Cylinder Diameter

The effect of cylinder diameter on the flow field at $AR = 1.0$, $Re = 100$, $Pr = 0.71$, $K = 5.0$ and $L_x = L_y = 0.5$ are displayed in figure 3.7 for the case 1 and case 2. In both of the cases, the flow structure in the absence of free convection effect ($Ri = 0.0$) and for the four different values of D is shown in the bottom row of the figure 3.7. Now at $Ri = 0.0$ and $D = 0.0$, it is seen that a comparatively large uni-cellular vortex appears at the left top corner of the cavity, due to the effect of buoyancy driven flow and a very small vortex of very low intensity appears at the right bottom corner of the cavity, which is owing to shear driven effect of the incoming fluid. Further with the increase of D at fixed Ri ($Ri = 0.0$) the size of the large vortex sharply decreases and the small vortex disappear. This is due to increasing the size of the cylinder which gives rise to a decrease in the space available for the flow induced by the heat source and shear force. Next for $Ri = 1.0$ and the different values of D ($D = 0.0$, 0.2, 0.4 and 0.6), it is clearly seen from the figure that the natural convection effect is present, but remains relatively weak at the higher values of D, since the open lines characterizing the imposed flow are still dominant.
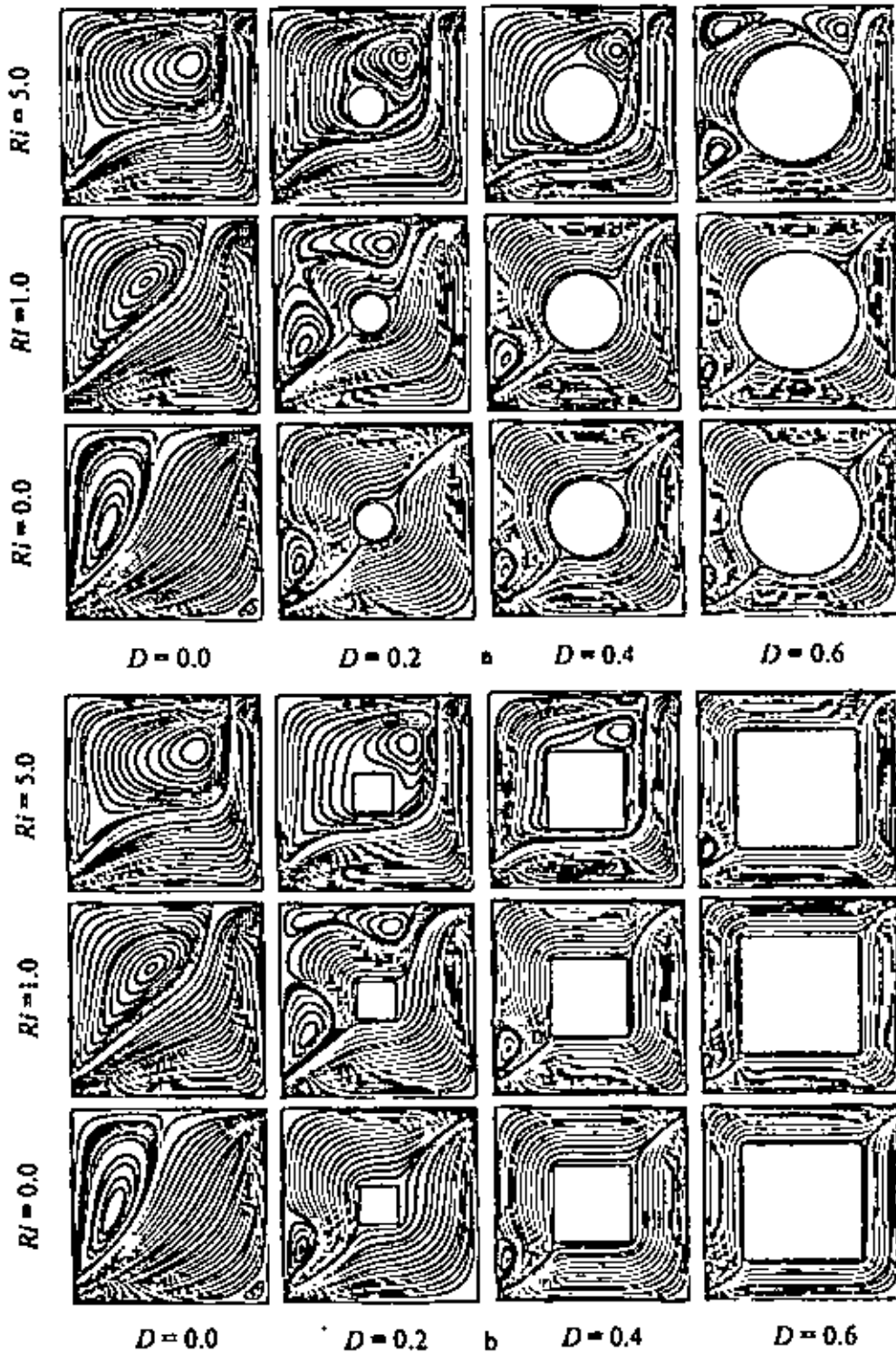
Figure 3.7: Streamlines for the (a) case 1 and (b) case 2 at different values of diameter D of the cylinder and Richardson number Ri, while $AR = 1.0$, $Re = 100$, $K = 5.0$, $Pr = 0.71$ and $L_x = L_y = 0.5$.

As Ri increase from 1.0 to 5.0, the size of the vortex increases sharply for the lower values of D (D = 0.0, 0.2 and 0.4) and divided into three small vortices at the highest value of D = 0.6. This expansion of the size of the vortex squeezes the induced forced flow path resulting almost same kinetic energy in the bulk-induced flow as that of the inlet port.

The effect of cylinder diameter on the thermal field at AR = 1.0, Re = 100, Pr = 0.71, K = 5.0 and $L_x = L_y$ = 0.5 are displayed in figure 3.8 for the case 1 and case 2. The isotherms in the absence of cylinder (D = 0.0) and for the three values of Ri are shown in the left column of figure 3.8. At Ri = 0.0 and D = 0.0, the high temperature region is concentrated near the hot wall and the isothermal lines are linear and parallel to the vertical walls in the cavity, indicating conduction and forced convection dominated heat transfer in the cavity. It is also seen that the thermally influenced region increases and the lower values isothermal lines become bend in the cavity with increasing values of D. As Ri increases to 1 0, the concentrated temperature region near the hot wall become thin for all values of D and the lower values isothermal lines become almost similar with increasing values of D when compared to that for the corresponding values of D at Ri = 0.0. As Ri increases further to 5.0, the nonlinearity in the isotherms become higher and plume formation is deep, it can also be seen that the thermal boundary layer near the hot wall become more concentrated than that of for the previous cases, indicating the well established conduction heat transfer at the vicinity of the hot wall and natural convection heat transfer in the remaining part of the cavity.

As compared the streamline and isotherm plots that are for both circular and square shape cylinders, a noteworthy difference is found in the streamline plots for the highest values of D at all values of Ri, but the isothermal lines are almost identical for both of the cases at all values of D and Ri considered.

The effects of cylinder diameters on average Nusselt number (Nu) at the heated wall, average temperature (θ_{av}) of the fluid in the cavity and the dimensionless temperature (θ_c) at the cylinder center as a function of Ri are shown in figures 3 9 for the aforementioned two cases. From these figures it is seen that as Ri increases, the values of average Nusselt number (Nu) increases monotonically for all values of D, which is due to increasing Ri enhances convective heat transfer.
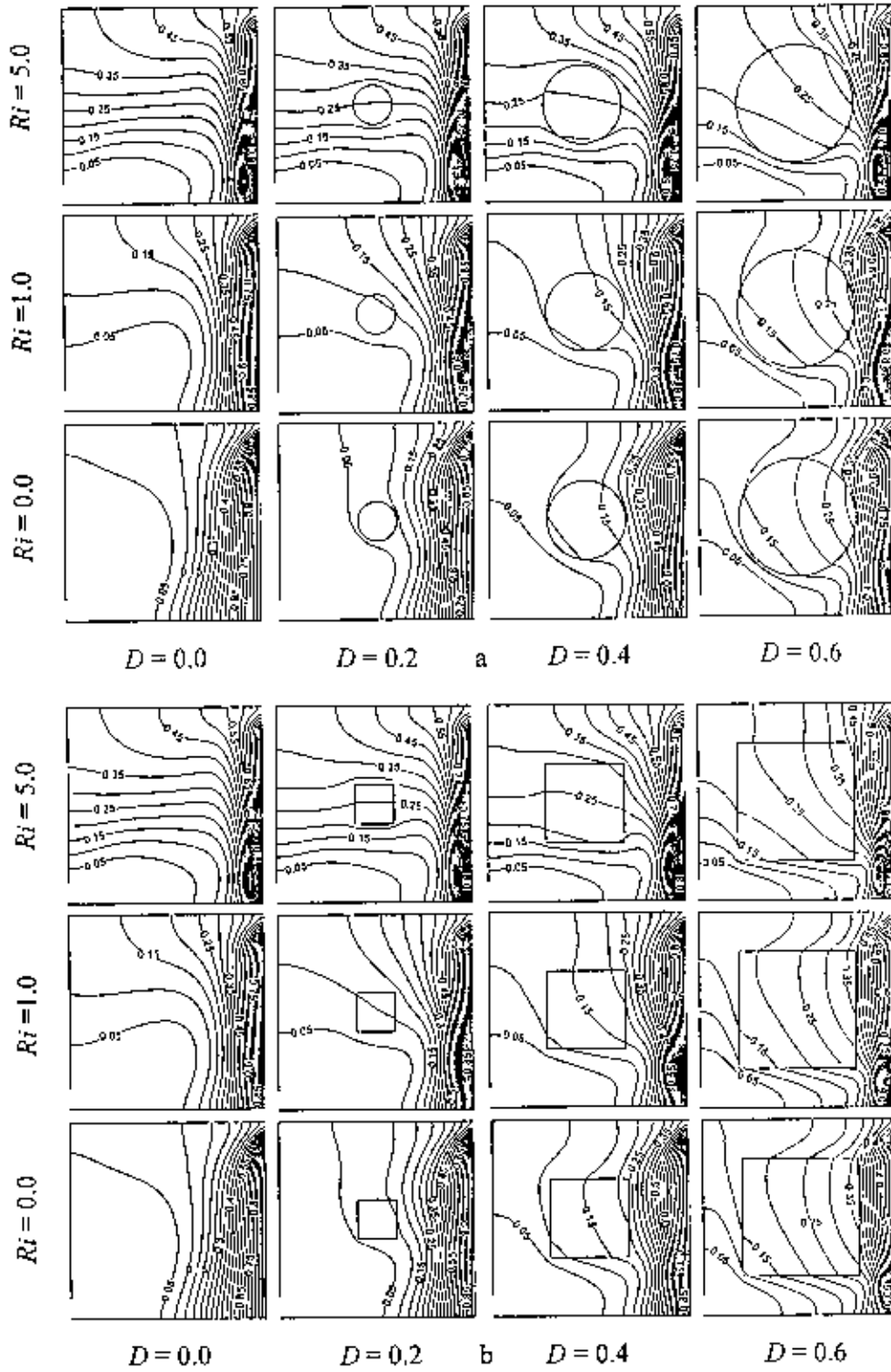
Figure 3.8: Isotherms for the (a) case 1 and (b) case 2 at different values of diameter D of the cylinder and Richardson number Ri, while $AR = 1.0$, $Re = 100$, $K = 5.0$, $Pr = 0.71$ and $L_x = L_y = 0.5$.
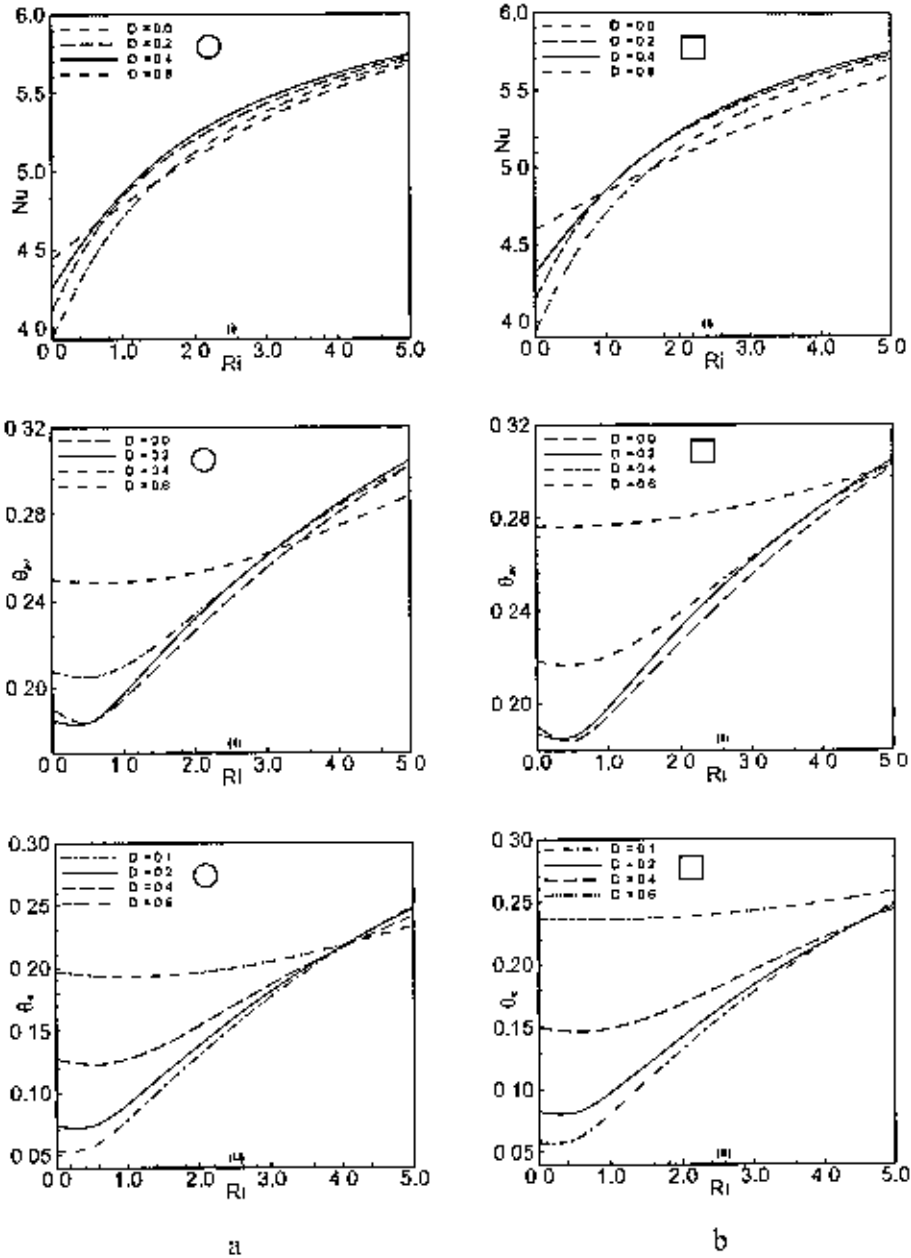
Figure 3.9: Effect of cylinder diameter D on (i) average Nusselt number, (ii) average fluid temperature and (iii) temperature at the cylinder center in the cavity for (a) case 1 and (b) case 2, while $AR = 1.0$, $Re = 100$, $Pr = 0.71$, $K = 5.0$ and $L_x = L_y = 0.5$.

Table 3.4 (a): Variation of average Nusselt number with cylinder diameter for the case 1

Ri	Nu			
	$D = 0.0$	$D = 0.2$	$D = 0.4$	$D = 0.6$
0.0	3.929590	4.112987	4.254335	4.438162
0.5	4.379906	4.532336	4.584969	4.617115
1.0	4.704789	4 832878	4.858178	4.786173
1.5	4.941247	5.044868	5.073061	4.943543
2.0	5.121619	5.203415	5.237451	5.088078
2.5	5.265161	5.329231	5 364877	5.219117
3.0	5.383142	5.433276	5 467139	5.336458
3.5	5.482503	5.521770	5 552104	5.440404
4.0	5.567771	5.598567	5.624698	5.531758
4.5	5.642055	5.666231	5.688059	5.611729
5.0	5.707576	5.726561	5.744269	5 681745

Table 3.4 (b): Variation of average Nusselt number with cylinder diameter for the case 2

Ri	Nu			
	$D = 0.0$	$D = 0.2$	$D = 0.4$	$D = 0.6$
0.0	3.929590	4.140904	4.310178	4.596143
0.5	4.379906	4.553558	4.603554	4 723150
1.0	4.704789	4.852818	4.855125	4.845404
1.5	4.941247	5.063939	5.062938	4.962107
2.0	5.121619	5.220678	5.229566	5.072681
2.5	5.265161	5.344344	5.362034	5.176729
3.0	5.383142	5.446298	5.468814	5.274025
3.5	5.482503	5.532912	5.557016	5.364493
4.0	5.567771	5 608074	5.631717	5.448196
4.5	5.642055	5.674337	5.696357	5.525318
5.0	5.707576	5.733475	5.753277	5.596145

On the other hand, average Nusselt number (Nu) is the highest for $D = 0.6$ in the forced convection dominated region ($0.0 \leq Ri \leq 1.0$), and for $D = 0.4$ in the free convection dominated region with increasing Ri in both of the aforementioned cases, which are also clearly observed in the Tables 3.4 (a) and 3.4 (b). However, average temperature (θ_{av}) of the fluid in the cavity decreases for the lower values of D ($D = 0.0$ and 0.2) at $Ri \leq 0.5$, but beyond these values of Ri it is gradually increases with Ri. It is also seen that the values of θ_{av} increases gradually with increasing Ri for the higher value of D ($D = 0.4$ and 0.6). Moreover, the values of average fluid temperature θ_{av} is the lowest for $D = 0.2$ at the pure forced convection ($Ri = 0.0$), for $D = 0.0$ at the mixed convection region and for $D = 0.6$ at the free convection dominated region for the case 1, but it is different for case 2. It is also seen that the dimensionless temperature (θ_c) at the cylinder center in the cavity increases gradually with Ri for all values of D. Furthermore, it is also seen that the values of θ_c is the lowest for the values of Ri up to 4.0 at the lowest values of D ($D = 0.1$), but beyond these values of Ri it is the lowest for the highest value of D ($D = 0.6$). Although the in general trends of the plots of the average Nusselt number (Nu), average fluid temperature (θ_{av}) and the temperature at the cylinder center (θ_c) are similar for both of the aforementioned cases, a considerable difference is found at the numerical values of these objects. Lastly, the numerical values of the average Nusselt number (Nu) for both of the cases are presented in Tables 3.4 (a) and 3.4 (b). It is clearly seen in Tables 3.4 (a) and 3.4 (b) that, the overall values of average Nusselt numbers, when square cylinder is considered (case 2) are always superior than those obtained with the circular cylinder (case 1) only for $D = 0.2$, but different nature are observed for the higher values of D ($D = 0.4$ and 0.6).

3.4.3 Effects of Thermal Conductivity Ratio

The effect of the solid-fluid thermal conductivity ratio K on streamlines at $AR = 1.0$, $Re = 100$, $Pr = 0.71$, $D = 0.2$, $L_x = L_y = 0.5$ and various Ri ($Ri = 0.0$, 1.0 and 5.0) for the case 1 and case 2 are presented in figure 3.10. At low Ri ($Ri = 0.0$) and for relatively small values of K ($K = 0.2$), a small recirculating cell is located just at the top of the inlet port of the cavity in both of the cases. The formation of circulation
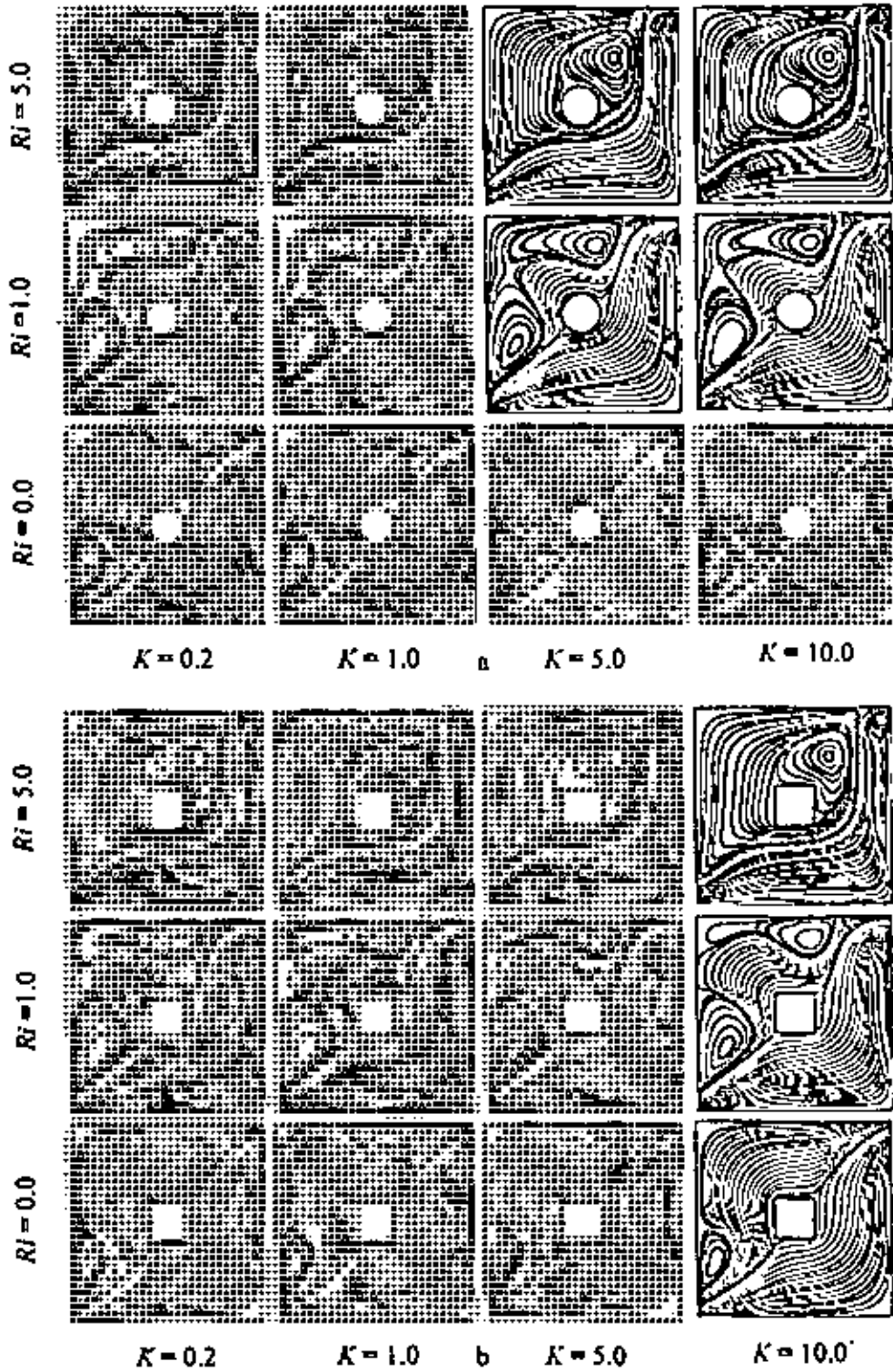
Figure 3.10: Streamlines for the (a) case 1 and (b) case 2 at different values of thermal conductivity ratio K and Richardson number Ri, while $AR = 1.0$, $Re = 100$, $Pr = 0.71$, $D = 0.2$ and $L_x = L_y = 0.5$.

cell is because of the mixing of the fluid due to the buoyancy driven and convective currents. In both of the cases, from the bottom row of figure 3.10, it is be seen that the streamlines for the different values of K (K = 0.2, 1.0, 5.0, 10.0) at Ri = 0.0 are almost identical. This is because thermal conductivity ratios have insignificant influence on velocity distribution. When Ri increases from 0.0 to 1.0, the natural convection effect is comparable with forced convection effect, as a result the size of the recirculating cell increases, compared with that for Ri = 0.0 and different values of K. Further when Ri increases to 5.0, the effect of natural convection is far more compared to the forced convection effect. In this case, conditions are strongly favoring the phenomena of natural convection and significant increase in recirculating cell is found.

The effect of the solid-fluid thermal conductivity ratio K on isotherms at AR = 1.0, Re = 100, Pr = 0.71, D = 0.2, $L_x = L_y$ = 0.5 and various Ri (Ri = 0.0, 1.0 and 5.0) for the case 1 and case 2 are presented in figure 3.11. From the figure 3.11, it is clearly seen that the thermal conductivity of the inner cylinder affects strongly on the isotherm structures in both of the cases. Now at Ri = 0.0 and K = 0.2, the isothermal lines are almost parallel and concentrated to the hot surface as shown in the bottom row of figure 3.11 in both of the cases, which implies that heat transfer between the heat source and the externally induced air flow is provided mainly by heat conduction and forced convection. Since the buoyancy effect is overwhelmed by the shear effect of the external induced flow. Moreover, making a comparison of the isothermal lines for Ri = 0.0 and various values of K, no significant difference is found except that the isothermal lines are shifted from the center of the cylinder with increasing K. As Ri increases to 1.0, nonlinearity of isotherms are seen and plume formation are initiated for all values of K, which indicates the launch of natural convection current. Further, as Ri increases to 5.0, plume formation become deep and isotherms becomes clustered near the heat source, which points to the conduction heat transfer at the vicinity of the heat source and convection, heat transfer in the remaining part of the cavity.

Therefore, the influence of the cylinder shapes on the fluid flow and heat transfer characteristics are almost considerable at all values of K and Ri.
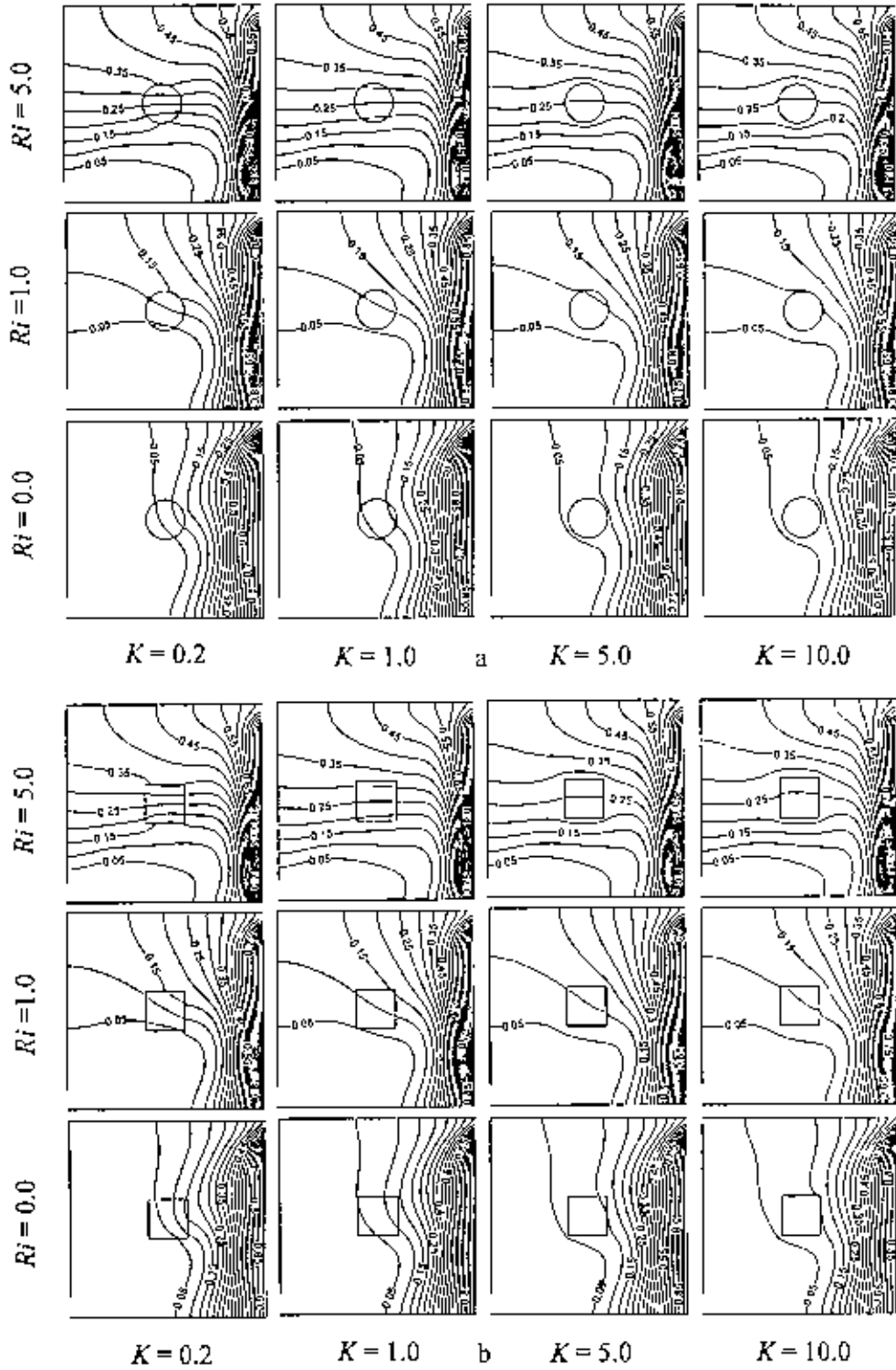
Figure 3.11: Isotherms for the (a) case 1 and (b) case 2 at different values of thermal conductivity ratio K and Richardson number Ri, while $AR = 1.0$, $Re = 100$, $L_x = L_y = 0.5$, $Pr = 0.71$ and $D = 0.2$.
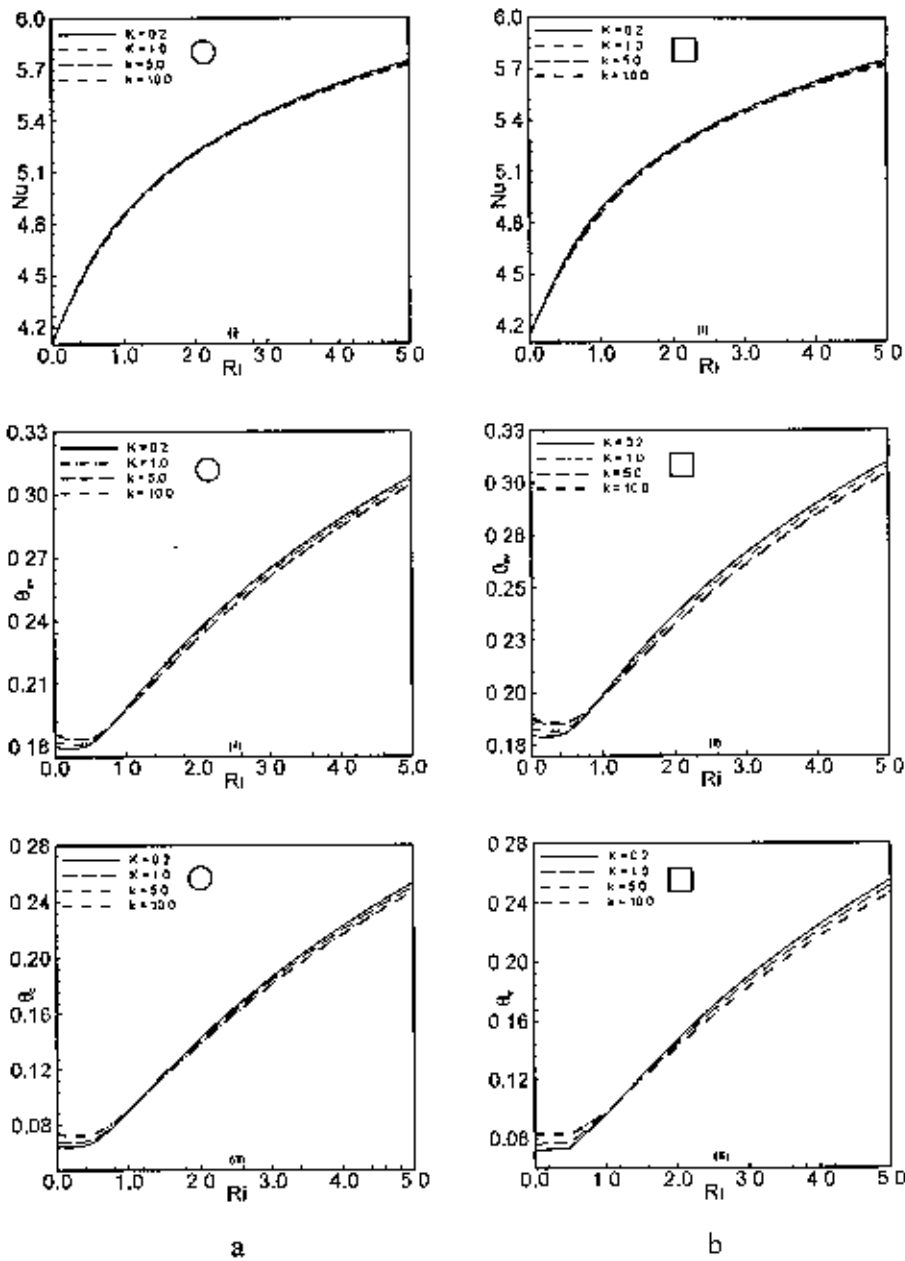
Figure 3.12: Effect of thermal conductivity ratio K on (i) average Nusselt number, (ii) average fluid temperature and (iii) temperature at the cylinder center in the cavity for (a) case 1 and (b) case 2, while AR = 1.0, $L_x = L_y = 0.5$, $Re = 100$, $Pr = 0.71$ and $D = 0.2$.

Table 3.5 (a): Variation of average Nusselt number with solid fluid thermal conductivity ratio for the case 1

Ri	Nu			
	$K = 0.2$	$K = 1.0$	$K = 5.0$	$K = 10.0$
0.0	4.115668	4.114514	4.112987	4.112573
0.5	4.552985	4.543402	4.532336	4.529588
1.0	4.851970	4.843239	4.832878	4.830251
1.5	5.059429	5.052769	5.044868	5.042852
2.0	5.216205	5.210251	5.203415	5.201697
2.5	5.342343	5.336126	5.329231	5.327537
3.0	5.447763	5.440815	5.433276	5.431454
3.5	5.538055	5.530204	5.521770	5.519752
4.0	5.616735	5.607964	5.598567	5.596329
4.5	5.686198	5.676565	5.666231	5.663773
5.0	5.748166	5.737760	5.726561	5.723895

Table 3.5 (b): Variation of average Nusselt number with solid fluid thermal conductivity ratio for the case 2

Ri	Nu			
	$K = 0.2$	$K = 1.0$	$K = 5.0$	$K = 10.0$
0.0	4.144315	4.143092	4.140904	4.140141
0.5	4.582596	4.569476	4.553558	4.549042
1.0	4.882094	4.869002	4.852818	4.848154
1.5	5.086654	5.076538	5.063939	5.060270
2.0	5.239650	5.231079	5.220678	5.217683
2.5	5.362401	5.354076	5.344344	5.341604
3.0	5.465065	5.456269	5.446298	5.443550
3.5	5.553184	5.543584	5.532912	5.530014
4.0	5.630170	5.619650	5.608074	5.604960
4.5	5.698319	5.686874	5.674337	5.670982
5.0	5.759270	5.746954	5.733475	5.718599

The effect of thermal conductivity ratio K on average Nusselt number (Nu) at the heated surface, average temperature (θ_{av}) of the fluid in the cavity and dimensionless temperature (θ_c) at the cylinder center for the case 1 and case 2 with $AR = 1.0$, $Re = 100$, $Pr = 0.71$, $D = 0.2$ and $L_x = L_y = 0.5$ are shown in figure 3.12. From these figures it is clearly observed that as Ri increases, average Nusselt number (Nu) at the hot surface sharply increases for all values of K. A careful observation on these figures also shows that the variation of Nu with the values of K is not significant at all values of Ri. However, as Ri increases average temperature (θ_{av}) of the fluid and the temperature (θ_c) at the cylinder center increases very slowly in the forced convection dominated region and very sharply in the free convection dominated region with increasing Ri for all values of K in the cavity. On the other hand, the average temperature (θ_{av}) of the fluid in the cavity and the temperature (θ_c) at the cylinder center are the lowest in the forced convection dominated region for the lowest value of K ($K = 0.2$) and in the free convection dominated region for the larger values of K ($K = 5.0, 10.0$). From these figures it is clearly observed that the plots for Nu, θ_{av} and θ_c are appear to be almost qualitatively similar but not quantitatively for both of the cases considered. Finally, the quantitative measurements for the values of Nu are tabulated in the Tables 3.5 (a) and 3.5 (b) to compare the values of average Nusselt number for the two shapes of cylinder (circular and square). It is clearly seen from the Tables 3.5 (a) and 3.5 (b) that the overall values of average Nusselt number for the case 2 are slightly higher than those obtained for the case 1 at all values of K.

3.4.4 Effects of Reynolds Number

The effect of Reynolds number on the flow field for the case 1 and case 2 are illustrated in the figure 3.13 by plotting the streamlines, while $AR = 1.0$, $Pr = 0.71$, $D = 0.2$, $L_x = L_y = 0.5$, $K = 5.0$ and $Ri = 0.0, 1.0$ and 5.0. The basic forced convection flow, presented in the left of the bottom row for $Ri = 0.0$ and $Re = 50$. is characterized by a perfect symmetry of the solution with respect to the diagonal joining the inlet and outlet ports. Because, of the small value of Re the thermal transport effect by the external cold air is little. Now for $Re = 100$ and $Ri = 0.0$ it can be seen that the symmetry already observed is destroyed and a small recirculating
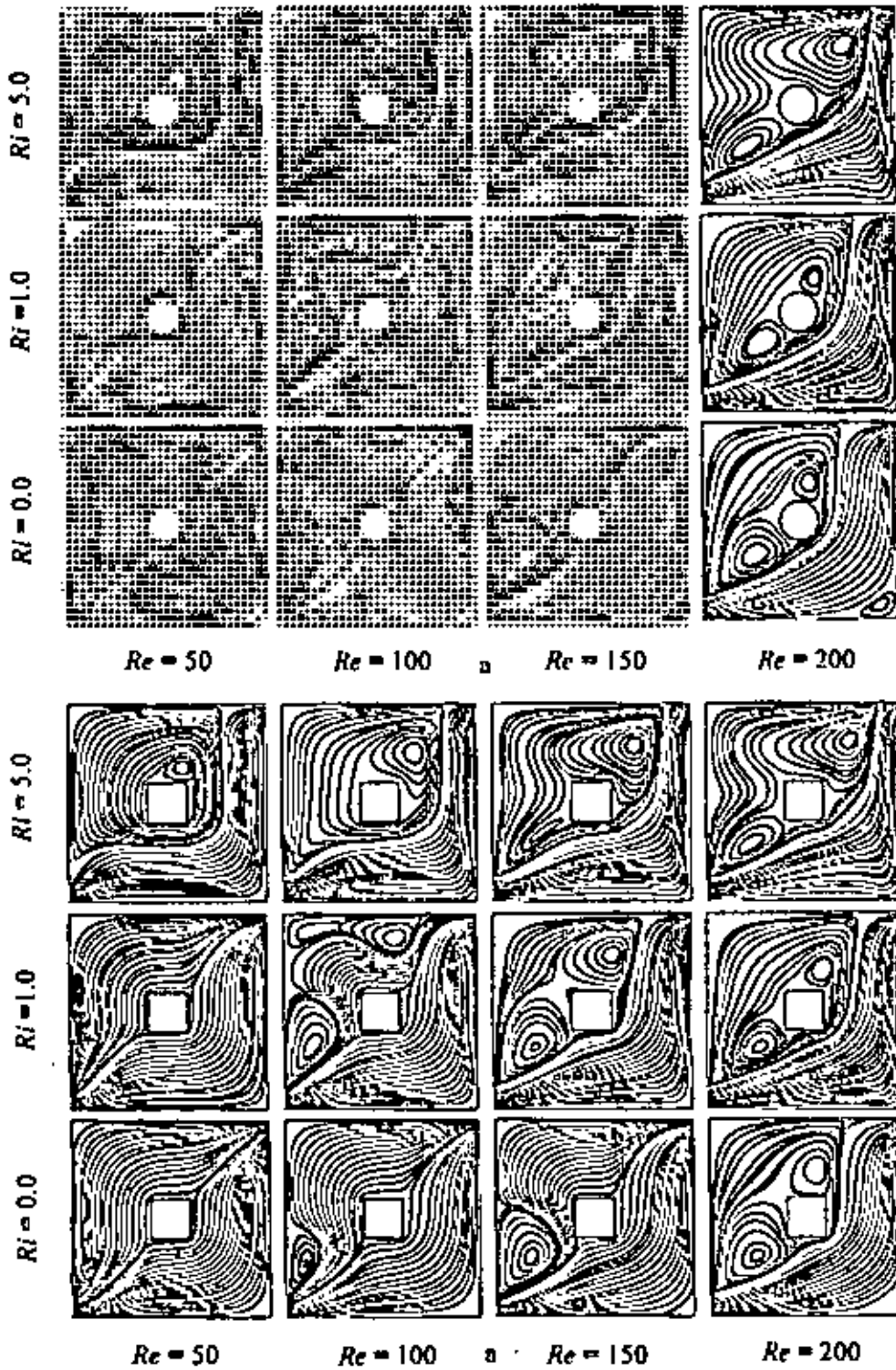
Figure 3.13: Streamlines for the (a) case 1 and (b) case 2 at different values of Reynolds numbers Re and Richardson number Ri, while $AR = 1.0$, $K = 5.0$, $D = 0.2$, $Pr = 0.71$ and $L_x = L_y = 0.5$.

cell is developed just at the top of the inlet port and the recirculating cell became large with the increased of Re (150 and 200). On the other hand, at any particular Reynolds number, there is a marked changed in flow patterns as the flow regime changes from dominant forced convection to dominant natural convection with increasing Ri.

The effect of Reynolds number on the temperature distributions for the case 1 and case 2 are illustrated in the figure 3.14 by plotting the isotherms, while $AR = 1.0$, $Pr = 0.71$, $D = 0.2$, $L_x = L_y = 0.5$, $K = 5.0$ and $Ri = 0.0$, 1.0 and 5.0. The corresponding isotherms results from combined effects of conduction and pure forced convection is shown in the left bottom corner of figure 3.14, which indicated that a large area of the cavity remains at higher temperature. On the other hand, at any particular Reynolds number, there is a marked changed in isotherms as the flow regime changes from dominant forced convection to dominant natural convection with increasing Ri. It is also observed that for a particular Ri, the isotherms became denser toward the hot wall as the Re increases. The main cause is that the region affected by the heat source became smaller due to the strong external flow.

Figures 3.13 and 3.14 are also be used for comparison of streamline and isotherm plots between the case 1 and case 2. A noteworthy dissimilarity is found on the resulting streamline and isotherm plots between the two-abovementioned cases.

The effect of Reynolds number on average Nusselt number (Nu) at the heat source, average fluid temperature (θ_{av}) in the cavity and the temperature (θ_c) at the cylinder center for the case 1 and case 2 are presented in figure 3.15 as a function of Richardson number. Keeping the values of Re constant, the average Nusselt number at the heated surface increases gradually with increasing values of Ri. Also, the average Nusselt number at the heated surface is found to increase as Re increases at fixed Ri in both of the cases. Therefore, it can be concluded that more heat transfer from the heat source is expected in the case of large parameter value of Re or Ri. The average temperature of the fluid domain and temperature at the cylinder center in the cavity increases gradually with Ri for all values of Re. Moreover, for a fixed value of Ri, the values of θ_{av} and θ_c are the lowest for the largest Re.
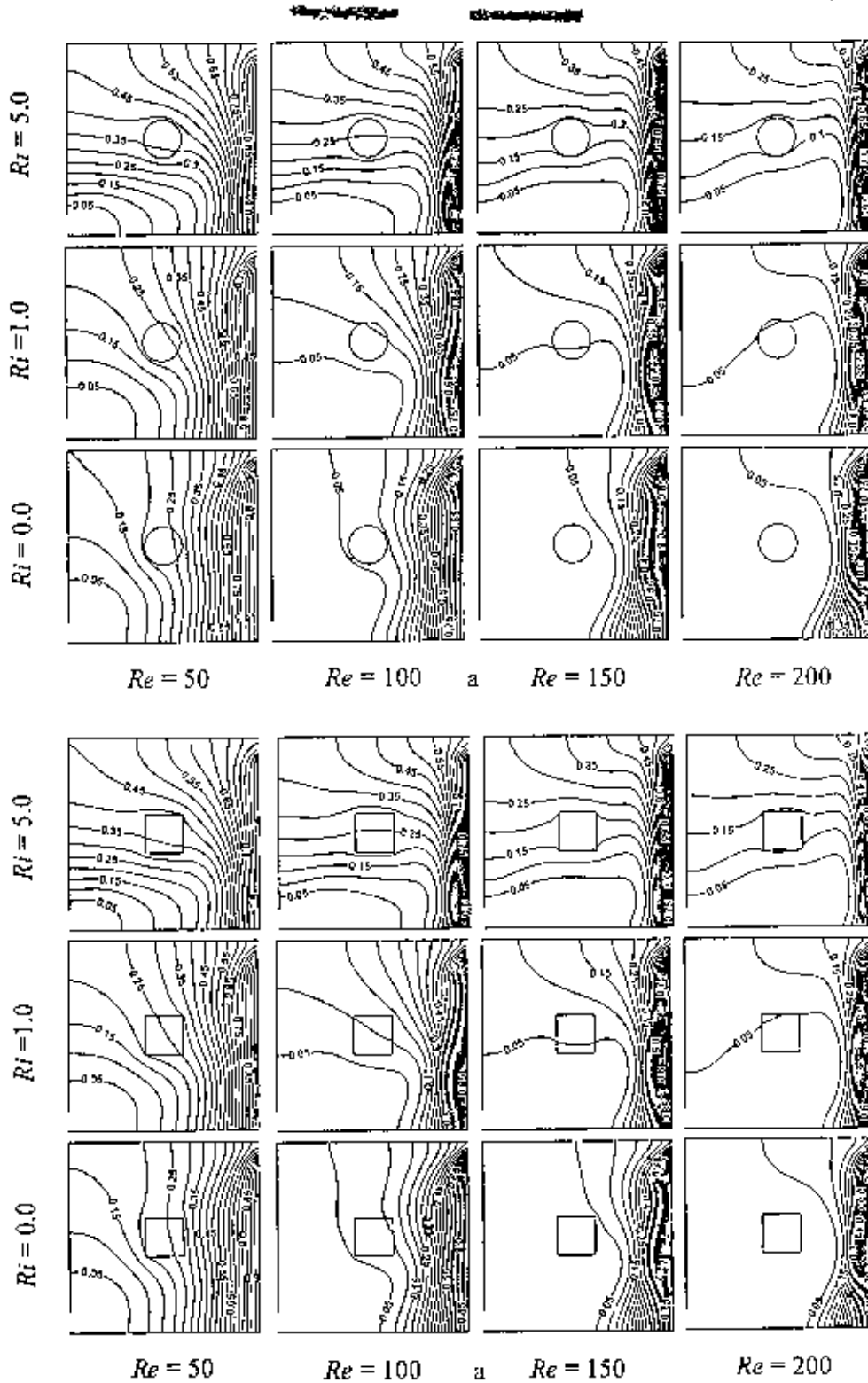
Figure 3.14: Isotherms for the (a) case 1 and (b) case 2 at different values of Reynolds numbers Re and Richardson number Ri, while $AR = 1.0$, $K = 5.0$, $L_x = L_y = 0.5$, $D = 0.2$ and $Pr = 0.71$.
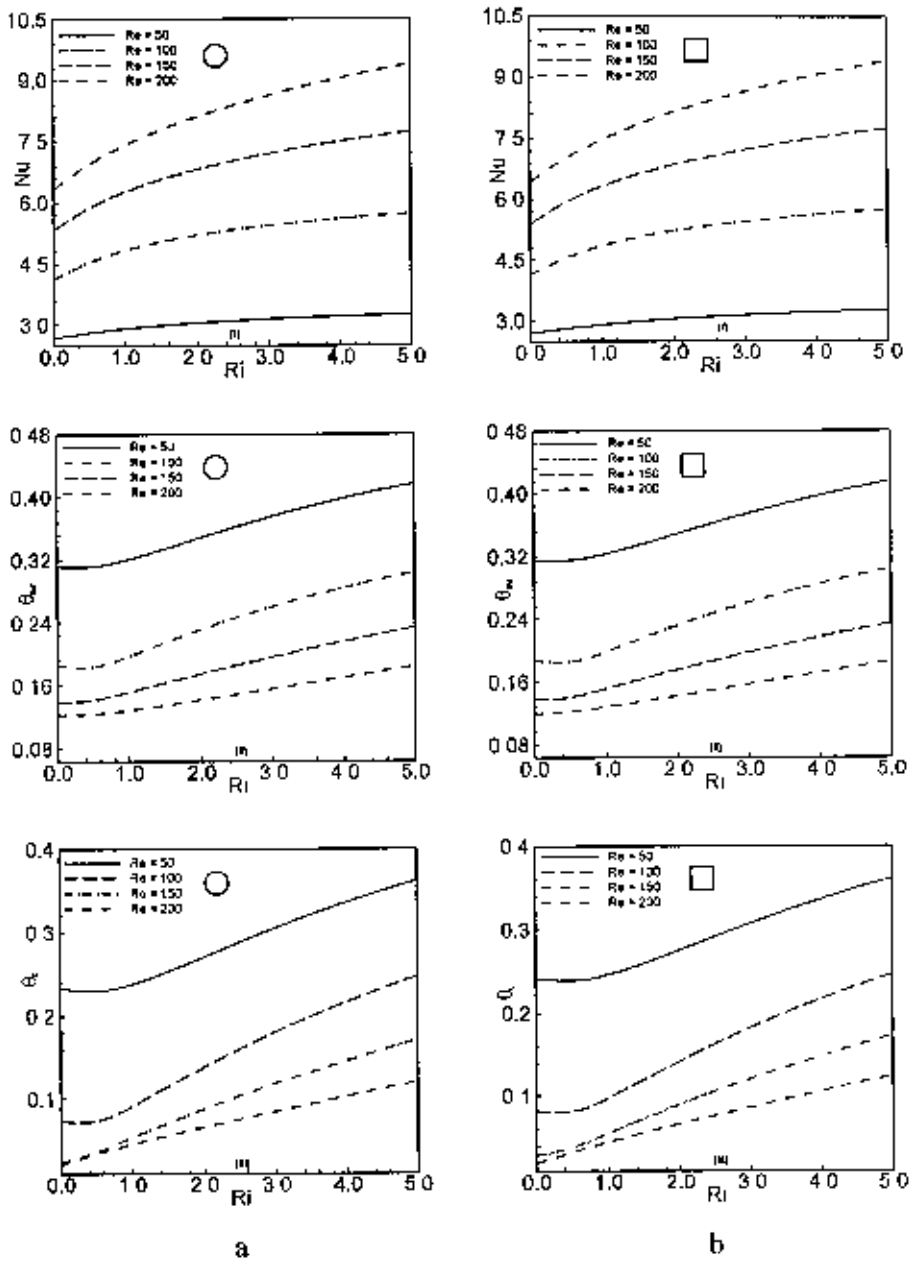
Figure 3.15: Effect of Reynolds number *Re* on (i) average Nusselt number, (ii) average fluid temperature and (iii) temperature at the cylinder center in the cavity for the (a) case 1 and (b) case 2, while *AR* = 1.0, $L_x = L_y = 0.5$, $K = 5.0$, $Pr = 0.71$ and $D = 0.2$.

Table 3.6 (a): Variation of average Nusselt number with Reynolds number for the case 1

Ri	Nu			
	Re = 50	Re = 100	Re = 150	Re = 200
0.0	2.687645	4.112987	5.321188	6.325433
0.5	2.802458	4.532336	5.867555	6.932840
1 0	2.902725	4.832878	6 259965	7.398234
1.5	2.983341	5.044868	6.562965	7 776306
2.0	3.046527	5.203415	6.809839	8 096685
2.5	3.096509	5.329231	7.017861	8.375714
3.0	3.136951	5.433276	7.197031	8.622583
3.5	3.170484	5.521770	7.353750	8.843093
4.0	3 198911	5.598567	7.492447	9.041450
4.5	3.223467	5.666231	7.616359	9.220957
5.0	3.245015	5.726561	7.727943	9.384296

Table 3.6 (b): Variation of average Nusselt number with Reynolds number for the case 2

Ri	Nu			
	Re = 50	Re = 100	Re = 150	Re = 200
0.0	2.695308	4.140904	5.383585	6.418461
0.5	2.803944	4.553558	5 927046	7.009310
1.0	2.900274	4.852818	6.315675	7.464387
1.5	2.979390	5.063939	6.612105	7.835280
2.0	3.042455	5.220678	6.851874	8.149303
2.5	3.092843	5.344344	7.053212	8.421941
3.0	3.133811	5.446298	7.226430	8.662465
3.5	3.167845	5.532912	7.377990	8.876971
4.0	3.196705	5.608074	7.512281	9.069858
4.5	3.221625	5.674337	7.632464	9.244498
5.0	3.243475	5.733475	7.740906	9.403565

Although the qualitative nature of the plots of average Nusselt number (Nu), average fluid temperature (θ_{av}) and cylinder center temperature (θ_c) for the case 2 are similar with that for the case 1, but are quantitatively different. Here only the average Nusselt number values comparison are shown in the Tables 3.6 (a) and 3.6 (b). It is clearly found in Tables 3.6 (a) and 3.6 (b) that the overall values of average Nusselt number for case 2 are considerably higher than those obtained for the case 1 at the higher values of Re (Re = 100, 150 and 200) and this trend is not true for the lowest value of Re (Re = 50)

3.4.5 Effects of Prandtl Number

We now discuss the effect of Prandtl number on the flow and heat transfer in mixed convection flow on taking AR = 1.0, Re = 100, D = 0.2, $L_x = L_y = 0.5$, K = 5.0 and various values of Ri (Ri = 0.0, 1.0 and 5.0) for the case1 and case2 Figure 3.16 depicts the streamlines for the values of Prandtl number Pr = 0.71, 1.0, 3.0 and 7.1 at the three values of Ri in boyh of the cases. At Ri = 0.0 and Pr = 0.71, The fluid flow is characterized by the imposed flow covering most of the cavity space and a small rotating cell is formed just at the top of the inlet port in the cavity. Moreover the size, position and strength of the rotating cell are almost identical for the four cases presented at Ri = 0.0. It is therefore confirmed that for Ri = 1 0. the flow in the cavity dominated by shear action of the incoming fluid and buoyancy induced flow at low Pr = 0.71. The buoyancy induced flow become relatively weak with increasing the value of Pr at Ri = 1.0, since the open lines characterizing the imposed flow are still dominant. Further at Ri = 5.0 a strong effect of buoyancy forced is observed for lower values of Pr (Pr = 0.71 and 1.0) and relatively weak effect of buoyancy forced is observed for higher values of Pr (Pr = 3.0 and 7.1). This phenomenon is very logical because, higher Prandtl number fluids are highly viscous.

The influence of Prandtl number on isotherms for different values of Ri and the above mentioned two cases are shown in the figure 3.17. From this figure we can ascertain that the isotherms are almost linear and distributed inside the cavity for Ri = 0.0 and Pr = 0.71, which is due to the combined effect of conduction and forced convection As Ri increases, nonlinearity of isotherms is found and plume formation
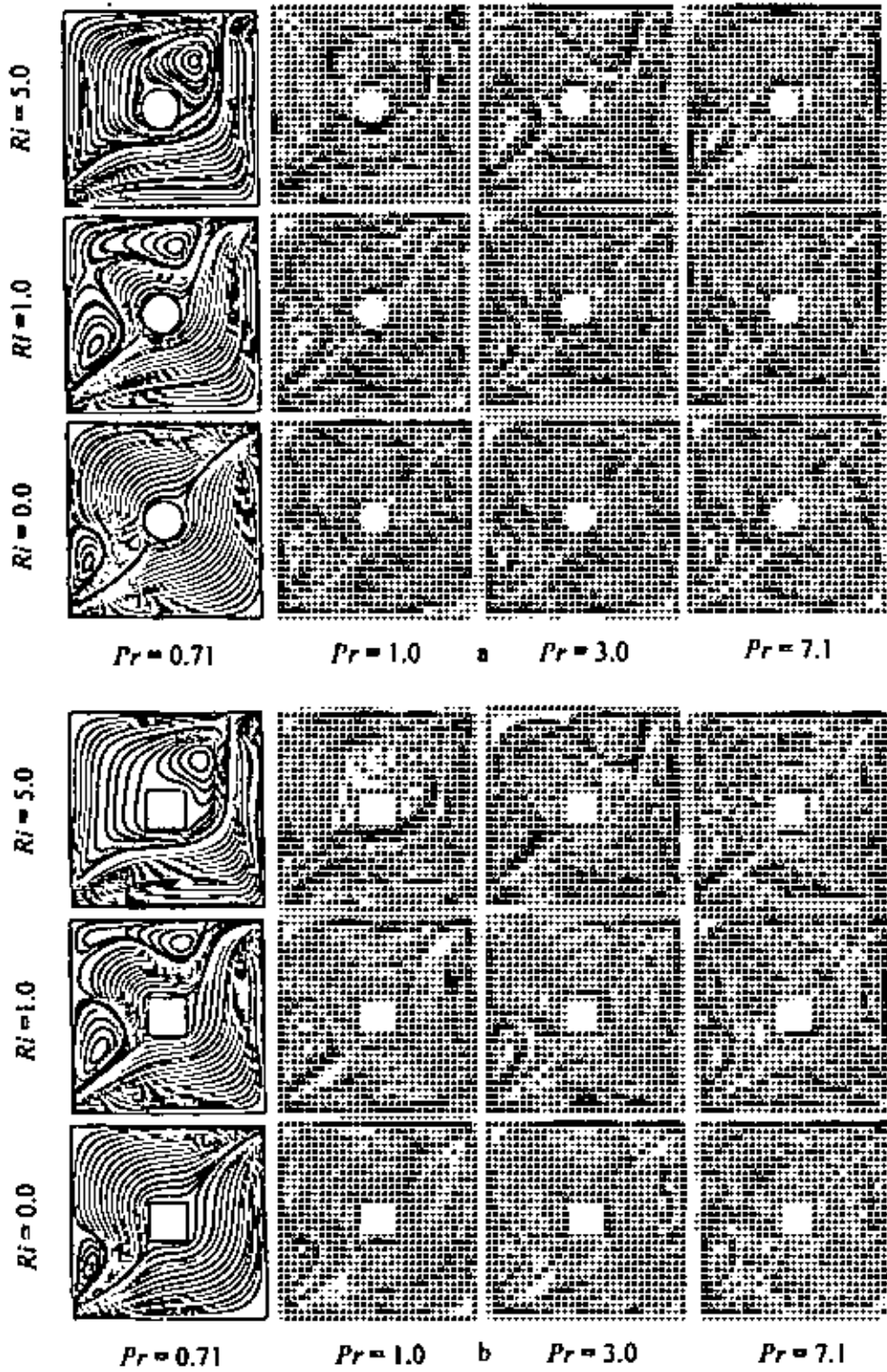
Figure 3.16: Streamlines for the (a) case 1 and (b) case 2 at different values of Prandtl numbers Pr and Richardson number Ri, while $AR = 1.0$, $Re = 100$, $K = 5.0$, $D = 0.2$ and $L_x = L_y = 0.5$.

is initiated for lower values of Pr ($Pr = 0.71$ and 1.0), which indicates the launch of natural convective current. Moreover, these trends in isotherms are not found for higher values of Pr ($Pr = 3.0$ and 7.1). On the other hand, an increase in Prandtl number also increases the crowding of isotherms for all values of Ri. It is also seen from the figure 3.17 that in both of the cases isotherms are confined to a smaller region at high values of the Prandtl number thereby suggesting the bulk of the resistance to heat transfer confined to a thin layer of fluid. This is clearly due to the thinning of the thermal boundary layer with the increasing Prandtl number. However, a visual examination of the streamline and isotherms plots does reveal a trivial difference between the two aforementioned cases.

The effect of Richardson number on the average Nusselt number (Nu) at the heated surface, average temperature (θ_{av}) of the fluid in the cavity and dimensionless temperature (θ_c) at the cylinder center at different Prandtl number is shown in figure 3.18 for the case 1 and case 2 respectively. In both of the aforesaid cases, as Ri increases, average Nusselt number (Nu) increases monotonically for all values of Pr. Maximum average Nusselt number is obtained, without the effect of Ri, for the highest $Pr = 7.1$. The average temperature of the fluid domain and the temperature at the cylinder center in the cavity increases gradually with the increases of Ri for the lower values of Pr ($Pr = 0.71$ and 1.0), while the average temperature of the fluid decreases gradually with increasing Ri for the higher values of Pr ($Pr = 3.0$ and 7.1). On the other hand, the temperature at the cylinder center is independent of Ri for the higher values of Pr ($Pr = 3.0$ and 7.1). However, minimum average temperature of the fluid and the temperature at the cylinder center in the cavity are obtained, without the effect of Ri, for the highest $Pr = 7.1$. It is further observed that, although the variation of the average Nusselt number (Nu) with Ri and Pr is qualitatively similar for both of the abovementioned cases, but has quantitatively dissimilarity, which are well documented in the Tables 3.7 (a) and 3.7 (b). By Comparing the values of average Nusselt number between the case 1 and case 2, it is clearly seen in Tables 3.7 (a) and 3.7 (b) that, the overall values of average Nusselt number, when circular cylinder is considered (case 1) are significantly lower than those obtained with the square cylinder (case 2) for all values of Pr.
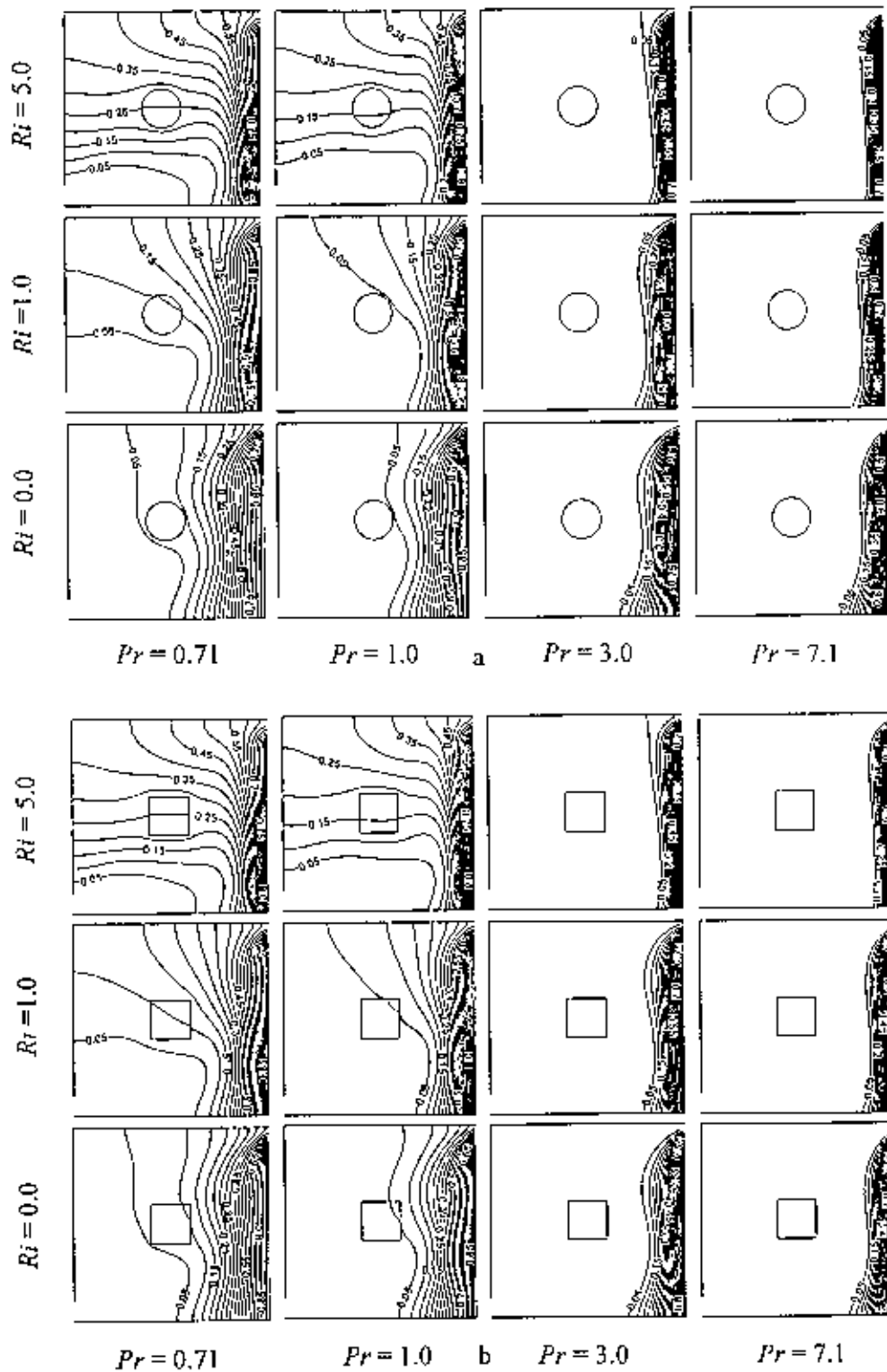
Figure 3.17: Isotherms for the (a) case 1 and (b) case 2 at different values of Prandtl numbers Pr and Richardson number Ri, while $AR = 1.0$, $Re = 100$, $L_x = L_y = 0.5$, $K = 5.0$ and $D = 0.2$.
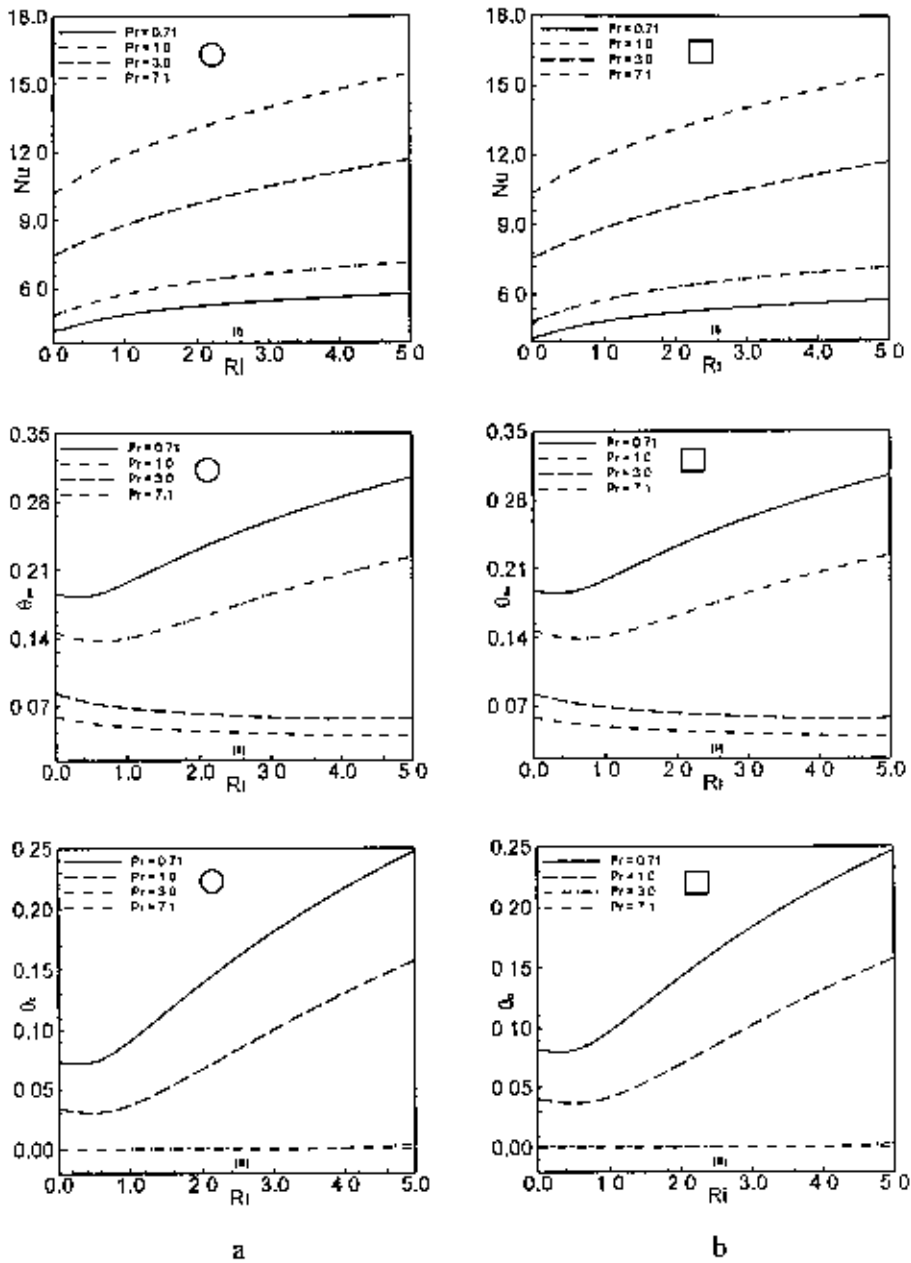
Figure 3.18: Effect of Prandtl number *Pr* on (i) average Nusselt number, (ii) average fluid temperature and (iii) temperature at the cylinder center in the cavity for the (a) case 1 and (b) case 2, while AR = 1.0, $L_x = L_y = 0.5$, $K = 5.0$, $Re = 100$ and $D = 0.2$.

Table 3.7 (a): Variation of average Nusselt number with Prandtl number for the case 1

Ri	Nu			
	$Pr = 0.71$	$Pr = 1.0$	$Pr = 3\,0$	$Pr = 7.1$
0.0	4.112987	4.818053	7.440991	10.187403
0.5	4.532336	5.334980	8.177176	11.104742
1.0	4.832878	5.737606	8.776704	11 850491
1.5	5.044868	6.044782	9.285501	12 483071
2.0	5.203415	6.283370	9.729844	13.036041
2.5	5.329231	6.476995	10.1258220	13.529678
3.0	5.433276	6.639949	10.483920	13.977156
3.5	5.521770	6.780603	10.811168	14.387546
4.0	5.598567	6 904201	11.112099	14.767386
4 5	5.666231	7.014271	11.389353	15.121558
5.0	5.726561	7 113319	11.644908	15 453813

Table 3.7 (b): Variation of average Nusselt number with Prandtl number for the case 2

Ri	Nu			
	$Pr = 0.71$	$Pr = 1.0$	$Pr = 3.0$	$Pr = 7.1$
0.0	4.140904	4 866317	7.559764	10.364761
0.5	4.553558	5.373153	8.270079	11.241093
1.0	4.852818	5.771176	8.852954	11.961860
1.5	5.063939	6.076713	9.350436	12.578009
2.0	5.220678	6.312980	9.786626	13.119316
2.5	5.344344	6.503511	10.176474	13.604200
3.0	5.446298	6.663233	10.529872	14.044830
3.5	5.532912	6.800845	10.853619	14.449694
4.0	5.608074	6.921710	11.152328	14.824962
4.5	5 674337	7.029374	11.428765	15.175277
5.0	5.733475	7.126324	11.684315	15.504224

3.4.6 Effects of Cylinder Locations

The distribution of streamlines and isothermal lines for the case 1 and case 2 in a square cavity at various locations of the inner cylinder, while $Re = 100$, $Pr = 0.71$, $D = 0.2$, $K = 5.0$ and $Ri = 0.0$, 1.0 and 5.0 are shown in figures 3.19 and 3.20 respectively. When the inner cylinder is placed near the left wall along the mid horizontal plane, a two cellular vortex is developed at the left top corner in the cavity and a very small pocket of fluid is seen at the right bottom corner in the cavity for $Ri = 0.0$ As Ri increases to 1.0, the two cellular vortex becomes large in size and the pocket of fluid becomes disappear. Further as Ri increases to 5.0, the two cellular vortex become uni-cellular and large in size. Next when the inner cylinder is placed near the right wall along the mid horizontal plane, a uni-cellular vortex is exist at the left top corner in the cavity for all values of Ri and a tiny vortex is seen only at $Ri = 0.0$. Another observation also shows that the size of the vortex increases with increasing Ri. Further when the inner cylinder is placed near the bottom wall along the mid vertical plane, the inner vortex become very small in size and placed just at the top of the inlet port for $Ri = 0.0$. But at $Ri = 1.0$, another small vortex is also appear at the left top corner in the cavity. Further as Ri increases to 5.0, the flow pattern changes drastically. Finally when the inner cylinder is placed near the top wall along the mid vertical plane, a uni-cellular vortex is formed just at the top of the inlet port and a pocket of fluid is seen further at the right bottom corner in the cavity at $Ri = 0.0$. As Ri increases to 1.0, the vortex increases in size and the pocket of fluid becomes disappear. As Ri increases further to 5.0, the vortex become large in size and squeezes the induced flow paths, due to the dominating behavior of the convective current.

The distribution of isotherms inside the cavity for the four various locations of the inner cylinder and fixed $Ri = 0.0$ is shown in the bottom row of the figure 3.20 for both of the cases. As the inner cylinder moves closer to the left wall along the mid-horizontal plane, the uniformly distributed isotherms around the heat source display that the heat is mainly transported by diffusion due to zero buoyancy force.
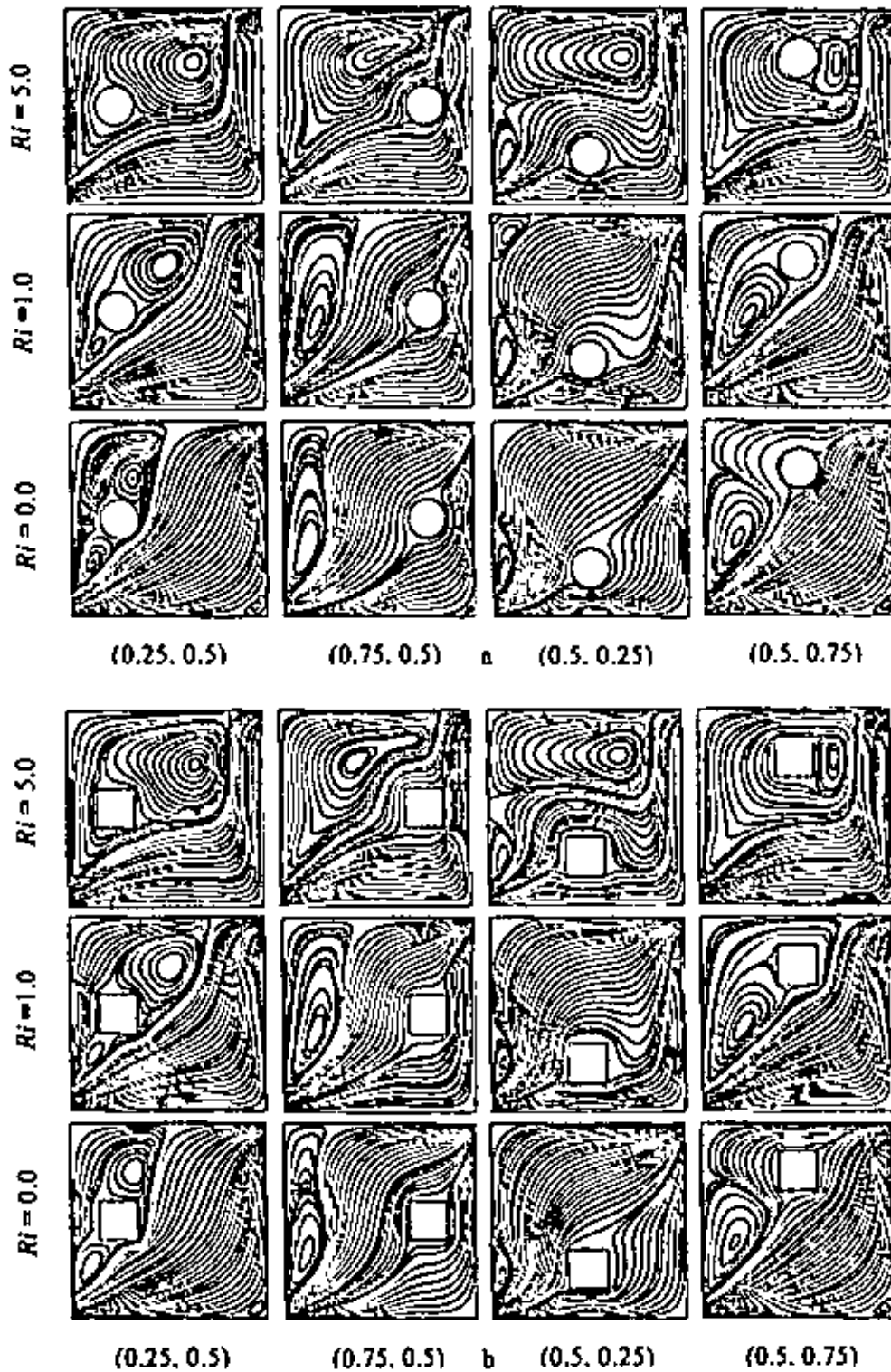
Figure 3.19: Streamlines for the (a) case 1 and (b) case 2 at different locations (L_x, L_y) of the inner cylinder and various values of Richardson number Ri, while $AR = 1.0$, $Re = 100$, $K = 5.0$, $D = 0.2$ and $Pr = 0.71$.
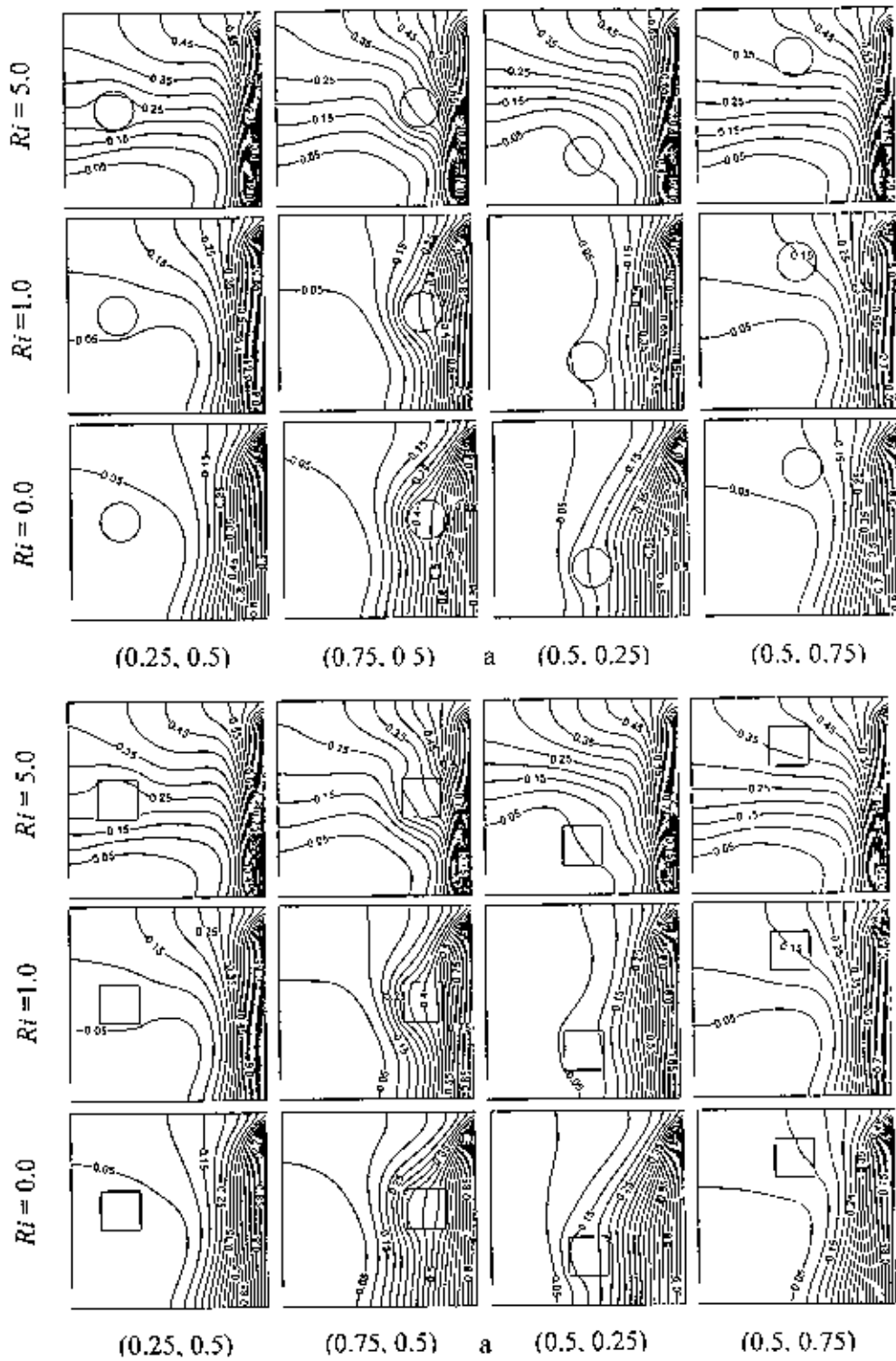
Figure 3.20: Isotherms for the (a) case 1 and (b) case 2 at different locations (L_x, L_y) of the inner cylinder and various values of Richardson number Ri, while $AR = 1.0$, $Re = 100$, $K = 5.0$, $D = 0.2$ and $Pr = 0.71$.

The isothermal lines surrounding the heat source seem to have no significant difference as the cylinder moves closer to the right wall along the mid-horizontal plane and closer to the top wall along the mid-vertical plane. In addition, more vertical isotherms near the hot wall generates when the inner cylinder moves closer to the bottom wall along the mid-vertical plane. Now going through the middle row of the figure 3.20, which is for $Ri = 1.0$ and different locations of the inner cylinder, we can observe an insignificant change in isotherms when compared with that for the case $Ri = 0.0$. The distribution of isotherms for the highest value of Ri at different locations of the inner cylinder in the cavity is significantly different from that at the lower values of Ri, because the buoyancy induced convection becomes more dominant than conduction at higher Ri.

However, a visual examination of the streamline and isotherms plots does reveal an important difference between the two aforementioned cases.

The effect of the inner cylinder locations on average Nusselt number (Nu) at the hot wall, average temperature (θ_{av}) of the fluid in the cavity and the temperature at the cylinder center (θ_c) corresponding to the aforementioned cases is shown in figure 3.21. For a fixed position of the inner cylinder, increasing the values of Ri enhances convection, as a result the average Nusselt numbers curves increases with increasing Ri. On the other hand, a maximum value of Nu is found when the cylinder center is at (0.25, 0.5) and (0.5, 0.75), which are also documented in the Tables 3.8 (a) and 3.8 (b). It is seen that average temperature (θ_{av}) of the fluid in the cavity decreases slowly as Ri increases up to a certain value and after then it increases smoothly with Ri when the cylinder center is at (0.25, 0.5) and (0.5, 0.75). It is also seen that the values of θ_{av} in the cavity decreases quickly as Ri increases up to a certain value and beyond these values of Ri it goes up gradually with Ri when the cylinder center is at (0.5, 0.25) and (0.75, 0.5). The values of temperature at the cylinder center (θ_c) increases sharply with increasing Ri when the cylinder center is at (0.25, 0.5) and (0.5, 0.75) and decreases gradually with increasing Ri when the cylinder center is at (0.5, 0.25) and (0.75, 0.5). Finally, the average Nusselt number is slightly higher for the case 2, as compared to the case 1 only when the cylinder center is at (0.25, 0.5).
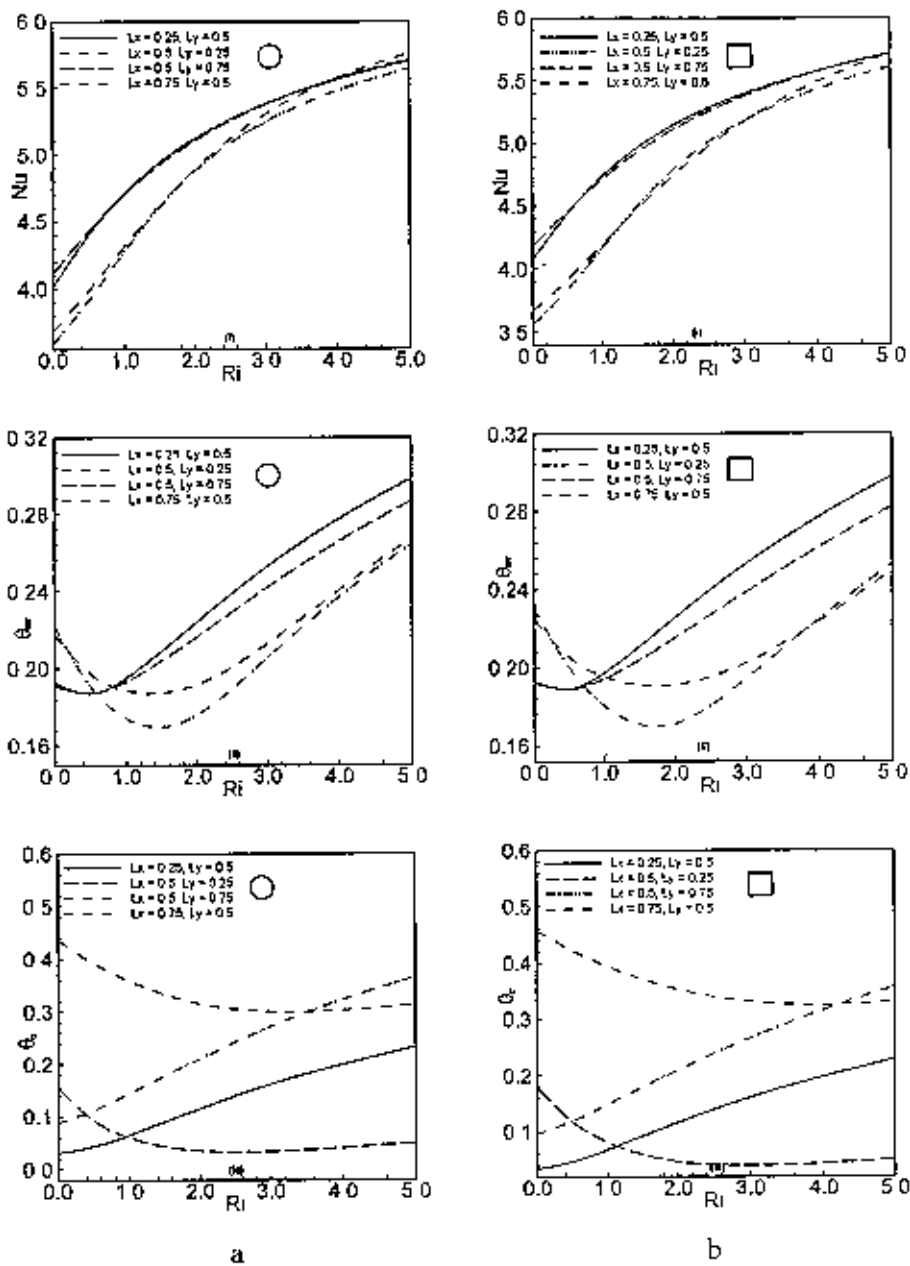
Figure 3.21: Effect of cylinder locations (L_x, L_y) on (i) average Nusselt number, (ii) average fluid temperature and (iii) temperature at the cylinder center in the cavity for the (a) case 1 and (2) case 2, while $AR = 1.0$, $Pr = 0.71$, $K = 5.0$, $Re = 0.71$ and $D = 0.2$.

Table 3.8 (a): Variation of average Nusselt number with cylinder locations for the case 1

Ri	Nu			
	(0.25, 0.5)	(0.5, 0.25)	(0.5, 0.75)	(0.75, 0.5)
0.0	4.013307	3.588855	4.110274	3.682389
0.5	4.402548	3.916998	4.430361	3.988678
1.0	4.711121	4.279096	4.703937	4.315789
1.5	4.944565	4.610498	4.926638	4.623480
2.0	5.124008	4.880849	5.107266	4.894137
2.5	5.266557	5.087932	5.255358	5.121223
3.0	5.383400	5.247661	5.378622	5.306178
3.5	5.481646	5.375210	5.482805	5.455489
4.0	5.565932	5.480391	5.572112	5.576830
4.5	5.639400	5.569321	5.649631	5.676813
5 0	5.704267	5.645980	5.717670	5 760499

Table 3.8 (b): Variation of average Nusselt number with cylinder locations for the case 2

Ri	Nu			
	(0.25, 0.5)	(0.5, 0.25)	(0.5, 0.75)	(0.75, 0.25)
0.0	4.070518	3.559750	4.175597	3.668232
0.5	4.443486	3.840374	4.463337	3.917497
1.0	4.740979	4.172244	4.717478	4.197024
1.5	4.967794	4.498648	4.930528	4.475881
2.0	5.143023	4.783805	5.107190	4.737571
2.5	5.282625	5.009991	5.254209	4.973039
3.0	5.397258	5.183636	5.377726	5.177381
3.5	5.493776	5.320598	5.482694	5.349676
4.0	5.576679	5.432590	5.572939	5.492745
4.5	5.649025	5.526805	5.651379	5.611370
5.0	5.712975	5.607783	5.720248	5.710447

3.4.7 Effects of Cavity Aspect Ratio

In order to assess the effect of geometric aspect ratio of the cavity, four different values of cavity aspect ratios AR (AR = 0.5, 1.0, 1.5 and 2.0) are considered here. Figures 3.22 show the streamlines in a cavity along with a circular cylinder (case 1) and square cylinder (case 2) at four different values of aspect ratios AR and three different values of Ri, while Re = 100, Pr = 0.71, D = 0.2, K = 5.0 and $L_x = L_y$ = 0.5. Now for AR = 0.5 and Ri = 0.0, it is observed that two small counter rotating cells are formed in the cavity for both of the cases The clockwise rotating cell is at the right bottom corner and the anti-clockwise rotating cell is at the top of the inlet port. As Ri increases to 1.0, the anti-clockwise cell remains unchanged and clockwise cell become disappear. Further at Ri = 5.0, comparatively large another anti-clockwise cell is also seen at the left top corner in the cavity. Next for AR =1.0 and zero buoyancy effect, a small recirculation cell exists in the cavity. With the increase of Ri to 1.0, the recirculation cell becomes into two cellular. These two cells merged and formed a single cell occupying the left top portion in the cavity at Ri = 5.0. Finally for the largest values of AR (AR = 1 5 and 2.0) and the low value of Ri (Ri = 0.0), a recirculation cell is developed just at the top of the inlet in the cavity. As Ri increases from 0.0 to 1.0, an additional recirculation cell is appeared, which is comparatively small and formed just at the left of the exit port near the top wall. As Ri increases further from 1.0 to 5.0, the recirculation cell becomes large in size which occupies the major portion of the cavity as a result the external induced flow becomes squeezes due to the buoyancy dominant effect in the cavity.

From the isotherm plots shown in figure 3.23, it is noticed that in both of the cases the high temperature zone is confined to a narrow region close to the hot wall for the higher values of AR (AR = 1.0, 1.5 and 2 0) at Ri = 0.0. The temperature gradient near the hot wall gets steeper as Ri increased for the mentioned cases. This is because, for low values of Ri, where forced convection dominates, the bulk of the cavity remains at a lower temperature, whereas the temperature distribution becomes more stratified when natural convection starts to dominate.
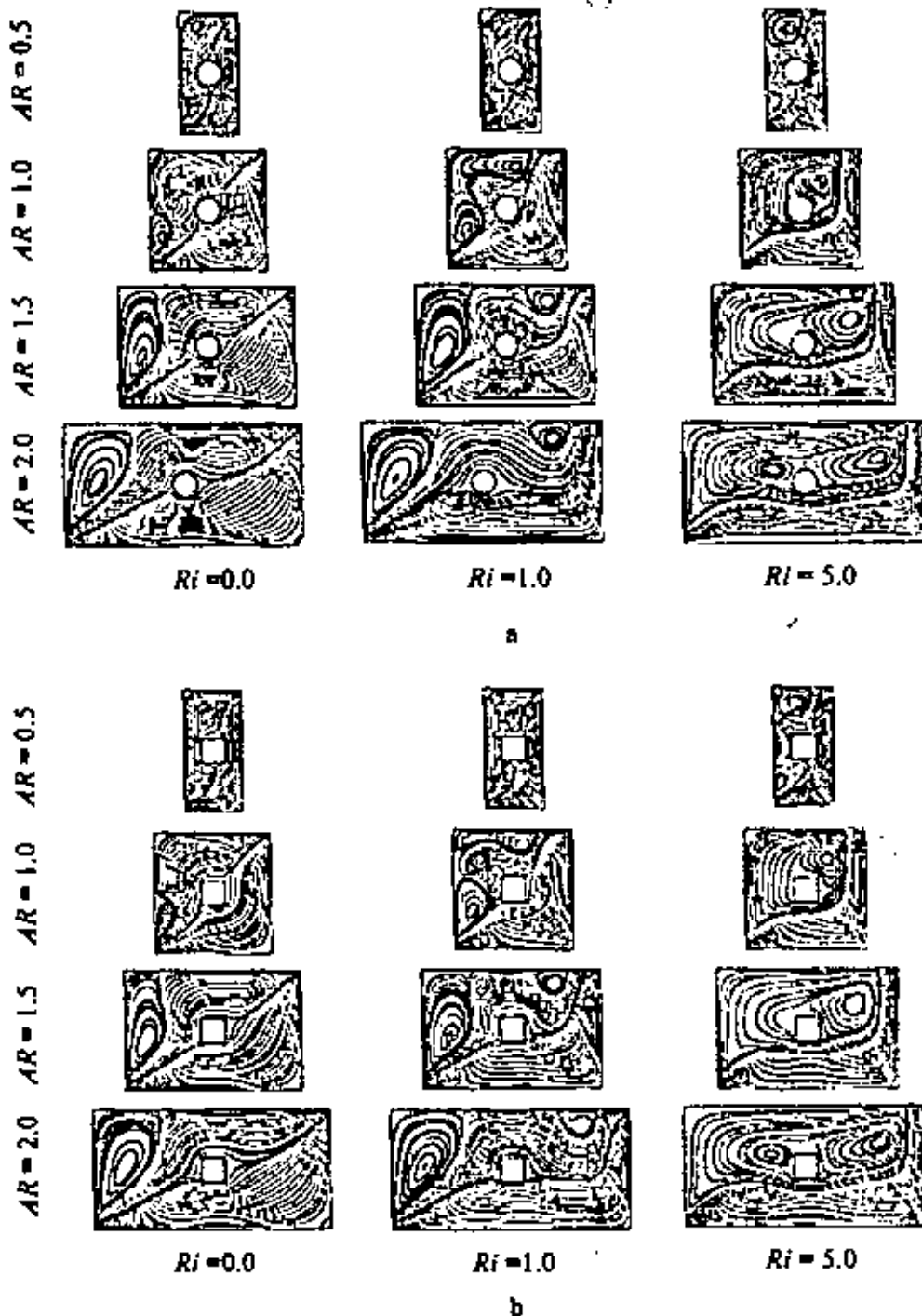
Figure 3.22: Streamlines for the (a) case 1 and (b) case 2 at different values of cavity aspect ratio AR and Richardson number Ri, while $Re = 100$, $L_x = L_y = 0.5$, $K = 5.0$, $D = 0.2$ and $Pr = 0.71$.
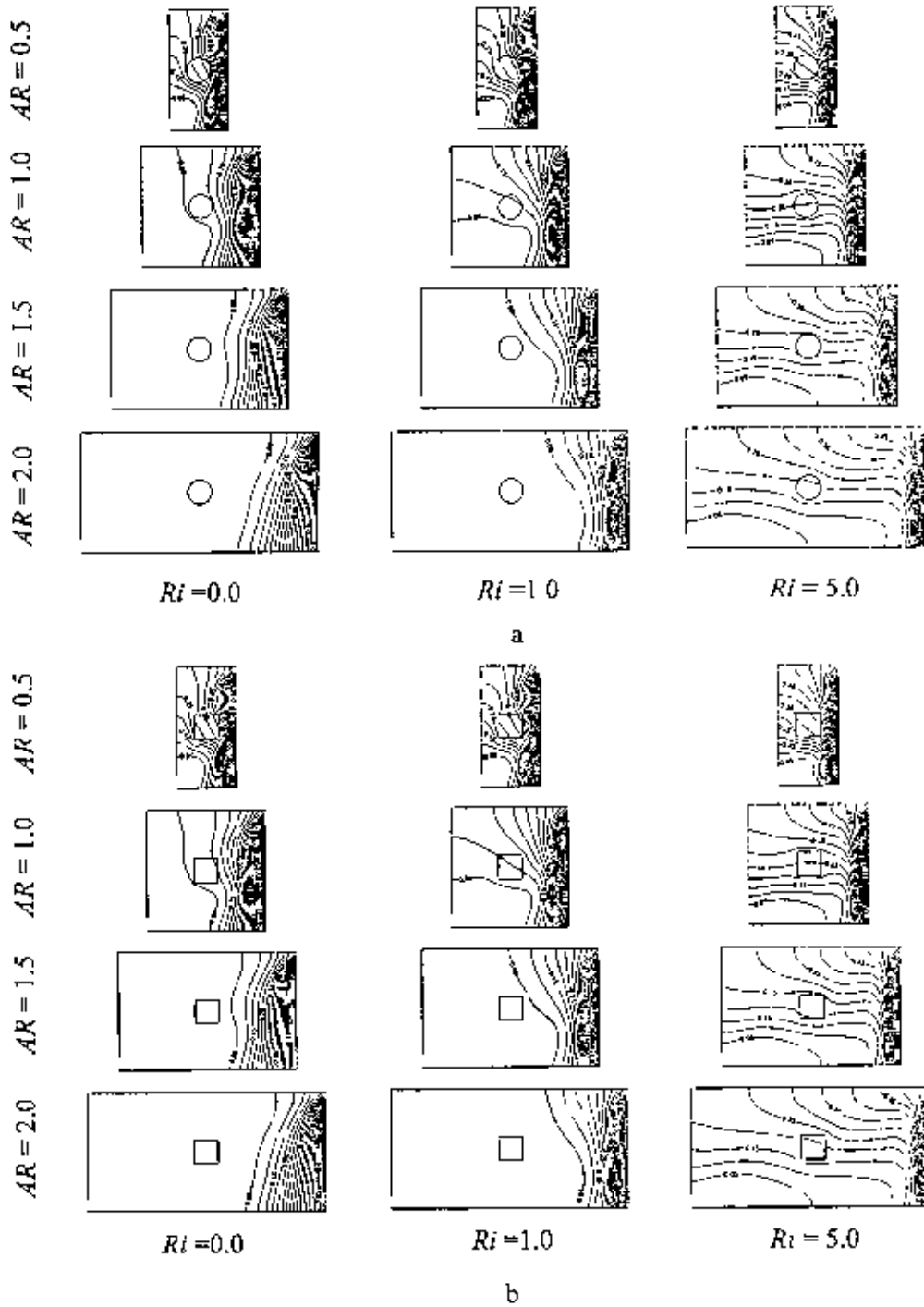
Figure 3.23: Isotherms for the (a) case 1 and (b) case 2 at different cavity aspect ratios AR and Richardson number Ri, while $Re = 100$, $L_x = L_y = 0.5$, $K = 5.0$, $D = 0.2$ and $Pr = 0.71$.
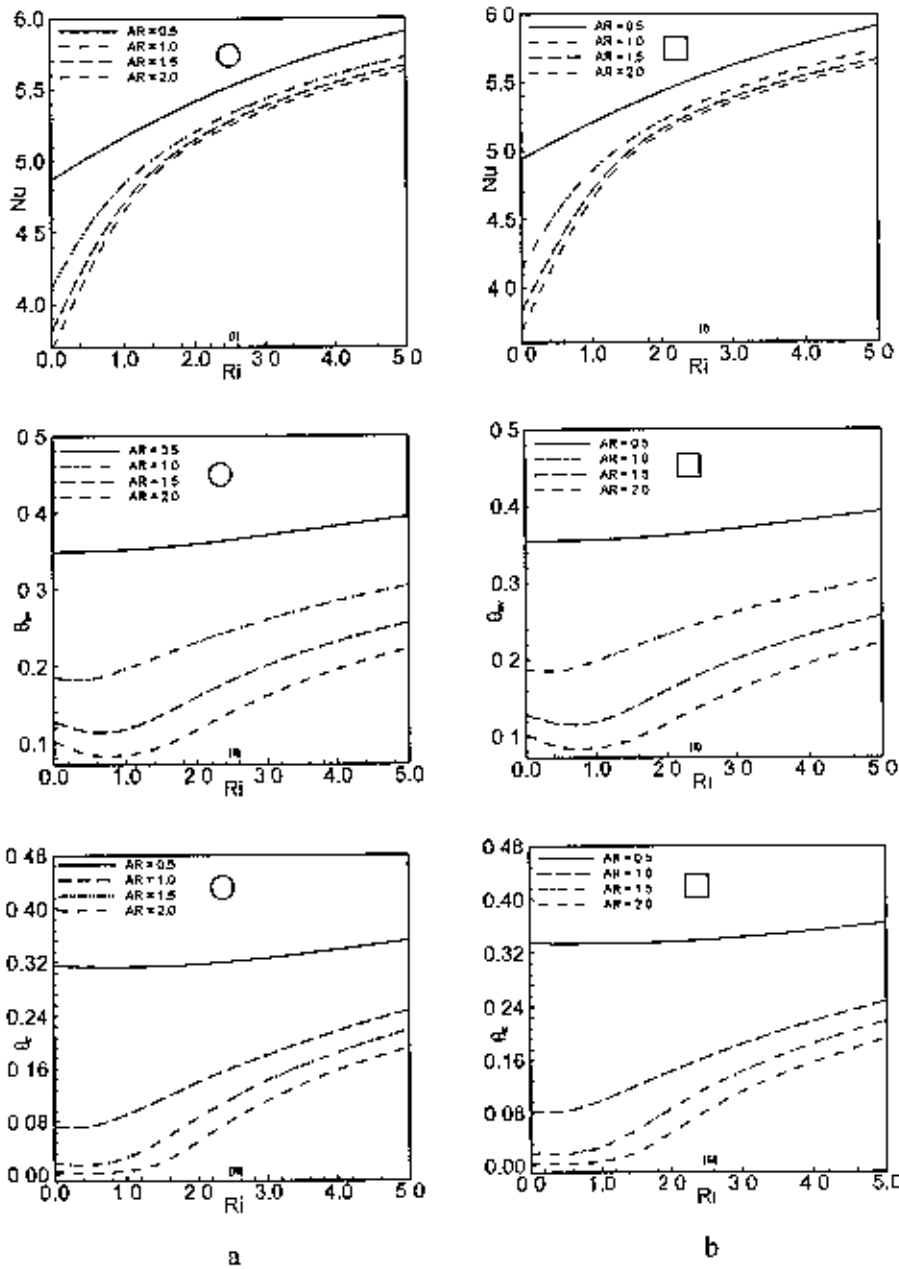
Figure 3.24: Effect of cavity aspect ratio AR on (i) average Nusselt number, (ii) average fluid temperature and (iii) temperature at the cylinder center in the cavity for the (a) case 1 and (b) case 2, while Re = 100, Pr = 0.71, K = 5.0, $L_x = L_y$ = 0.5 and D = 0.2.

81

Table 3.9 (a): Variation of average Nusselt number with cavity aspect ratio for the case 1

Ri	Nu			
	AR = 0.5	AR = 1.0	AR = 1.5	AR = 2.0
0.0	4.865716	4.112987	3.809091	3.675664
0.5	5.021038	4 532336	4.307424	4.211941
1.0	5.165367	4.832878	4.700704	4.644760
1.5	5.297432	5.044868	4.970890	4.939920
2.0	5.416783	5.203415	5.149616	5 120957
2.5	5.523620	5.329231	5.280363	5.249831
3.0	5.618664	5.433276	5.383899	5.351866
3.5	5.702990	5.521770	5.469789	5.436549
4 0	5.777845	5.598567	5.543210	5.508891
4.5	5.844491	5.666231	5.607320	5.571975
5.0	5.904104	5.726561	5.664197	5.627849

Table 3.9 (b): Variation of average Nusselt number with cavity aspect ratio for the case 2

Ri	Nu			
	AR = 0.5	AR = 1.0	AR = 1.5	AR = 2 0
0.0	4.939903	4.140904	3.825512	3.687188
0.5	5.076266	4.553558	4.316535	4.219868
1.0	5.204888	4.852818	4.707114	4.649877
1.5	5.324715	5.063939	4.978836	4.944845
2.0	5.435172	5.220678	5.157762	5.126336
2.5	5.536080	5.344344	5.287461	5.254608
3.0	5.627608	5.446298	5.389795	5.356062
3.5	5.710221	5.532912	5.474616	5.440302
4.0	5.784600	5.608074	5.547139	5.512301
4.5	5.851546	5.674337	5.610498	5.575107
5.0	5.911893	5.733475	5.666747	5.630748

But at the lowest value of AR ($AR = 0.5$), most of the area of the cavity remains the high temperature due to strong buoyancy for all values of Ri. This happens because as aspect ratio decreases, the hot wall comes closer to the incoming cold fluid.

By comparing the simulation results between the two aforementioned cases, it is observed that the cylinder shapes has insignificant effect on both flow and thermal fields for different cavity aspect ratio and Richardson number.

Variation of average Nusselt number (Nu) at the hot wall, average temperature (θ_{av}) of the fluid in the cavity and the temperature (θ_c) at the cylinder center with Ri at different values of AR is shown in figure 3.24 for the aforementioned cases. In both of the cases, average Nusselt number increases sharply with increasing Ri for all values of AR. On the other hand, average temperature of the fluid in the cavity and the temperature at the cylinder center increase gradually with Ri. Moreover, maximum values of Nu is found at $AR = 0.5$, which is owing to the shortest distance between the hot wall and the inlet port. Also the minimum values of θ_{av} and θ_c are found at $AR = 2.0$, which is due to the fact that the cavity volume increases with aspect ratio and more volume of the cavity is involved in cooling the fluid. Finally, Tables 3.9 (a) and 3.9 (b) compare the values of average Nusselt number for the two cases. It is clearly seen in Tables 3.9 (a) and 3.9 (b) that the overall values of average Nusselt number, when square cylinder is considered are noticeably higher than those obtained with the circular cylinder for all values of AR.

3.5 Concluding Remarks

In this chapter, different characteristics of a two dimensional conjugate mixed convection problem in vented cavities with a heat-conducting horizontal cylinder (circular/square) are studied numerically using a finite element method. Results are obtained for wide ranges of parameters Reynolds number Re, Richardson number Ri, Prandtl number Pr, solid and fluid thermal conductivity ratio K and various physical parameters i.e. the inlet and outlet position of the cavity, the sizes and locations of the cylinder and aspect ratio of the cavity. The major results are drawn as follows:

- Cavity orientation has a great influence on the streamlines and isotherms distributions at the three convective regimes. The average Nusselt numbers at the

hot wall have been used to compare the heat transfer rate among different configurations. Results show that the configuration BT has the highest heat transfer rate, whereas the configuration BB has the less effective heat transfer rate at the three convective regimes. Moreover, bulk average temperature and cylinder center temperature are the lowest for BT configuration in the forced convection dominated region and for TT configuration in the free convection dominated region.

- Cylinder size affects strongly the streamline distribution in the cavity. As a result, buoyancy-induced circulation cell reduces with increasing cylinder diameter A significant influence of cylinder diameter on isothermal lines is also established. However, maximum average Nusselt number (Nu) is found for $D = 0.6$ in the forced convection dominated region ($0.0 \leq Ri \leq 1.0$), and for $D = 0.4$ in the free convection dominated region. Moreover, the values of average fluid temperature θ_{av} is the lowest at the pure forced convection ($Ri = 0.0$) for $D = 0.2$, at the mixed convection region for $D = 0.0$ and at the free convection dominated region for $D = 0.6$. Also the values of θ_c is the lowest for the values of Ri up to 4.0 at the lowest values of D ($D = 0.1$), but beyond these values of Ri it is the lowest for the highest value of D ($D = 0.6$).

- Material properties (K) have insignificant effect on the flow field, and have significant effect on the thermal fields. The variation of average Nusselt number, Nu, average fluid temperature θ_{av} and temperature at the cylinder center θ_c with the values of K is not significant at all values of Ri for the smallest value of D. On the other hand, the variation of average Nusselt number Nu, average fluid temperature θ_{av} and temperature at the cylinder center θ_c with the values of K is more significant at all values of Ri for the largest value of D.

- Forced convection parameter Re has a great significant effect on the streamlines and isotherms field. Buoyancy-induced vortex in the streamlines increased and thermal layer near the heated surface become thin and concentrated with increasing Re. The average Nusselt numbers at the heated surface is always upper and the average temperature in he cavity is inferior for the largest value of Re.

- Recirculation cell in the streamline plot decreases and thermal boundary layer thickness near the heated wall decreases strongly with increasing values of Pr. Maximum average Nusselt number, minimum average fluid temperature and cylinder center temperature are obtained, without the effect of Ri, for the highest $Pr = 7.1$.

- Cylinder locations have significant effect on the flow and thermal fields. Comparatively large recirculation cell is developed for the cases when the cylinder moves near the left, top and right wall, this cell becomes into two parts and small in size when the cylinder is located near the bottom wall. Maximum value of Nu is found when the cylinder center is at (0.25, 0.5) and (0.5, 0 75) Average fluid temperature is the lowest at the forced convection dominated region when the cylinder center is at (0.25, 0.5) and (0.5, 0.75) and at the free convection dominated region when the cylinder center is at (0.5, 0.25).

- Cavity aspect ratio has significant effect on the streamlines and isotherms plots. Buoyancy effect increases with decreasing the cavity aspect ratio. The average Nusselt number at the heated surface is always higher for $AR = 0.5$ and the average temperature of the fluid in the cavity and temperature at the cylinder center are always lower for the highest values of AR ($AR = 2.0$).

- The difference of the values of average Nusselt number between the case of circular cylinder and the case of square cylinder are not significant from the engineering point of view.

Chapter 4

Effect of Joule Heating in the coupling of Conduction with Magnetohydrodynamics Mixed Convection Flow in a Rectangular Lid-Driven Cavity along with a Heat Conducting Horizontal Cylinder

The problem of combined free and forced convection heat transfer in a closed cavity has received considerable attention now a day. Such a problem customary grouped under the lid-driven cavity problems. Flow and heat transfer investigation in lid-driven cavities is one of the most widely studied problems in thermo-fluids area. Numerous investigations have been conducted in the past on lid-driven cavity flow and heat transfer considering various combinations of the imposed temperature gradients and cavity configurations. This is because the driven cavity configuration is encountered in many practical engineering and industrial applications. Analysis of mixed convective flow in a lid-driven cavity finds applications in materials processing, flow and heat transfer in solar ponds, dynamics of lakes, reservoirs and cooling ponds, crystal growing, float glass production, metal casting, food processing, galvanizing, and metal coating, among others. Combined forced and free convective flow in lid-driven cavities occurs as a result of two competing mechanisms. The first is due to shear flow caused by the movement of one of the walls in the cavity, while the second is due to buoyancy flow produced by thermal non-homogeneity of the cavity boundaries. Understanding of these mechanisms is of great significance from technical and engineering standpoints. When a temperature gradient is imposed such that the shear driven and buoyancy effects are of comparable magnitude then the resulting flow falls under the mixed convection regime and the interaction or coupling of these effects makes the analysis more complex. This problem has been studied in detail in the past, most of the research is directed toward the fluid mechanics studies (Aydin (1999), Aydin and wang (2000), Chamkha (2002), Gau and Sharif (2004) Luo and Yang (2007)). However, the mechanism of heat transfer under such flow in a lid-driven cavity with the insertion of a cylinder has not been investigated yet.

In the present chapter the major objective is to examine the effect of Joule heating in the coupling of conduction with magnetohydrodynamics mixed convection flow in a rectangular lid-driven cavity along with heat conducting horizontal cylinder. The governing equations along with appropriate boundary conditions for the present problem are first transformed into a non-dimensional form and the resulting non linear system of partial differential equations are then solved numerically using Galerkin's finite element method. The variation of streamlines, isotherms, average Nusselt number at the heated surface, average temperature of the fluid in the cavity and the temperature at the cylinder center for the various relevant dimensionless parameters Hartmann number Ha, Joule heating parameter J, Reynolds number Re, Richardson number Ri, Prandtl number Pr, solid-fluid thermal conductivity ratio K and various physical parameters i.e. the sizes and locations of the inner cylinder and aspect ratio of the cavity are shown graphically. In addition, numerical values of the average Nusselt number at the heated surface for the above mentioned parameters have been presented in tabular form.

The rest of this chapter is as follows. In section 4.1, the physical models of the current investigation are presented. Then the suitable mathematical model (both governing equations and boundary conditions) is considered in section 4 2. After that a brief description of solution method along with grid sensitivity test and validation of the numerical scheme are presented in the section 4.3. Subsequently parametric results are presented in the section 4.4. Finally, section 4.5 gives a summary of our conclusions

4.1 Physical Configurations

The physical configuration under consideration and coordinates chosen are depicted in figures 4.1 and 4.2. A Cartesian co-ordinate system is used with origin at the lower left corner of the computational domain. It is a two dimensional rectangular lid-driven cavity with a fixed amount of conducting solid material in the form of circular cylinder (case 1) and square cylinder (case 2). The left wall of the cavity is allowed to move upward in its own plane at a constant velocity U_0 and to be kept at a constant temperature T_c. Horizontal walls of the cavity are insulated while the right vertical wall is assumed to be heated isothermally at a constant temperature T_h.
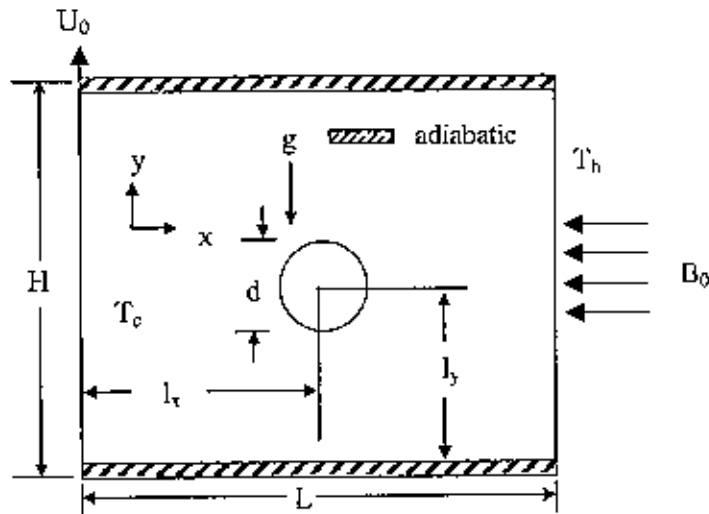
Figure 4.1: Schematic of the problem with the domain and boundary conditions for the case 1
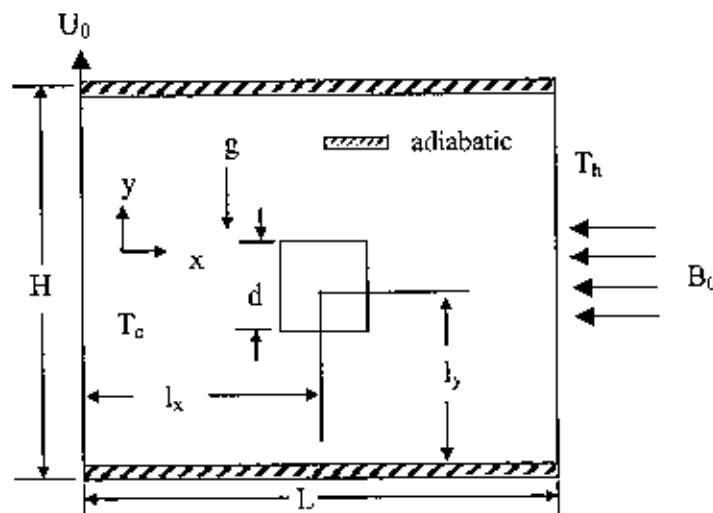
Figure 4.2: Schematic of the problem with the domain and boundary conditions for the case 2

In these figures, H and L are the height and length of the cavity respectively Here the fluid is assumed to be electrically conducting, all walls of the cavity are assumed to be electrically insulating. However, gravity acts in vertical directions and magnetic field is effective in the horizontal direction normal to the moving wall. The magnetic Re is assumed to be small so that the induced magnetic field is neglected and the Hall effects of magneto-hydrodynamics are to be negligible. All fluid physical properties

are assumed to be constant except the density variation in the body force term of the momentum equation according to the Boussinesq approximation. In addition, the effect of Joule heating is considered, but pressure work and viscous dissipation are assumed to be negligible.

4.2 Mathematical Formulation

The several steps of the mathematical formulation for the above problem are shown as follows

4.2.1 Governing Equations

Thermophysical properties of the fluid in the flow model are assumed to be constant except the density variations causing a body force term in the momentum equation. The Boussinesq approximation is invoked for the fluid properties to relate density changes to temperature changes and to couple in this way the temperature field to the flow field. The governing equations for steady mixed convection flow using conservation of mass, momentum, and energy modified to account for the presence of magnetic field, Joule heating term, and thermal conductivity of the solid can be written as

Continuity Equation

$$\frac{\partial u}{\partial x} + \frac{\partial v}{\partial y} = 0 \tag{4.1}$$

Momentum Equations

$$u\frac{\partial u}{\partial x} + v\frac{\partial u}{\partial y} = -\frac{1}{\rho}\frac{\partial p}{\partial x} + \upsilon\left(\frac{\partial^2 u}{\partial x^2} + \frac{\partial^2 u}{\partial y^2}\right) \tag{4.2}$$

$$u\frac{\partial v}{\partial x} + v\frac{\partial v}{\partial y} = -\frac{1}{\rho}\frac{\partial p}{\partial y} + \upsilon\left(\frac{\partial^2 v}{\partial x^2} + \frac{\partial^2 v}{\partial y^2}\right) + g\beta(T - T_c) - \frac{\sigma B_0^2 v}{\rho} \tag{4.3}$$

Energy Equations

$$u\frac{\partial T}{\partial x} + v\frac{\partial T}{\partial y} = \frac{k}{\rho c_p}\left(\frac{\partial^2 T}{\partial x^2} + \frac{\partial^2 T}{\partial y^2}\right) + \frac{\sigma B_0^2 v^2}{\rho c_p} \tag{4.4}$$

For solid

$$0 = \frac{k_s}{\rho c_p} \left(\frac{\partial^2 T_s}{\partial x^2} + \frac{\partial^2 T_s}{\partial y^2} \right) \tag{4 5}$$

where x and y are the coordinate directions. The variables u, v, p, T, and T_s are the fluid velocity components in the x and y directions, pressure, fluid temperature and solid temperature respectively. The parameters β, ρ, k, k_s, σ, c_p, g, B_0 are the fluid volumetric thermal expansion coefficient, fluid density, thermal conductivity of the fluid, thermal conductivity of the solid, electrical conductivity, the fluid specific heat, the acceleration due to gravity, magnetic induction respectively.

4.2.2 Boundary Conditions

The boundary conditions for the present problem can be written as follows:

At the left wall: $u = 0, v = U_0, T = T_c$

At the heated right vertical wall: $u = 0, v = 0, T = T_h$

At the cylinder surface: $u = 0, v = 0$

At the top and bottom walls: $u = 0, v = 0, \frac{\partial T}{\partial n} = 0$

At the fluid-solid interface: $\left(\frac{\partial T}{\partial n} \right)_{fluid} = \frac{k_s}{k} \left(\frac{\partial T_s}{\partial n} \right)_{solid}$

where n is the non-dimensional distances either along x or y direction acting normal to the surface and k and k_s are the thermal conductivity of the fluids and the solid respectively.

Heat transfer rate is measure by local and average value of Nusselt number. Local Nusselt number at the heated surface of the cavity defined by Cengel (2007) is calculated by using the equations:

$$Nu_l = h(y) L / k$$

The average value of Nusselt number is calculated by integrating the local value over the total length of the hot wall using the relation

$$Nu = \frac{1}{L_s} \int_0^{L_s} Nu_j \, dy$$

where L_s and $h(y)$ are the length and the local convection heat transfer coefficient of the heated wall respectively.

4.2.3 Dimensional Analysis

The following dimensionless variables are used for making the governing equations (4.1–4.5) in dimensionless from as:

$$X = \frac{x}{L}, Y = \frac{y}{L}, U = \frac{u}{U_0}, V = \frac{v}{U_0}, P = \frac{p}{\rho U_0^2}, D = \frac{d}{L}, L_x = \frac{l_x}{L}, L_y = \frac{l_y}{L},$$

$$\theta = \frac{(T - T_c)}{(T_h - T_c)}, \theta_s = \frac{(T_s - T_c)}{(T_h - T_c)}$$

where X and Y are the coordinates varying along horizontal and vertical directions, respectively, U and V are, the velocity components in the X and Y directions, respectively, θ and θ_s are the dimensionless temperature of fluid and solid respectively, and P is the dimensionless pressure.

Introducing the above dimensionless dependent and independent variables into the governing equations (4.1–4.5) yields the following equations

Continuity Equation

$$\frac{\partial U}{\partial X} + \frac{\partial V}{\partial Y} = 0 \tag{4.6}$$

Momentum Equations

$$U \frac{\partial U}{\partial X} + V \frac{\partial U}{\partial Y} = -\frac{\partial P}{\partial X} + \frac{1}{Re} \left(\frac{\partial^2 U}{\partial X^2} + \frac{\partial^2 U}{\partial Y^2} \right) \tag{4.7}$$

$$U \frac{\partial V}{\partial X} + V \frac{\partial V}{\partial Y} = -\frac{\partial P}{\partial Y} + \frac{1}{Re} \left(\frac{\partial^2 V}{\partial X^2} + \frac{\partial^2 V}{\partial Y^2} \right) + Ri\theta - \frac{Ha^2}{Re} V \tag{4.8}$$

Energy Equations

$$U\frac{\partial\theta}{\partial X}+V\frac{\partial\theta}{\partial Y}=\frac{1}{Re\,Pr}\left(\frac{\partial^2\theta}{\partial X^2}+\frac{\partial^2\theta}{\partial Y^2}\right)+JV^2 \qquad (4.9)$$

$$0=\frac{K}{RePr}\left(\frac{\partial^2\theta_s}{\partial X^2}+\frac{\partial^2\theta_s}{\partial Y^2}\right) \qquad (4.10)$$

where

$$Re=U_0L/\upsilon,\,Gr=g\beta\Delta TL^3/\upsilon^2,\;Ha^2=\sigma B_0^2L^2/\mu,\;J=\sigma B_0^2LU_0/\rho C_p\Delta T,$$
$$Pr=v/\alpha,\;Ri=Gr/Re^2\;and\;K=k_s/k_f$$

(here $\Delta T=T_h-T_c$ and $\alpha=k/\rho C_p$ are the temperature difference and thermal diffusivity respectively) are the Reynolds number, Grashof number, square of the Hartmann number, Joule heating parameter, Prandtl number, Richardson number and solid fluid thermal conductivity ratio respectively.

The dimensionless boundary conditions of the present problem under consideration can be written as follows:

At the left wall: $U=0,V=1,\theta=0$

At the heated right vertical wall: $U=0,V=0,\theta=1$

At the cylinder surface: $U=0,V=0$

At the top and bottom walls: $U=0,\,V=0,\,\frac{\partial\theta}{\partial N}=0$

At the fluid-solid interface: $\left(\frac{\partial\theta}{\partial N}\right)_{fluid}=K\left(\frac{\partial\theta_s}{\partial N}\right)_{solid}$

Where N is the non-dimensional distances either along X or Y direction acting normal to the surface.

The average Nusselt number at the heated wall of the cavity based on the dimensionless quantities may be expressed by $Nu=-\int_0^1\frac{\partial\theta}{\partial X}dY$ and the average temperature of the fluid in the cavity is defined by $\theta_{av}=\int\theta\,d\overline{V}/\overline{V}$, where $\overline{V}$ is the cavity volume as recommended by Singh and Sharif (2003).

4.3 Numerical Analysis

In this section numerical method adopted in the present study is discussed briefly.

4.3.1 Solution Method

The solution of the governing equations along with initial and boundary conditions are solved through the Galerkin finite element formulation. The continuum domain is divided into a set of non-overlapping regions called elements. Six node triangular elements with quadratic interpolation functions for velocity as well as temperature and linear interpolation functions for pressure are utilized to discretize the physical domain. Moreover, interpolation functions in terms of local normalized element coordinates are employed to approximate the dependent variables within each element. Substitution of the obtained approximations into the system of the governing equations and boundary conditions yields a residual for each of the conservation equations. These residuals are reduced to zero in a weighted sense over each element volume using the Galerkin method. Details of this method have already been discussed in the Chapter 3.

4.3.2 Grid Size Sensitivity Test

In order to determine the proper grid size for this study, a grid independence test are conducted for the case 1 with $Re = 100$, $Ri = 1.0$, $K = 5.0$, $D = 0.2$ and $Pr = 0.71$. The following five types of mesh are considered for the grid independence study. These grid densities are 24427 nodes, 3774 elements; 29867 nodes, 4640 elements; 37192 nodes, 5814 elements; 38229 nodes, 5968 elements and 48073 nodes, 7524 elements The extreme value of the average Nusselt number Nu, that relates to the heat transfer rate of the heated surface and average and average temperature θ_m of the fluid in the cavity are used as a sensitivity measure of the accuracy of the solution and are selected as the monitoring variables for the grid independence study. Table 4.1 shows the dependence of the quantities Nu and θ_{av} on the grid size and the computational time. Considering both the accuracy of the numerical values and the computational time, the following calculations are performed with 38229 nodes and 5968 elements grid system.

Table 4.1: Grid Sensitivity Check at $Re = 100$, $Ri = 1.0$, $K = 5.0$, $D = 0.2$ and $Pr = 0.71$ for the case 1

Nodes (elements)	24427 (3774)	29867 (4640)	37192 (5814)	38229 (5968)	48073 (7524)
Nu	1.022636	1.022643	1.022650	1.022651	1.022651
θ_{av}	0.525566	0.525567	0.525566	0.525567	0.525567
Time (s)	226.265	292.594	388.157	421.328	627.375

The present numerical technique will discretize the computational domain into unstructured triangles by Delaunay Triangular method. The Delaunay triangulation is a geometric structure that has enjoyed great popularity in mesh generation since the mesh generation was in its infancy. In two dimensions, the Delaunay triangulation of a vertex set maximizes the minimum angle among all possible triangulations of that vertex set. The mesh modes for the present numerical computation are shown in figures 4.3. Mesh generation has been done meticulously.

Case 1   Case 2
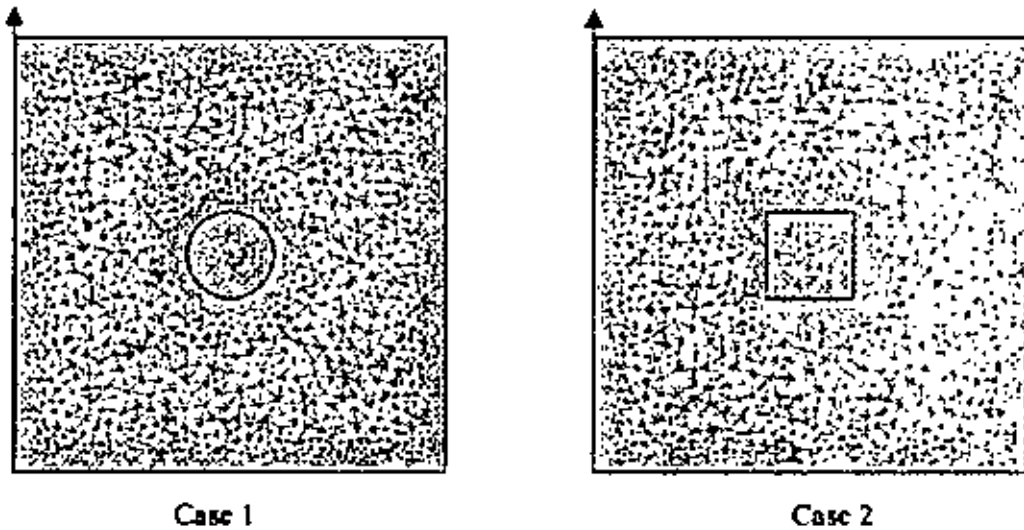
Figure 4.3: Grid used for numerical simulations at the case 1 and case 2.

94

4.3.3 Validation of the Numerical Scheme

To validate the present numerical scheme, a two-dimensional lid-driven square cavity flow problem Chamkha (2002) has been solved and compared. The enclosure geometry treated in Chamkha (2002) is a two-dimensional lid-driven square cavity filled with an electrically conducting fluid that generates or absorbs heat at a rate. The left wall is moving upward with a velocity and maintained at cooled condition. The right wall is hooted whereas the two horizontal walls are under adiabatic condition. In the present work numerical predictions, using the modified numerical scheme, have been obtained for Hartmann number between 0.0 to 50 0 and Grashof number between 10^2 to 10^5. The comparison of the results obtained by the present numerical scheme with those of Chamkha (2002) for average Nusselt number (at the hot wall) are shown in Tables 4.2 and 4.3. The computed results are in very good agreement with the Chamkha (2002) solution.

Table 4.2: Comparison of the present data with those of Chamkha (2002) for Ha

Parameter Ha	Present study Nu	Chamkha (2002) Nu	Error (%)
0.0	2.2069	2.2692	2.75
10.0	2.1132	2.1050	0.82
20.0	1.8206	1.6472	10.53
50.0	1.1862	0.9164	29 44

Table 4.3: Comparison of the present data with those of Chamkha (2002) for Gr

Parameter Gr	Present study Nu	Chamkha (2002) Nu	Error (%)
10^2	1.0298	0.9819	4.88
10^3	1.1059	1.0554	4.78
10^4	1.5231	1.4604	4.29
10^5	2.4622	2.3620	4.24

4.4 Results and Discussion

As stated earlier, the overall objective of the current chapter is to explore the conjugate effects of conduction and laminar mixed convection heat transfer in a lid-driven cavity in the presence of a magnetic field, Joule heating and heat conducting horizontal cylinder. The implications of varying the Reynolds number Re, Richardson number Ri, Prandtl number Pr, Hartmann number Ha, Joule heating parameter J, solid fluid thermal conductivity ratio K and physical parameters for the system are the cavity aspect ratio AR, cylinder diameter and locations of the inner cylinder in the cavity will be emphasized. The results are presented in terms of streamline and isotherm patterns at the three different regimes of flow, viz., pure forced convection, mixed convection and dominating natural convection with $Ri =$ 0.0, 1.0 and 5.0 respectively. The variations of the average Nusselt number at the heated surface, average fluid temperature in the cavity and temperature at the cylinder are plotted for the different values of the parameters. Moreover, the variation of the average Nusselt number at the heated surface is also highlighted in tabular form.

4.4.1 Effect of Cylinder Diameter

The effect of cylinder diameter (placed at the center of the cavity) on the flow fields as streamlines in a square cavity operating at three different values of Ri, while the values of K, Re, Ha, Pr, and J are keeping fixed at 5.0, 100, 10.0, 0.71 and 1 0 are presented in the figure 4.4 for the circular cylinder situation (case 1) and the square cylinder situation (case 2). As well known from the literature, the values of the Richardson number is a measure of the importance of natural convection to forced convection. First, in the case 1, figure 4.4 (a) shows that the forced convection plays a dominant role and the recirculation flow is mostly generated only by the moving lids at low Ri ($Ri = 0.0$) and D ($D = 0.0$). The recirculation flow rotates in the clockwise direction, which is expected since the lid is moving upwards. Further at low Ri ($Ri = 0.0$) and the higher values of D ($D = 0.2$, 0.4 and 0.6), the flow patterns inside the cavity remain unchanged except the shape and position of the core of the circulatory flow. Next at $Ri = 1.0$, the natural convection effect is comparable with

the forced convection effect, a pair of counter rotating rolls appear in the flow domain for the lower values of D (D = 0.0, 0.2 and 0.4), whereas the fluid flow is characterized by a clockwise rotating vortex generated by the movement of the left wall and two minor counter clockwise vortices generated by the buoyant force at the highest value of D (D = 0.6). This behavior is very logical because the large cylinder reduces the available space for the buoyancy-induced recirculation. Further at Ri = 5.0, which is a buoyancy dominated regime, the counter clockwise rotating roll due to buoyancy force grows rapidly as a result the clockwise rotating roll due to shear driven flow becomes weaker and smaller at the four different values of D (D = 0 0, 0.2, 0 4 and 0.6) considered. Now in the case 2, it is clearly observed from the figure 4.4 (b) that the distribution of streamlines are almost similar at the lower values of D (D = 0.0 and 0.2) and have significant difference at the higher values of D (D = 0.4 and 0.6) for all values of Ri, compared with that for the case 1 as shown in figure 4.4 (a).

The corresponding effect of the cylinder diameter on thermal fields as isotherms at various values of Ri is shown in the figure 4.5 for the abovementioned two cases. In both of the cases, we can ascertain that for Ri = 0.0 and D = 0.0, the isothermal lines near the hot wall are parallel to the heated surface and parabolic shape isotherms are seen at the left top corner in the cavity, which is similar to forced convection and conduction like distribution. Making a comparison of the isothermal lines for the higher values of D (D = 0.2, 0.4 and 0.6) with those for the case of without cylinder (D = 0.0) at Ri = 0.0, a significant difference is found at the left top corner in the cavity for the aforementioned two cases. Further for Ri = 1.0 and the case of without cylinder (D = 0.0), the isothermal lines are nearly parallel to the vertical walls in the cavity and parabolic shape isotherms at the left top corner in the cavity becomes insignificant. Furthermore, similar trend is observed in the isotherms for different values of D at Ri = 1.0, which is due to the conjugate effect of conduction and mixed convection flow in the cavity. As Ri increases further from 1.0 to 5.0, the isothermal lines near the cold wall are almost parallel to the vertical walls and parabolic shape isotherms are developed at the right top corner in the cavity, which is owing to the strong influence of the convective current in the cavity.
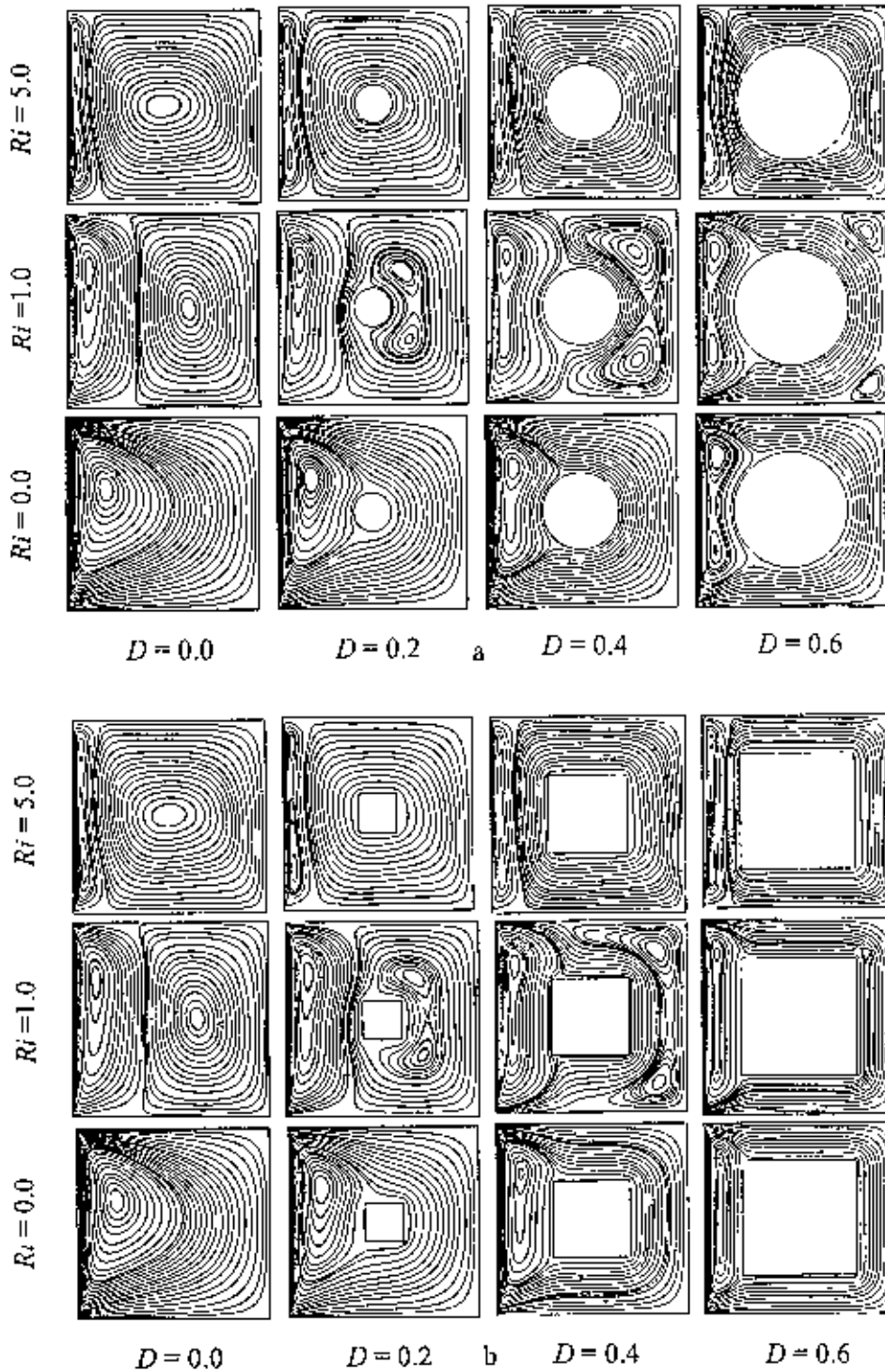
Figure 4.4: Streamlines for the (a) case 1 and (b) case 2 at different values of cylinder diameter D and Richardson number Ri, while $AR = 1.0$, $Re = 100$, $Ha = 10.0$, $J = 1.0$, $L_x = L_y = 0.5$, $K = 5.0$ and $Pr = 0.71$.
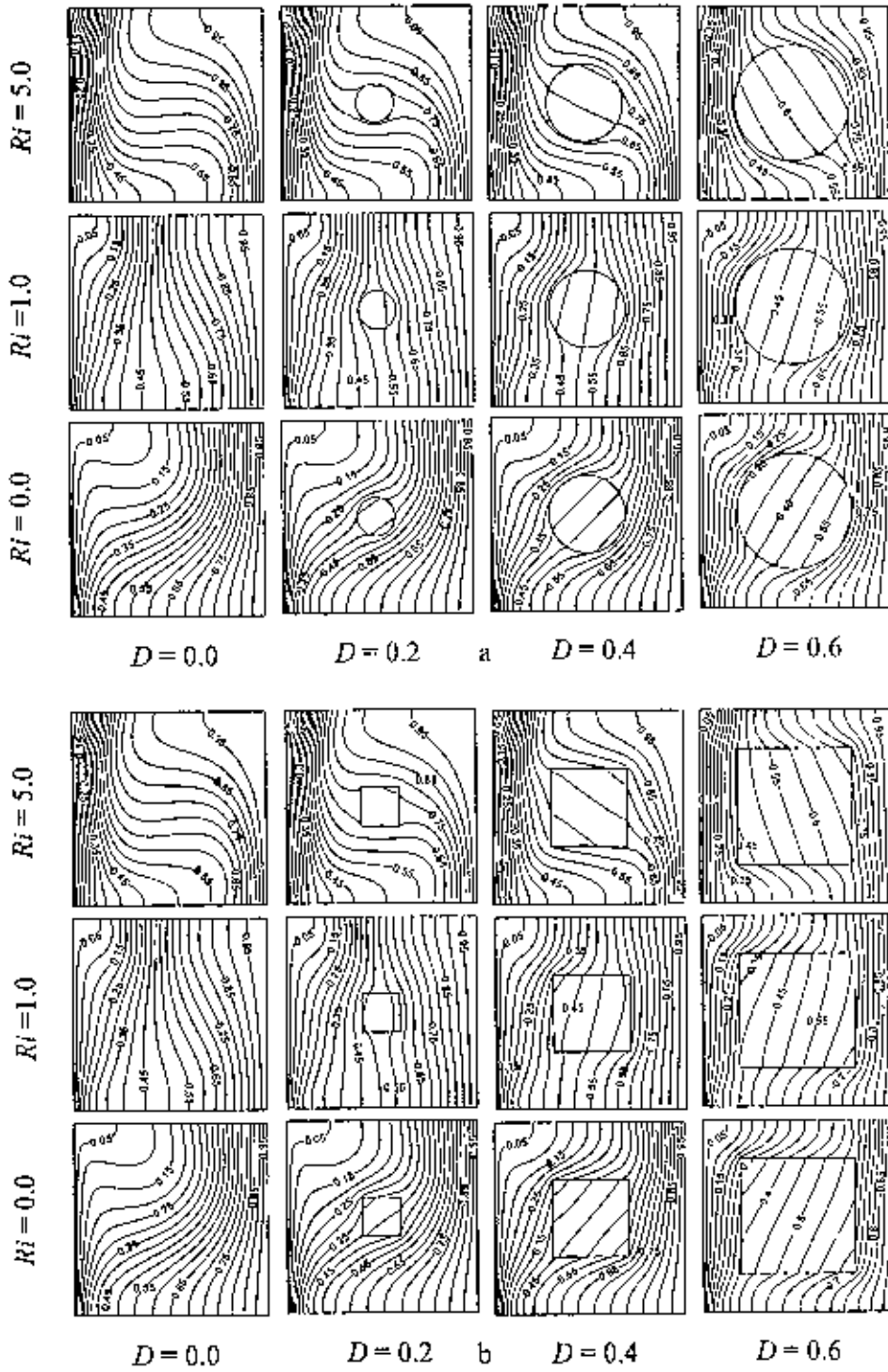
Figure 4.5: Isotherms for the (a) case 1 and (b) case 2 at different values of cylinder diameter D and Richardson number Ri, while $AR = 1.0$, $Re = 100$, $Ha = 10.0$, $J = 1.0$, $L_x = L_y = 0.5$, $K = 5.0$ and $Pr = 0.71$.
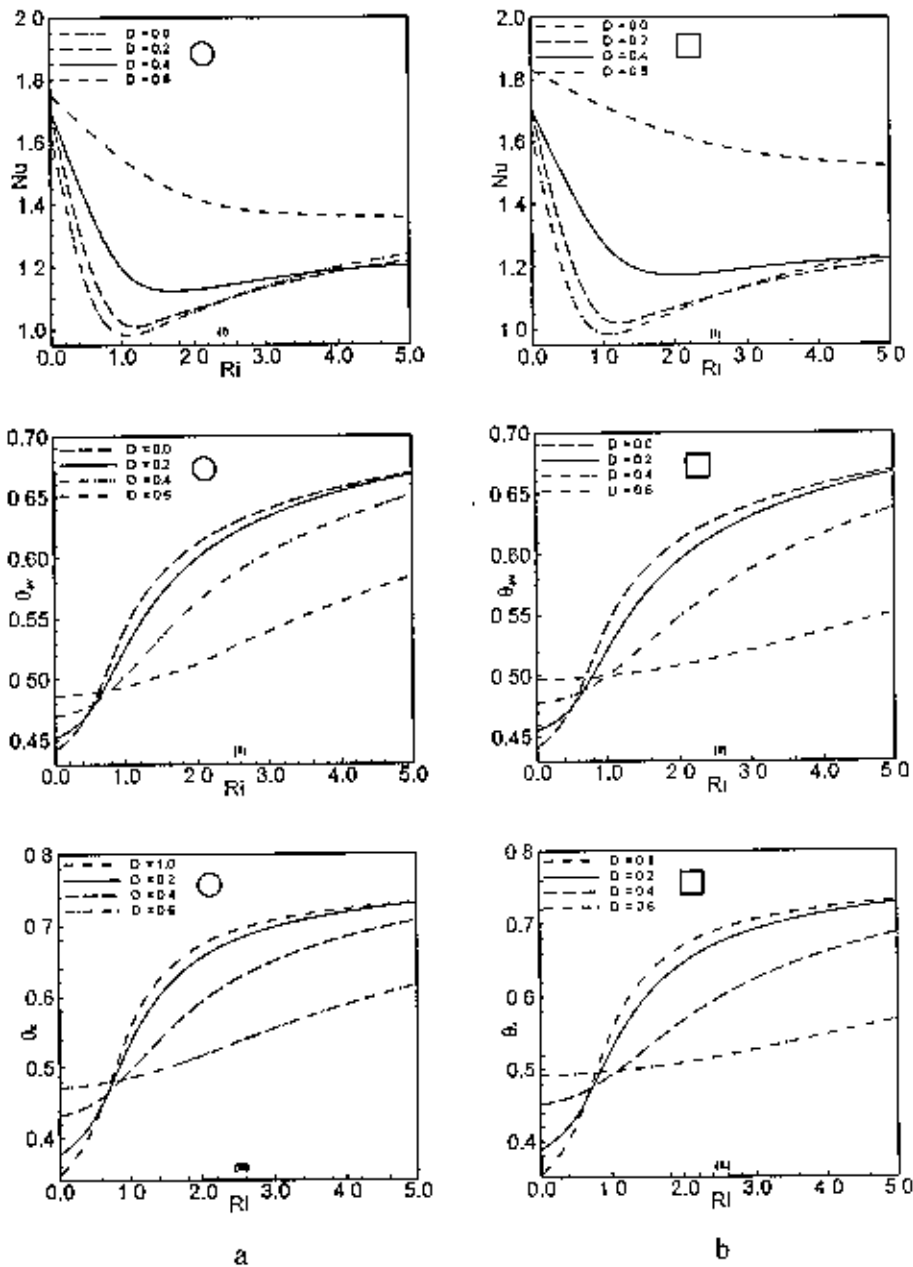
Figure 4.6: Effect of cylinder diameter D on (i) average Nusselt number, (ii) average fluid temperature and (iii) temperature at the cylinder center for (a) case 1 and (b) case 2. while $AR = 1.0$, $Re = 100$, $Ha = 10.0$, $J = 1.0$, $L_x = L_y = 0.5$, $Pr = 0.71$ and $K = 5.0$.

Table 4.4 (a): Variation of average Nusselt number with cylinder diameter for the case 1

Ri	Nu			
	$D = 0.0$	$D = 0.2$	$D = 0.4$	$D = 0.6$
0.0	1.643882	1.710726	1.706358	1.753162
0.5	1.141781	1.239607	1.410516	1.645498
1.0	0.985516	1.022651	1.195203	1.547871
1.5	1.009741	1.028463	1.127099	1.471043
2.0	1.055573	1.064352	1.126294	1.419329
2.5	1.099580	1.100379	1.142134	1.389025
3.0	1.137945	1.132416	1.159809	1.373009
3.5	1.170392	1.159872	1.175287	1.365026
4.0	1.197434	1.182924	1.187559	1.360839
4.5	1.219715	1.201949	1.196579	1.357858
5.0	1.237833	1.217358	1.202627	1.354560

Table 4.4 (b): Variation of average Nusselt number with cylinder diameter for the case 2

Ri	Nu			
	$D = 0.0$	$D = 0.2$	$D = 0.4$	$D = 0.6$
0.0	1.643882	1.712326	1.706780	1.830880
0.5	1.141781	1.260904	1.469466	1.771889
1.0	0.985516	1.034922	1.278355	1.715880
1.5	1.009741	1.034097	1.189873	1.665830
2.0	1.055573	1.068257	1.171764	1.623963
2.5	1.099580	1.103024	1.179114	1.591151
3.0	1.137945	1.133777	1.192075	1.566817
3.5	1.170392	1.159927	1.204092	1.549360
4.0	1.197434	1.181688	1.213212	1.536788
4.5	1.219715	1.199469	1.219018	1.527199
5.0	1.237833	1.213701	1.221634	1.519032

In addition, the convective distortion in the isothermal lines near the right top corner in the cavity gradually decreases with increasing the values of D for both of the mentioned cases. This behavior is very logical because the larger cylinder reduces the buoyancy force effects. From these figures it also seen that cylinder shapes have insignificant effects on isothermal lines at each values of Ri.

The variation of the average Nusselt number (Nu) at the heated surface, average temperature (θ_{av}) of the fluid in the cavity and temperature (θ_c) at the cylinder center against Ri at various values of D is shown in the figure 4.6 for the aforementioned cases. From these figures it is observed that in the pure forced convection region ($Ri = 0.0$) the values of Nu is the top for the highest value of D but the values of Nu decreases very quickly in the forced convection dominated region and increases gradually in the free convection dominated region at the lower values of D ($D = 0.0$, 0.2 and 0.4). On the other hand, the average Nusselt number (Nu) decreases mildly with increasing Ri for the highest value of D and maximum average Nusselt number is always found at the highest D for both the aforesaid cases. This is also supported from the obtained actual numerical values of Nu as shown in the Tables 4.4 (a) and 4.4 (b). From these Tables it is also observed that the values of Nu for case 1 is quantitatively lesser compared to that for the case 2 at the higher values of D, owing to poor mixing and heat transfer from the isothermal wall. However, average temperature (θ_{av}) of the fluid in the cavity and temperature at the cylinder center increases slightly at the highest D ($D = 0.6$) and rapidly at lower values of D ($D = 0.0$, 0.2 and 0.4) with increasing Ri for both of the abovementioned cases.

4.4.2 Effect of Solid Fluid Thermal Conductivity Ratio

The flow fields in terms of computed streamlines for the four representative values of the solid fluid thermal conductivity ratio K ($K = 0.2$, 1.0, 5 0 and 10.0), while $AR = 1.0$, $Re = 100$, $D = 0.2$, $L_x = L_y = 0.5$, $Ha = 10.0$, $J = 1.0$ and $Pr = 0.71$ are shown in figure 4.7 for the case of circular cylinder and the case of square cylinder. For $Ri = 0.0$ and $K = 0.2$, it is be seen from the figures 4.7 that a unicellular clockwise vortex is developed in the cavity for both of the cases, due to the only shear force induced by the left moving wall.

Figure 4.7: Streamlines for the (a) case 1 and (b) case 2 at different values of thermal conductivity ratio K and Richardson number Ri, while $AR = 1.0$, $Re = 100$, $Ha = 10.0$, $J = 1.0$, $L_x = L_y = 0.5$, $D = 0.2$ and $Pr = 0.71$.
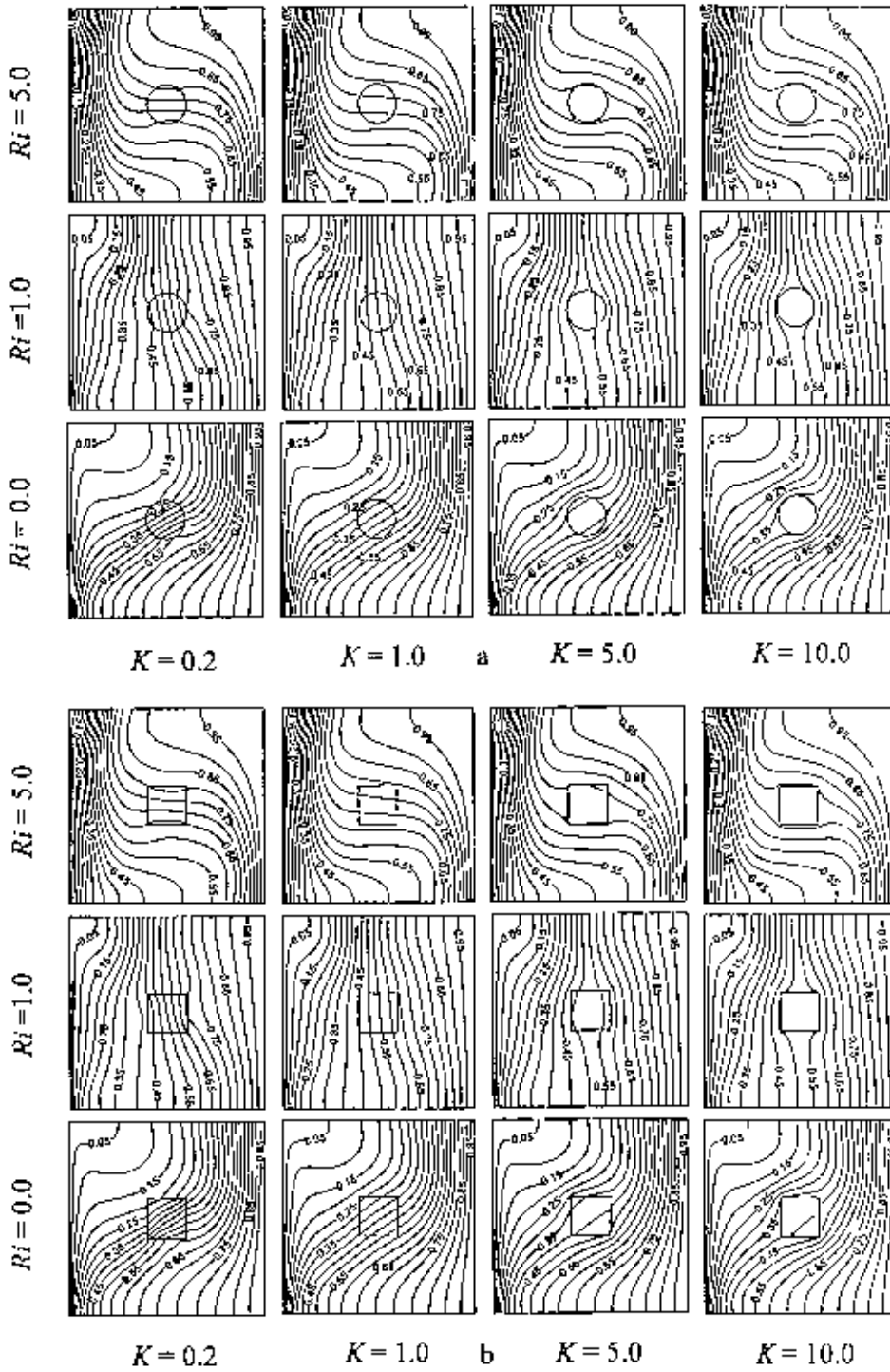
Figure 4.8: Isotherms for the (a) case1 and (b) case 2 at different values of thermal conductivity ratio K and Richardson number Ri, while $AR = 1.0$, $Re = 100$, $Ha = 10.0$, $J = 1.0$, $L_x = L_y = 0.5$, $D = 0.2$ and $Pr = 0.71$.

However, the streamlines for the four values of K at $Ri = 0.0$ appear to be almost identical. This behavior is rational because thermal conductivity of the solid has negligible effect in flow field. Now for $Ri = 1.0$ and $K = 0.2$, it can be seen from the figure 4.7 that a pair of counter rotating vortices are formed in the flow domain, of which the clockwise vortex near the left wall is small in size than the counter clockwise vortex near the right wall. It is also observed that the counter clockwise vortex is two-cellular. In addition, visual examination of the streamlines does not reveal any significant difference among the different values of K at $Ri = 1.0$, owing to the same reason as stated beforehand. Further at $Ri = 5.0$ and different values of K it is clearly seen that the counter clockwise vortex spreads and thereby squeezes the clockwise vortex, indicating a sign of supremacy of natural convection in the cavity. It is also seen that the streamline plots are independent of the thermal conductivity ratios K. In addition, the cylinder shape has insignificant effect on streamlines at the pure forced convection region and has significant effect on streamlines at the pure mixed convection and free convection dominated region.

Now from the figure 4.8 it is reminder that the thermal conductivity of the inner cylinder affects strongly the isotherm structures in both of the cases At low $Ri = 0.0$ and $K = 0.2$, the isotherms near the hot wall are parallel to the vertical walls and the isothermal lines start to turn back towards the hot wall near the left top corner of the cavity, which gives a clear indication that a conduction dominated heat transfer at the vicinity of the hot wall and higher forced convection and conduction dominated heat transfer in the upper part of the cavity. Making a comparison of the isothermal lines for different values of K at $Ri = 0.0$, no significant difference is found except the shift of the isothermal lines from the center of the inner cylinder As Ri increases from 0.0 to 1.0, the distortion in isothermal lines become immaterial, as a result the isotherms become parallel to the vertical walls, indicating the comparable effect of the conduction and mixed convection mechanisms. As Ri increases further to 5.0, convective distortion of the isotherms occur throughout the cavity due to the strong influence of the convective current in the cavity. In this case it is also seen that a thermal boundary layer is developed near the cold wall for the four different values of K. However, the effects of the cylinder shape on isotherms are not noticeable.

Figure 4.9: Effect of thermal conductivity K on (i) average Nusselt number, (ii) average fluid temperature and (iii) temperature at the cylinder center for (a) case 1 and (b) case 2, while $AR = 1 0$, $Re = 100$, $Ha = 10.0$, $J = 1.0$, $L_x = L_y = 0.5$, $Pr = 0.71$ and $D = 0.2$.

Table 4.5 (a): Variation of average Nusselt number with solid fluid thermal conductivity ratio for the case 1

Ri	Nu			
	$K = 0.2$	$K = 1.0$	$K = 5.0$	$K = 10.0$
0.0	1.735829	1.722377	1.710726	1.708439
0.5	1.136467	1.187800	1.239607	1.251436
1.0	0.950693	0.981962	1.022651	1.033299
1.5	1.015338	1.018857	1.028463	1.031755
2.0	1.078242	1.069832	1.064352	1.063740
2.5	1.128226	1.113792	1.100379	1.097649
3.0	1.168726	1.150669	1.132416	1.128377
3.5	1.202060	1.181486	1.159872	1.154919
4.0	1.229628	1.207111	1.182924	1.177271
4.5	1.252361	1.228240	1.201949	1.195726
5.0	1.270942	1.245442	1.217358	1.210650

Table 4.5 (b): Variation of average Nusselt number with solid fluid thermal conductivity ratio for the case 2

Ri	Nu			
	$K = 0.2$	$K = 1.0$	$K = 5.0$	$K = 10.0$
0.0	1.742490	1.725562	1.712326	1.709784
0.5	1.131933	1.195332	1.260904	1.277769
1.0	0.934124	0.977425	1.034922	1.051808
1.5	1.008590	1.016403	1.034097	1.040593
2.0	1.079863	1.071453	1.068257	1.068680
2.5	1.134641	1.117716	1.103024	1.099981
3.0	1.177762	1.155640	1.133777	1.128537
3.5	1.212499	1.186784	1.159927	1.153146
4.0	1.240778	1.212332	1.181688	1.173735
4.5	1.263829	1.233166	1.199469	1.190574
5.0	1.282502	1.249960	1.213701	1.204016

Average Nusselt number (Nu) at the hot wall, average fluid temperature (θ_{av}) in the cavity and temperature at the cylinder center (θ_c) is plotted as a function of Richardson number at four different values of solid fluid thermal conductivity ratio (K) is shown in the figure 4.9 for the aforesaid two cases. Concentrating on each plot separately for a particular values of K, the trend of the values of Nu are decreasing with increasing Ri up to 1.0 and beyond these values of Ri, the values of Nu is found to increases gradually with Ri. However, in the pure forced convection ($Ri = 0.0$) the value of Nu is highest for the lowest value of K, in the forced convection dominated region it is the top for the highest values of K and beyond these values of Ri, the average Nusselt number Nu is also the peak at the lowest value of K, which are documented in the Tables 4.5 (a-b). Referring to these Tables, markedly different values of Nu are found due to the cylinder shape at the four values of K and the three different flow regimes. Finally, from these figures it is also observed that the average temperature (θ_{av}) of the fluid in the cavity and the temperature (θ_c) at the cylinder center increase monotonically with Ri.

4.4.3 Effects of Hartmann Number

The influence of Hartmann number Ha on the flow patterns at three different values of Ri is shown in the figure 4.10 for the case 1 and case 2, where $AR = 1.0$, $Re = 100$, $K = 5.0$, $D = 0.2$, $J = 1.0$, $L_x = L_y = 0.5$ and $Pr = 0.71$ are kept fixed. In the absence of the magnetic field ($Ha = 0.0$) and the natural convection effect ($Ri = 0.0$), the fluid flow is characterized by a primary rotating uni-cellular vortex of the size of the cavity generated by the movement of the left wall. Again for $Ri = 0.0$ and the different higher values of Ha (10.0, 20.0 and 50.0), it is evident from these figures that the size of the vortex remain unchanged, but the core of the vortex shifted towards the left top corner of the cavity with increasing Ha up to 20.0 and the core divided into two parts located at the bottom and top corner near the left wall at the highest value of $Ha = 50.0$. When natural convection and forced convection become equally dominant, namely $Ri = 1.0$, the fluid flow is characterized by a clockwise rotating vortex generated by the movement of the left wall and two minor counter clockwise vortices generated by the buoyant force at the highest value of $Ha = 50.0$.
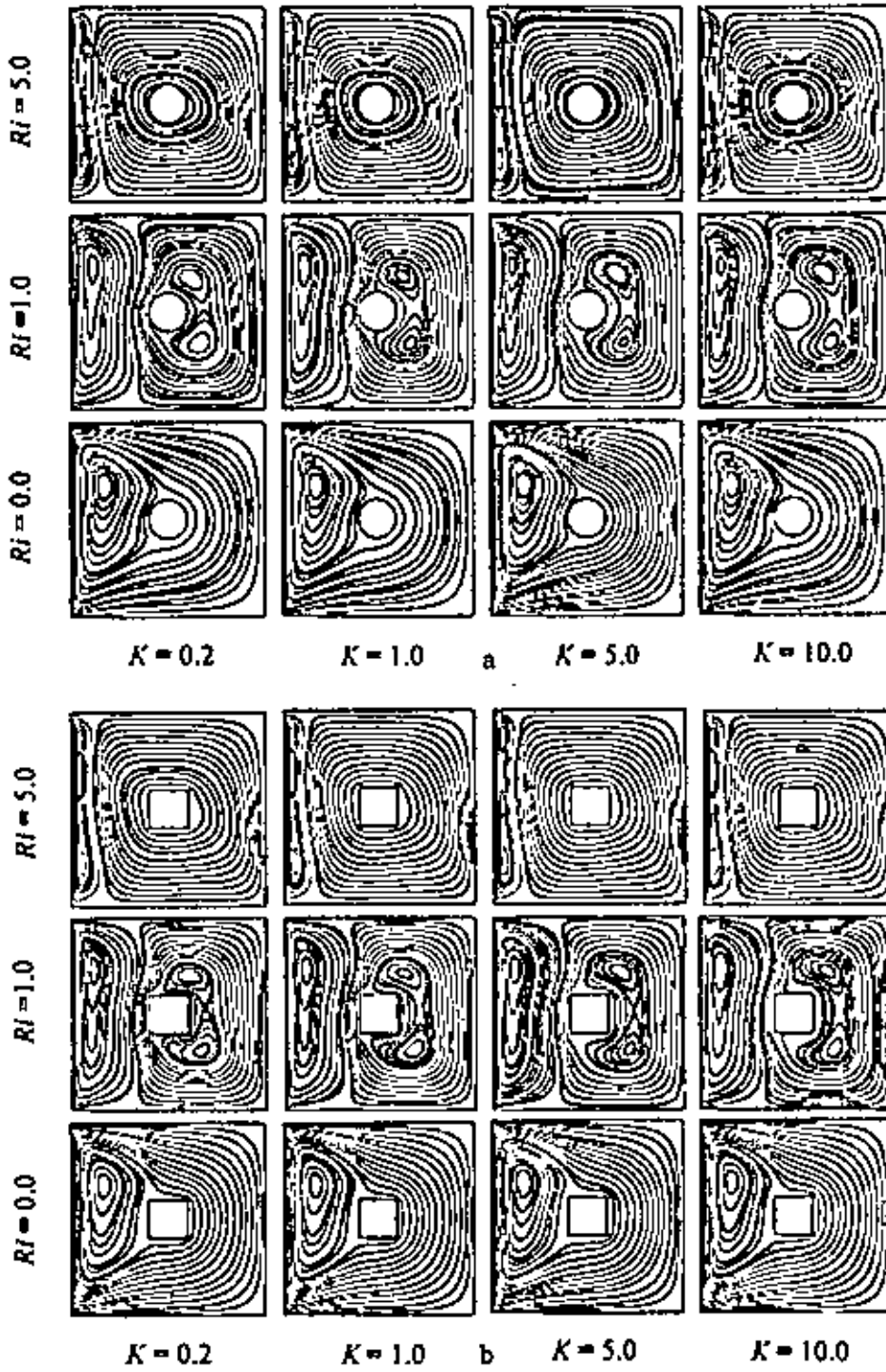
Figure 4.10: Streamlines for the (a) case 1 and (b) case 2 at different values of Hartmann number Ha and Richardson number RI, while $AR = 1.0$, $Re = 100$, $J = 1.0$, $L_x = L_y = 0.5$, $Pr = 0.71$, $K = 5.0$ and $D = 0.2$.
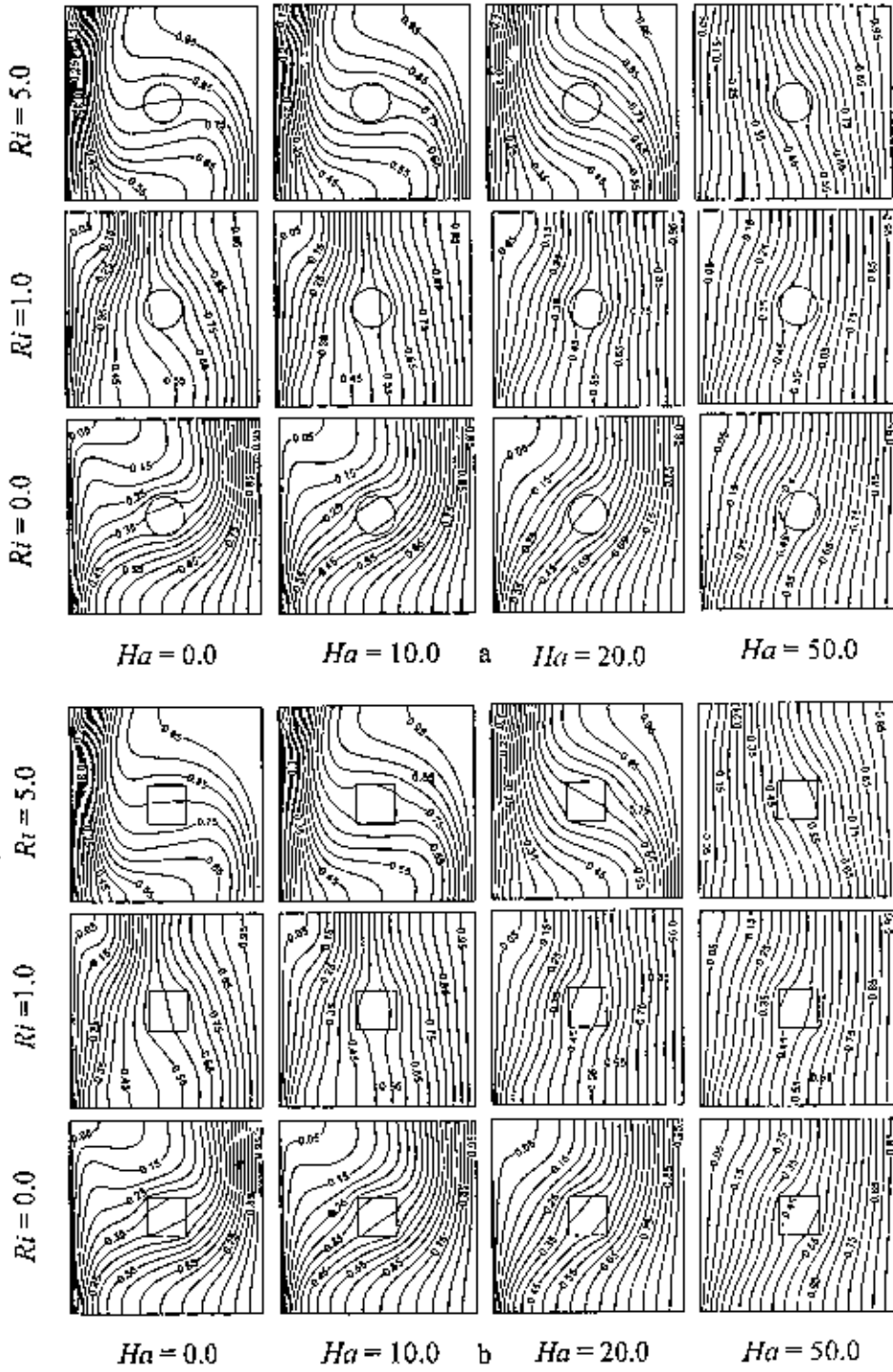
Figure 4.11: Isotherms for the (a) case 1 and (b) case 2 at different values of Hartmann number Ha and Richardson number Ri, while $AR = 1.0$, $Re = 100$, $J = 1.0$, $L_x = L_y = 0.5$, $Pr = 0.71$, $K = 5.0$ and $D = 0.2$

As *Ha* decreases from 50.0 to 20.0, the minor counter clockwise vortices merge into a two cellular single one and become comparatively large, as a result the clockwise rotating vortex become smaller in size. Furthermore, the size of the clockwise vortex decreases and counter clockwise vortex increases with decreasing *Ha* at *Ri* = 1.0. This is because application of a transverse magnetic field has the tendency to slow down the movement of the buoyancy-induced flow in the cavity. Further when *Ri* = 5.0, the effect of natural convection is far more compared to the forced convection effect, consequently the size of the counter clockwise vortices at *Ri* = 5.0 are larger than that at *Ri* = 1.0. It is also note that slight differences in streamlines are found between the abovementioned two cases.

The corresponding effects of Hartmann number *Ha* on the isotherms is shown in the figures 4.11 for the two aforesaid cases. From these figures it can be seen easily that the isotherms are almost parallel to the vertical walls for the highest value of *Ha* (*Ha* = 50.0) at the three values of *Ri*, indicating that most of the heat transfer process is carried out by conduction. However, some deviations in the conduction dominated isothermal lines are initiated near the left top surface of the cavity for the value of *Ha* = 20.0 at *Ri* = 0.0. The distortion of the isotherms near the left top surface of the cavity increases quickly with decreasing values of *Ha* at *Ri* = 0.0. From these figures, it is also be seen that the isothermal lines are dominated by conduction and mixed convection heat transfer in the cavity for different *Ha* at *Ri* = 1.0. Although the isotherms are almost parallel to the vertical surface for the highest value of *Ha* at *Ri* = 5.0, but the isotherms are drastically changed with decreasing the values of *Ha* at *Ri* = 5.0. Moreover, the formation of the thermal boundary layer near the left cold wall is to be initiated here for the lower values of *Ha* at *Ri* = 5.0. This is owing to the dominating influence of the convective current in the cavity. Furthermore, no major differences in isotherms are found between the two aforementioned cases.

The effects of Hartmann number on average Nusselt number (*Nu*) at the hot wall, average temperature (θ_{av}) of the fluid in the cavity and the temperature (θ_c) at the cylinder center for the case of circular cylinder and the case of square cylinder along with Richardson number is shown in the figure 4.12, while *AR* = 1.0, *Re* = 100, *K* = 5.0, *D* = 0.2, $L_x = L_y = 0.5$, *J* = 1.0 and *Pr* = 0.71.
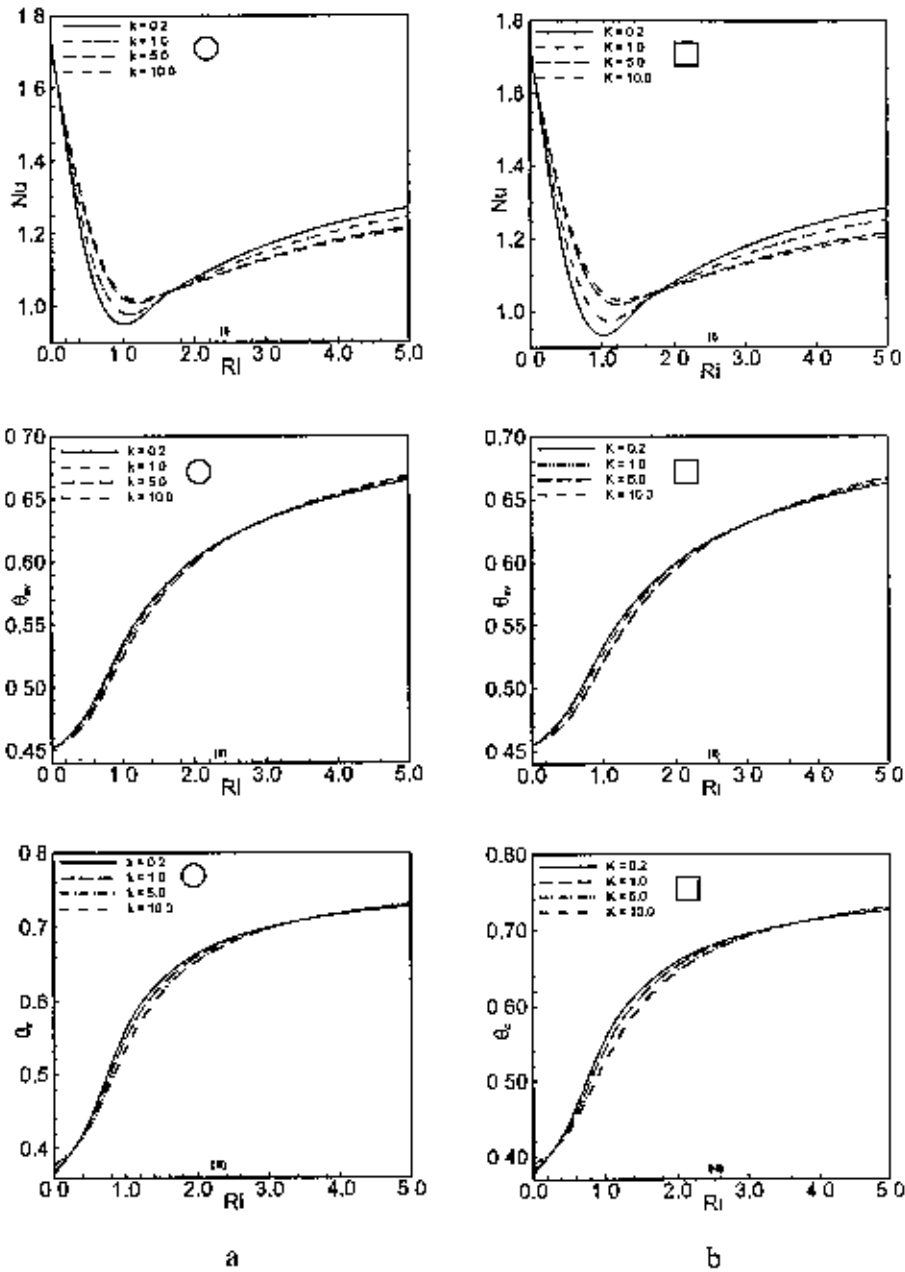
Figure 4.12: Effect of Hartmann number *Ha* on (i) average Nusselt numbers, (ii) average fluid temperature and (iii) temperature at the cylinder center for the (a) case 1 and (b) case 2, while $AR = 1.0$, $Re = 100$, $J = 1.0$, $L_x = L_y = 0.5$, $Pr = 0.71$ and $D = 0.2$.

Table 4.6 (a): Variation of average Nusselt number with Hartmann number for the case 1

Ri	Nu			
	$Ha = 0.0$	$Ha = 10.0$	$Ha = 20.0$	$Ha = 50.0$
0.0	1.915505	1.710726	1.453429	1.163656
0.5	1.178991	1.239607	1.238799	1.129542
1.0	0.971513	1.022651	1.090087	1.100485
1.5	0.951170	1.028463	1.040413	1.077260
2.0	0.942201	1.064352	1.055125	1.060369
2.5	0.941420	1.100379	1.096165	1.049969
3.0	0.945165	1.132416	1.144865	1.045867
3.5	0.950924	1.159872	1.193686	1.047576
4.0	0.957196	1.182924	1.239733	1.054409
4.5	0.963109	1.201949	1.281993	1.065591
5.0	0.968160	1.217358	1.320236	1.080339

Table 4.6 (b): Variation of average Nusselt number with Hartmann number for the case 2

Ri	Nu			
	$Ha = 0.0$	$Ha = 10.0$	$Ha = 20.0$	$Ha = 50.0$
0.0	1.916441	1.712326	1.458135	1.175298
0.5	1.212084	1.260904	1.252004	1.142403
1.0	0.984203	1.034922	1.105978	1.114291
1.5	0.969411	1.034097	1.052516	1.091673
2.0	0.961875	1.068257	1.062562	1.075018
2.5	0.959547	1.103024	1.100104	1.064485
3.0	0.960528	1.133777	1.146354	1.059919
3.5	0.963127	1.159927	1.193424	1.060894
4.0	0.966226	1.181688	1.238171	1.066798
4.5	0.969116	1.199469	1.279425	1.076922
5.0	0.971356	1.213701	1.316859	1.090543

From these figures, it is observed that the average Nusselt number (Nu) goes down very rapidly with increasing Ri in the forced convection dominated region and goes up gradually with increasing Ri in the free convection dominated region for the lower values of Ha (0.0, 10.0 and 20.0). But the average Nusselt number (Nu) decreases mildly with increasing Ri for the highest value of Ha (Ha = 50.0). On the other hand, the values of Nu is the uppermost in the pure forced convection (Ri = 0.0) at Ha = 0.0, in the mixed convection region (Ri = 1.0) at Ha = 50.0 and in the natural convection dominated region at Ha = 20.0. However, the average temperature (θ_{av}) of the fluid in the cavity and temperature (θ_c) at the cylinder center increases sharply with Ri for the lower values of Ha (0.0, 10.0 and 20.0) and increase very slowly with Ri at the highest value of Ha. Last of all, the quantitative differences of the values of Nu at different values of Ha between the two aforementioned cases are listed in the Tables 4.6 (a) and 4.6 (b). From these tables it is found that the values of Nu for the case 1 are slightly lower than that for the case 2 only at the highest value of Ha.

4.4.4 Effects of Joule Heating Parameter

The flow fields in terms of computed streamlines for the both case 1 and 2 at the four representative values of the dimensionless Joule heating parameter J (J = 0.0, 1.0, 5.0 and 7.5) is shown in the figure 4.13. Plots are shown for AR = 1.0, Re = 100, K = 5.0, D = 0.2, $L_x = L_y$ = 0.5, Ha = 10.0, Pr = 0.71 and Ri = 0.0, 1.0 and 5.0 for each case. In the absence of free convection effects (Ri = 0.0) the flow exhibits a simple clockwise recirculation pattern, which becomes concentrated along the cold moving wall for all values of J. As Ri increases from 0.0 to 1.0, two counter rotating cells appear in the cavity at all values of J, i.e. the fluid flow in the cavity is established by a relatively balanced interaction of the two driving mechanisms. Finally, for Ri = 5.0, which is a buoyancy dominated regime, the counter clockwise circulating cell on the right grows further and occupies most of the part of the cavity at J = 0.0, as a result the clockwise cell becomes weaker and smaller. A similar phenomena is also observed at Ri = 5.0 and J = 1.0. However, for Ri = 5.0 and J = 5.0, another clockwise circulating cell is developed at the right top corner in the cavity. It is also seen that the third cell increases significantly at the highest value of J (J = 7.5). Moreover, the streamlines for both of the aforementioned cases are almost identical
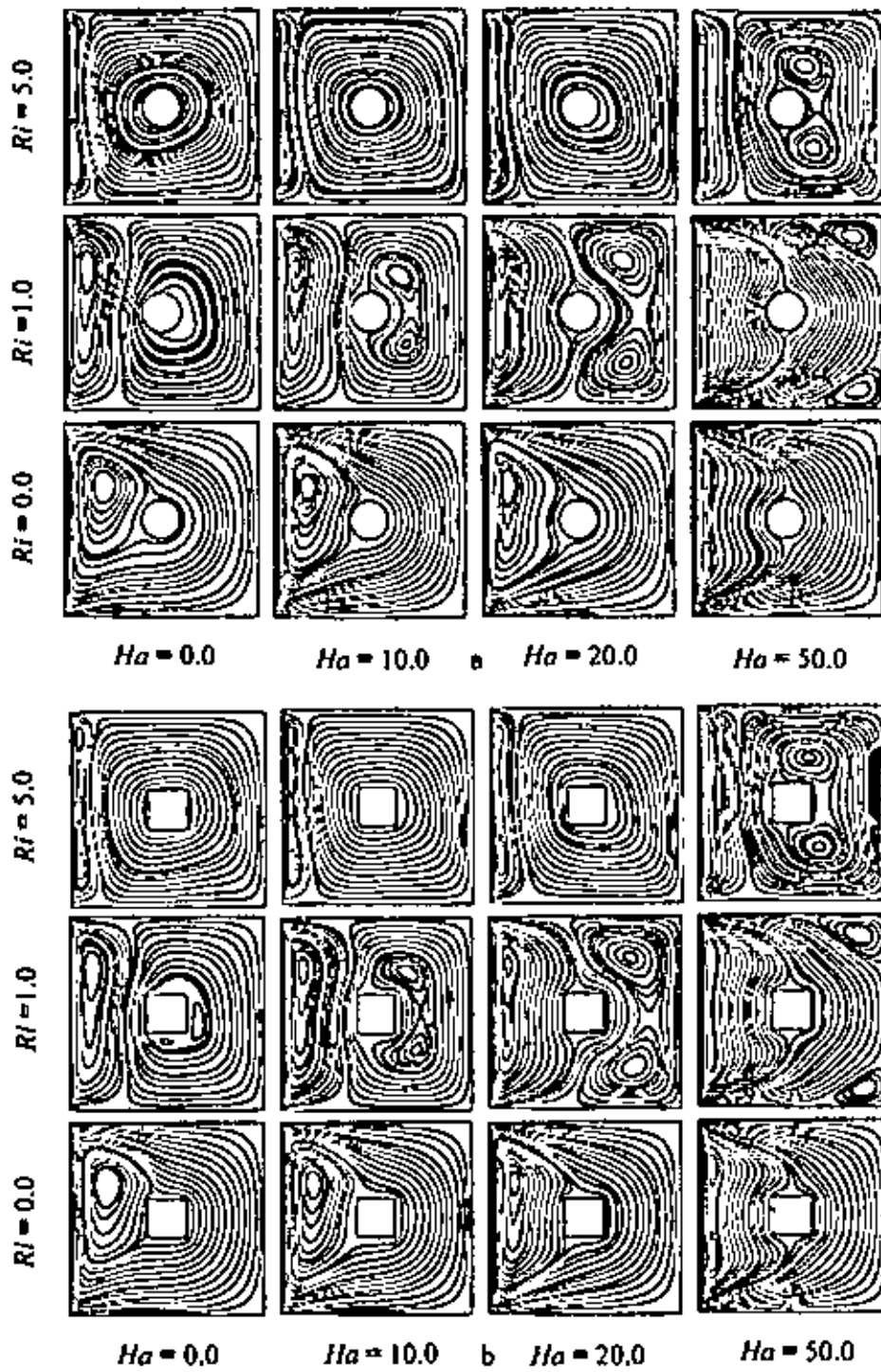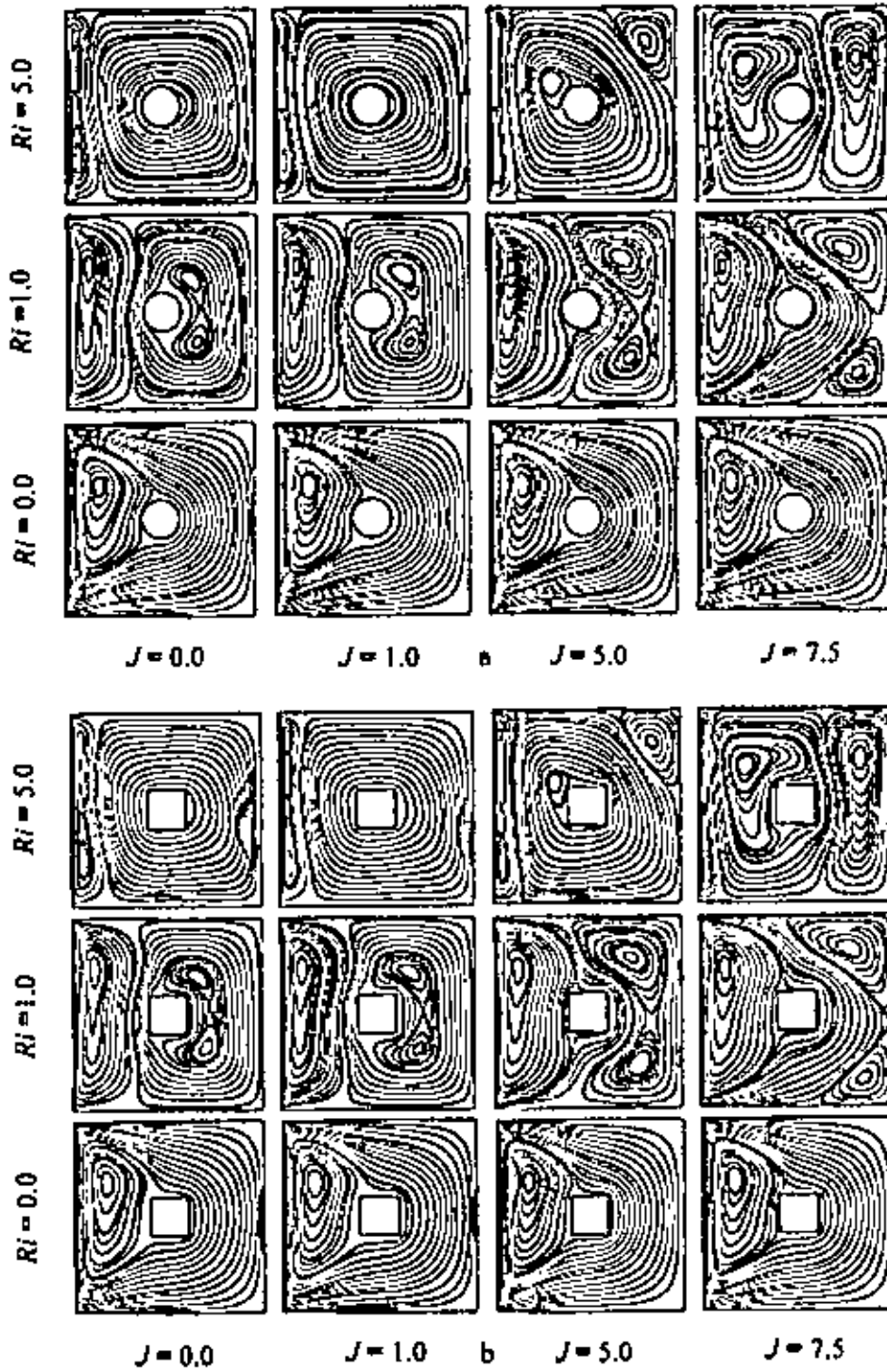
Figure 4.13: Streamlines for the (a) case 1 and (b) case 2 at different values of Joule heating parameter J and Richardson number Ri, while $AR = 1.0$, $Re = 100$, $Ha = 10.0$, $L_x = L_y = 0.5$, $K = 5.0$, $D = 0.2$ and $Pr = 0.71$.

Figure 4.14: Isotherms for the (a) case 1 and (b) case 2 at different values of Joule heating parameter J and Richardson number Ri, while $AR = 1.0$, $Re = 100$, $Ha = 10.0$, $L_x = L_y = 0.5$, $K = 5.0$, $D = 0.2$ and $Pr = 0.71$.

Figure 4.14 illustrate the isotherms for the case 1 and case 2 at different values of Joule heating parameter J and Ri (Ri = 0.0, 1.0 and 5.0), while AR = 1.0, Re = 100, K = 5.0, Ha = 10.0, L_x = L_y = 0.5, Pr = 0.71]. From these figures, it is seen that conductive distortion of isothermal lines start to appear at the vicinity of the heated surface and upper part of the cavity at the lower values of J (J = 0.0 and 1.0) and Ri = 0.0. But the conductive distortion in the isothermal lines become disappears and convective current becomes active with increasing the values of Joule heating parameter J at Ri = 0.0, as a result isothermal lines are concentrated at the cold wall with a clear indication of the existence of thermal spots. The isothermal lines at Ri = 1.0 and lower values of J (J = 0.0 and 1.0) are nearly parallel to the vertical walls of the cavity, which gives a clear indication of conduction and mixed convection dominated heat transfer in the cavity. Further, the isothermal lines at Ri = 1.0 and higher values of J (J = 5.0 and 7.5) start to turn back (convective distortion) towards the cold wall near the top wall due to the dominating influence of the convective current. Finally, at Ri = 5.0, the convective distortion of isothermal lines occurs throughout the cavity for all values of J due to the strong influence of the convective current. Moreover, in this case the extreme convective distortion in isotherms is observed at the higher values of J. In addition, the effect of cylinder shape on isotherms is trivial for all values of J and Ri.

In order to evaluate how the presence of Joule heating in the cavity affects the heat transfer rate along the hot wall, average Nusselt number (Nu) is plotted as a function of Richardson number Ri in the figure 4.15 for the above two cases at the four different values of Joule heating parameters J. It is observed that average Nusselt number decreases very slowly with the increase of Ri in the forced convection dominated region and increases gradually with Ri in the free convection dominated region for J = 0.0. Further, the values of Nu decreases with increasing Ri in the forced convection dominated region and become independent of Ri in the free convection dominated region for J = 1.0. But for the higher values of J, the values of Nu decreases with increasing Ri. It is also note that Nu is always higher at J = 0.0 for the two cases, which is expected. Figure 4.15 also explain the average temperature of the fluid (θ_{av}) in the cavity and temperature at the cylinder center (θ_c) as a function of Richardson number (Ri) for the two cases at different values of J.
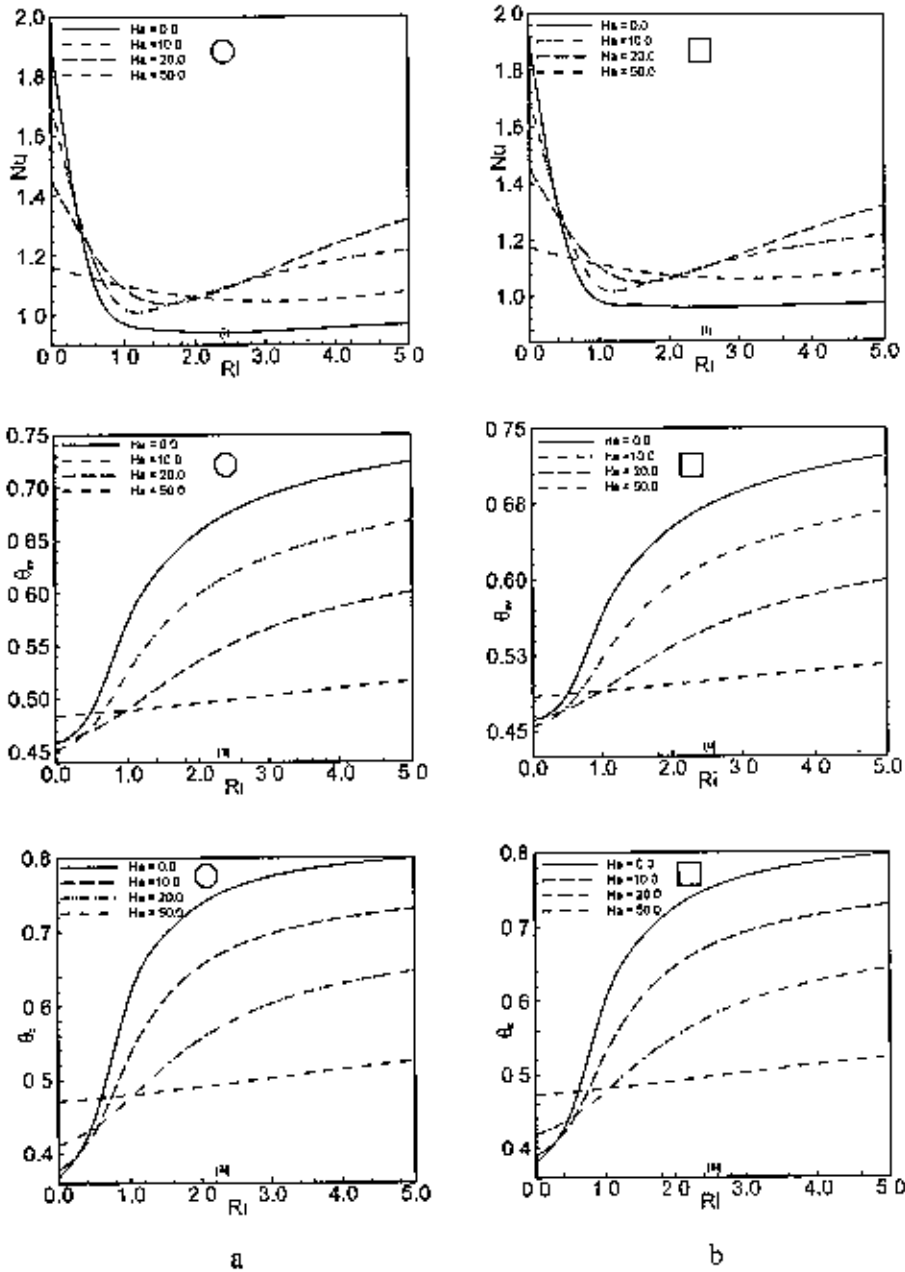
Figure 4.15: Effect of Joule heating parameter J on (i) average Nusselt number, (ii) average fluid temperature and (iii) temperature at the cylinder center for the (a) case 1 and (b) case 2, while $AR = 1.0$, $Re = 100$, $Ha = 10.0$, $L_x = L_y = 0.5$, $K = 5.0$, $Pr = 0.71$ and $D = 0.2$.

Table 4.7 (a): Variation of average Nusselt number with Joule heating parameter for the case 1

Ri	Nu			
	$J = 0.0$	$J = 1.0$	$J = 5.0$	$J = 7.5$
0.0	1.896161	1.710726	0.968986	0.505398
0.5	1.323444	1.239607	0.873431	0.584622
1.0	1.224756	1.022651	0.650031	0.718246
1.5	1.391699	1.028463	0.387293	0.332607
2.0	1.562487	1.064352	0.165841	0 098974
2.5	1 715601	1.100379	0.001544	-0.100411
3.0	1.853496	1.132416	-0 116069	-0.248419
3.5	1.979290	1.159872	-0.196830	-0.367913
4.0	2.095305	1.182924	-0.249595	-0.566521
4.5	2.203237	1.201949	-0.284071	-3.700918
5.0	2.304356	1.217358	-0.310494	-7.869844

Table 4.7 (b): Variation of average Nusselt number with Joule heating parameter for the case 2

Ri	Nu			
	$J = 0.0$	$J = 1.0$	$J = 5.0$	$J = 7.5$
0.0	1.899899	1.712326	0.962035	0.493103
0.5	1.344722	1.260904	0.883866	0.587414
1.0	1.218293	1.034922	0.683504	0.542879
1.5	1.376441	1.034097	0.435438	0.374161
2.0	1.548035	1.068257	0.209266	0.146429
2.5	1.703224	1.103024	0.028319	-0.068742
3.0	1.843106	1.133777	-0.109801	-0.244820
3.5	1.970588	1.159927	-0.210907	-0.394927
4.0	2.087981	1.181688	-0.281762	-0.637893
4.5	2.197012	1.199469	-0.331545	-3.627633
5.0	2.298994	1.213701	-0.371923	-7.928919

The values of θ_{av} and θ_c are increases mildly with increasing Ri at the lower values of J ($J = 0.0$ and 1.0) also increase steeply with increasing Ri at the higher values of J ($J = 5.0$ and 7.5). Moreover, the values of θ_{av} and θ_c are found minimum for the lowest value of J, which are very logical. Although the overall trends of the streamlines, isotherms, average Nusselt number, average fluid temperature and temperature at the cylinder center are the same, some differences in the values of Nu between the mentioned two cases are tabulated in the Tables 4.7 (a) and 4.7 (b).

4.4.5 Effect of Reynolds Number

The fluid flow patterns inside the cavity for the case 1 and case 2 are presented in terms of streamlines in the figure 4.16 at the four values of Reynolds number Re ($Re = 50, 100, 150,$ and 200) and the three different values of Ri ($Ri = 0.0, 1.0$ and 5.0), while $AR = 1.0$, $K = 5.0$, $D = 0.2$, $L_x = L_y = 0.5$, $Ha = 10.0$, $J = 1.0$, $Pr = 0.71$. As expected due to the upward motion of the left wall fluid rise up along the side of the cold vertical wall and flow down along the right vertical wall forming a roll with clockwise rotation inside the cavity for the four values of Re at $Ri = 0.0$. It is also observed that the orientation of the core in the recirculation cell changes as Reynolds number Re changes. Next at $Ri = 1.0$, two counter rotating cells are developed in the cavity for all values of Re, which indicates both the buoyant force and the shear driven force are present in the cavity. In this folder at low $Re = 50$ the clockwise cell, which is due to shear driven force occupies most of the part of the cavity and two small anticlockwise rotating cells due to buoyant force are developed at the bottom and top corner in the cavity near the right wall. However, as Re increases the anticlockwise rotating cells come together into one and become large in size. It is also seen from the right column of these figures, that size of the anticlockwise rotating cell increases sharply and thereby squeezes the clockwise cell, indicating a sign of supremacy of natural convection in the cavity at $Ri = 5.0$ and different Re. However, in both of the aforementioned cases, a little influence on the streamlines by the cylinder shapes is observed.

Now we draw the attention to see the effect of increasing Reynolds number Re on the temperature distribution in the cavity.
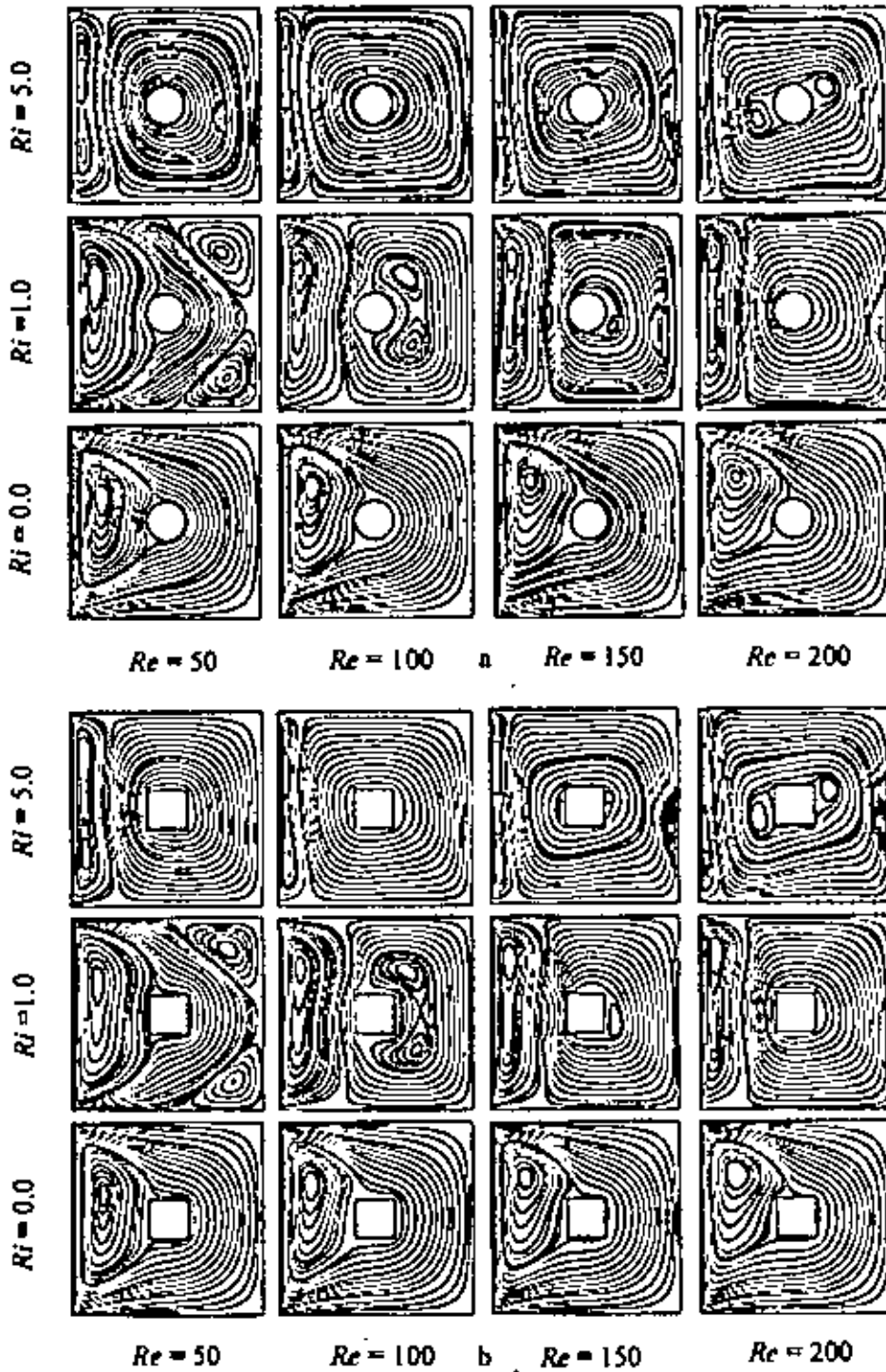
Figure 4.16: Streamlines for the (a) case 1 and (b) case 2 at different values of Reynolds number Re and Richardson number Ri, while $AR = 1.0$, $Ha = 10.0$, $J = 1.0$, $L_x = L_y = 0.5$, $K = 5.0$, $D = 0.2$ and $Pr = 0.71$.
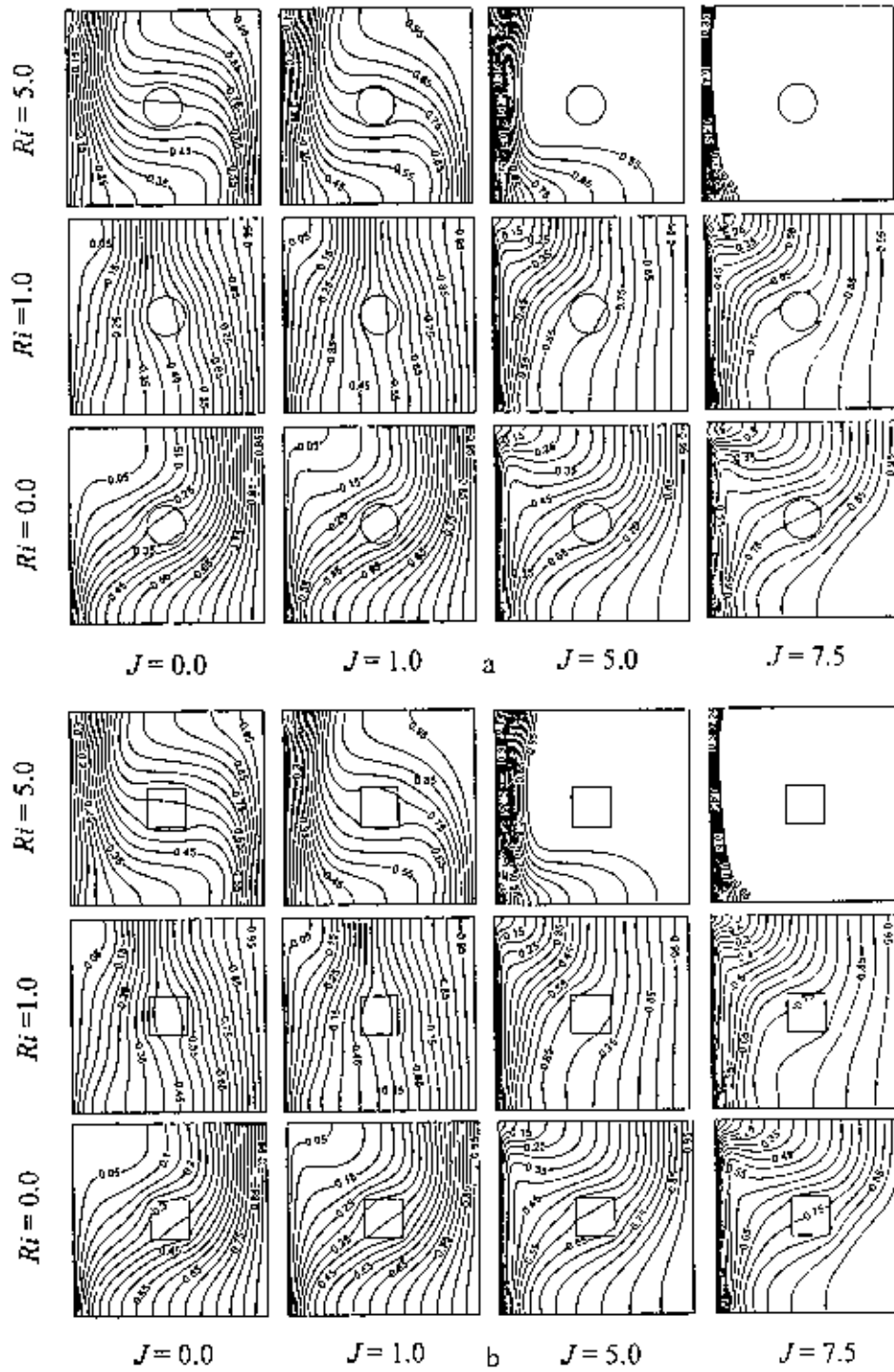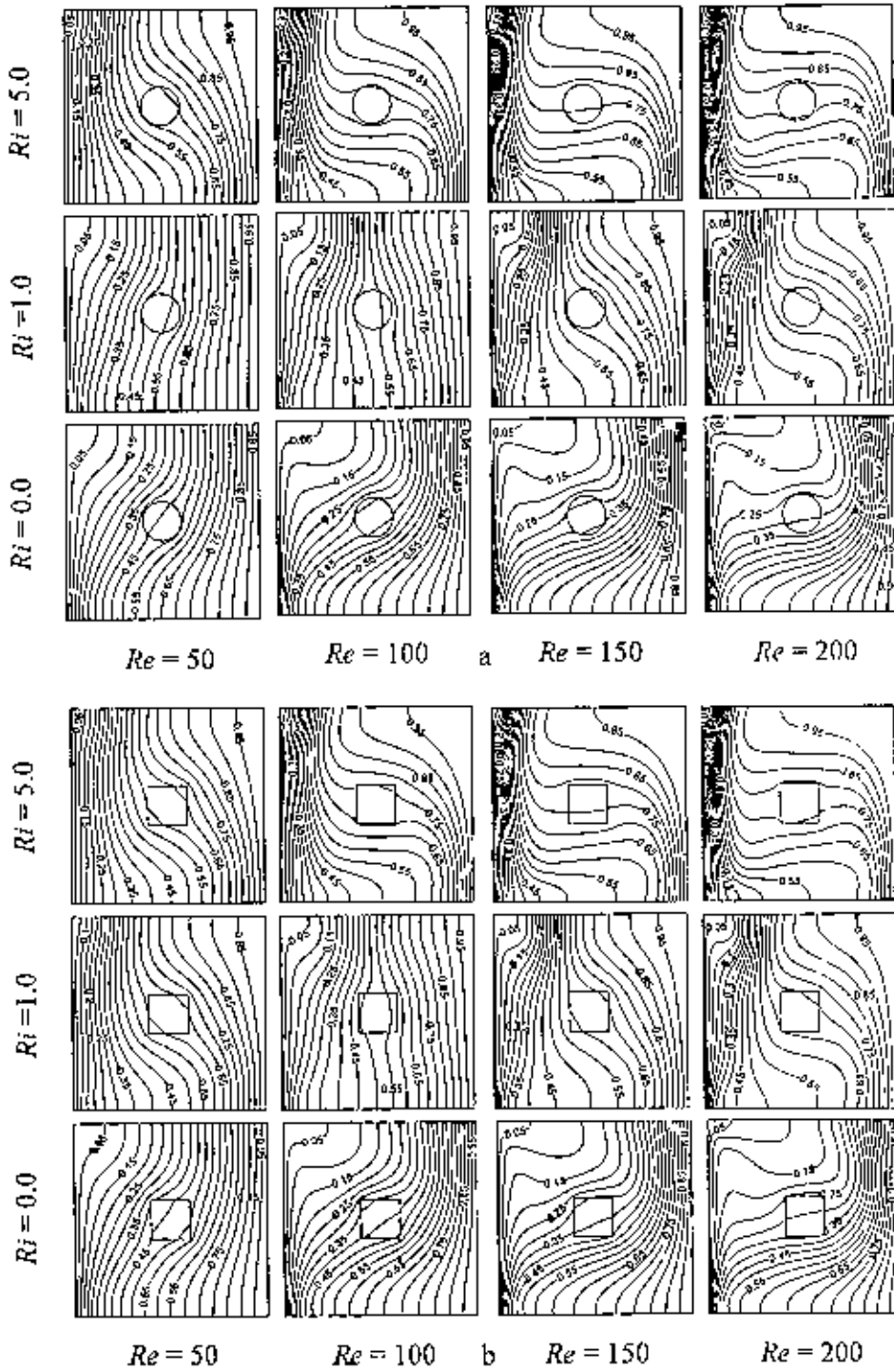
Figure 4.17: Isotherms for the (a) case 1 and (b) case 2 at different values of Reynolds number Re and Richardson number Ri, while $AR = 1.0$, $Ha = 10.0$, $J = 1.0$, $L_x = L_y = 0.5$, $K = 5.0$, $D = 0.2$ and $Pr = 0.71$.

From the figures 4.17, it can be seen that isothermal lines are nearly parallel to the hot wall at $Re = 50$ and $Ri = 0.0$ for both of the cases, which is similar to conduction-like distribution. It is also seen that isothermal lines start to turn back from the cold wall to the hot wall near the top wall at $Ri = 0.0$ and $Re = 50$ due to the dominating influence of conduction and forced convection in the upper part of the cavity. More significant distortion in isothermal lines near the left top corner of the cavity are observed at the higher values of Re. Further at $Ri = 1.0$, both the buoyant force and the shear force are same order of magnitude, the isotherm patterns reflects a conductive pattern of energy transfer at the lower values of Re ($Re = 50$, 100) and a convective pattern of energy transfer at the higher values of Re ($Re = 150$, 200) for both of the cases. On the other hand, the convective distortion of isothermal lines start to appear at $Re = 50$ and $Ri = 5.0$. Next at $Ri = 5.0$ and $Re = 100$, it is seen that the isothermal lines turn back towards the left cold wall near the top of the cavity and a thermal boundary layer is developed near the left vertical (cold) wall due to the dominating influence of the convective current in the upper part of the cavity. Finally at $Ri = 5.0$, the convective distortion in the isotherms become more and the thermal boundary layer near the cold wall becomes more concentrated with further increasing the values of Reynolds number due to the strong influence of the convective current. However, the streamlines and isotherms for the mentioned two cases appear to be almost identical at different values of Reynolds number.

The effect of Reynolds number on average Nusselt number (Nu) at the heat source, average fluid temperature (θ_{av}) in the cavity and the temperature (θ_c) at the cylinder center are displayed as a function of Richardson number at some particular Reynolds number in figure 4.18 for the aforesaid two shapes of cylinder. It is observed that in both of the cases the average Nusselt number at the hot wall decreases very sharply in the forced convection dominated region and increases gradually in the free convection dominated region with increasing Ri for the higher values of Reynolds number Re ($Re = 100$, 150 and 200), but is different for the lowest value of Reynolds number Re ($Re = 50$). However, maximum values of Nu is found for the highest value of Re ($Re = 200$) at the pure forced convection region ($Ri = 0 0$), at the pure mixed convection region ($Ri = 1.0$) and free convection dominated region.
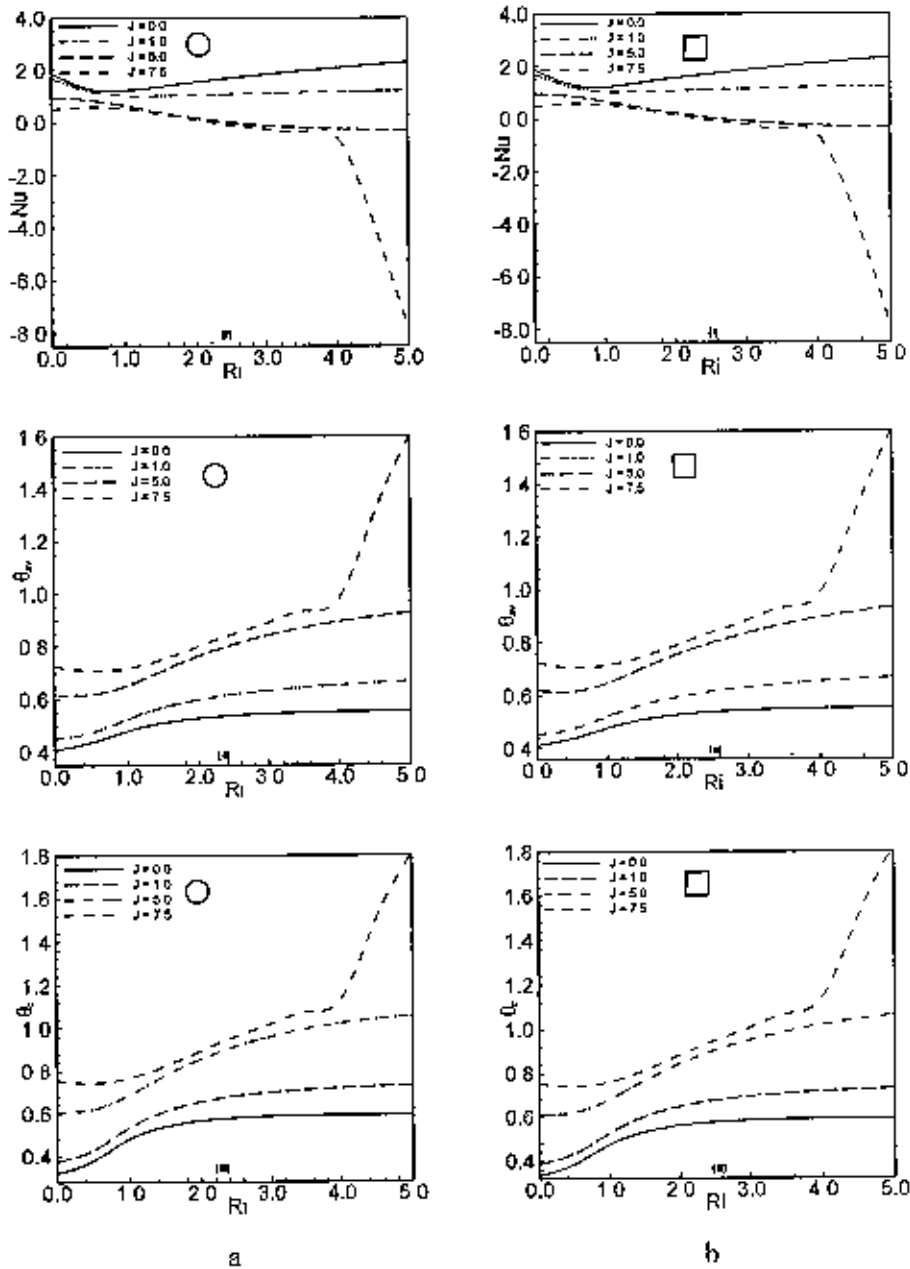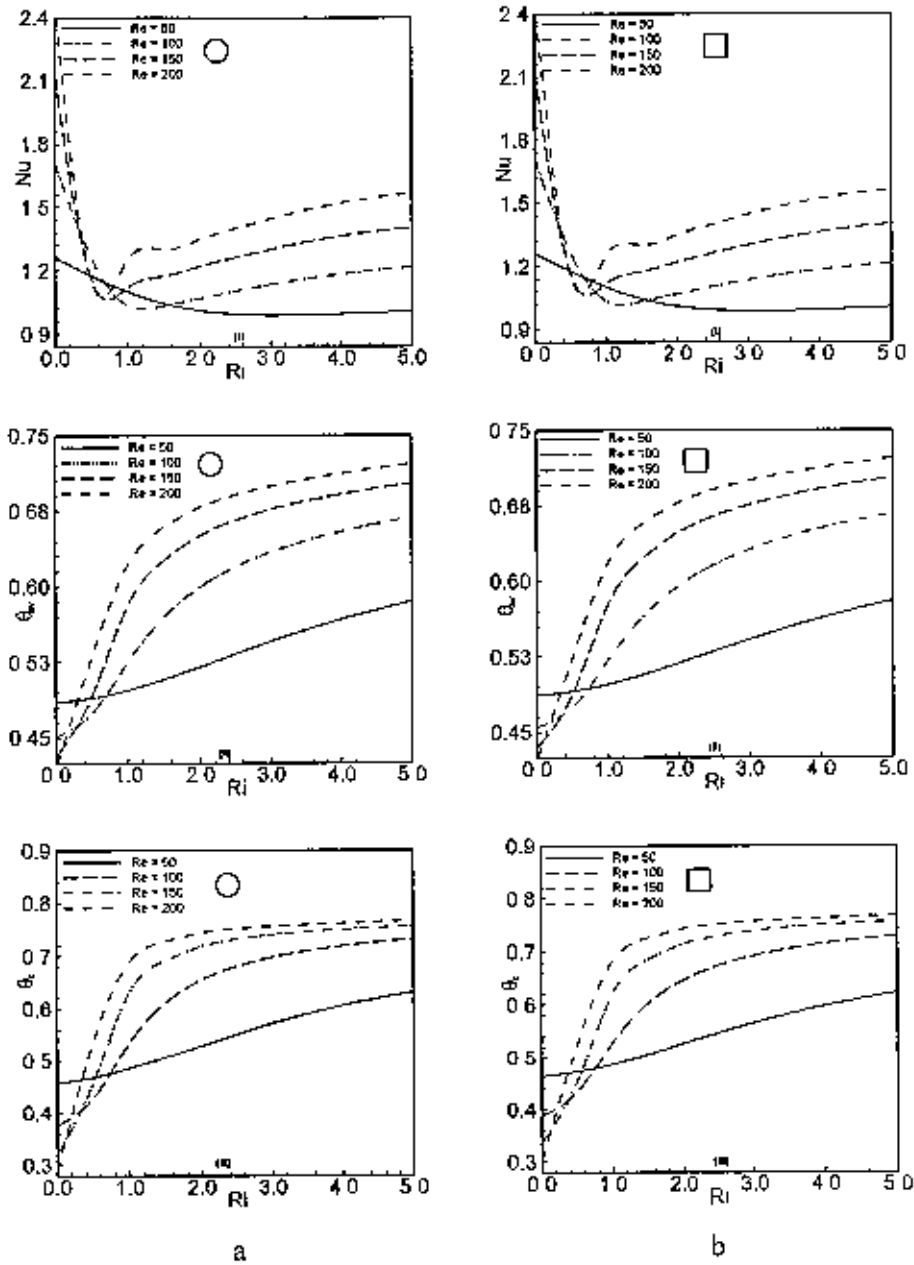
Figure 4.18: Effect of Reynolds number Re on (i) average Nusselt number, (ii) average fluid temperature and (iii) temperature at the cylinder center for the (a) case 1 and (b) case 2, while $AR = 1.0$, $Ha = 10.0$, $J = 1.0$, $L_x = L_y = 0.5$, $K = 5.0$, $Pr = 0.71$ and $D = 0.2$.

Table 4.8 (a): Variation of average Nusselt number with Reynolds number for the case 1

Ri	Nu			
	$Re = 50$	$Re = 100$	$Re = 150$	$Re = 200$
0.0	1.259431	1.710726	2.113681	2.440418
0.5	1.167179	1.239607	1.140568	1.155502
1.0	1.086457	1.022651	1.120741	1.252180
1.5	1.027479	1.028463	1.173439	1.299310
2.0	0.992551	1.064352	1.220219	1.351091
2.5	0.976718	1.100379	1.263960	1.403617
3.0	0.973097	1.132416	1.303509	1.451683
3.5	0.976214	1.159872	1.338008	1.492843
4.0	0.982533	1.182924	1.367189	1.526451
4.5	0.989973	1.201949	1.391163	1.552771
5.0	0.997365	1.217358	1.410237	1.572461

Table 4.8 (b): Variation of average Nusselt number with Reynolds number for the case 2

Ri	Nu			
	$Re = 50$	$Re = 100$	$Re = 150$	$Re = 200$
0.0	1.261492	1.712326	2.130720	2.479329
0.5	1.176203	1.260904	1.161391	1.148622
1.0	1.101123	1.034922	1.121194	1.253349
1.5	1.044776	1.034097	1.175372	1.299454
2.0	1.009633	1.068257	1.220769	1.348373
2.5	0.992108	1.103024	1.262476	1.398488
3.0	0.986443	1.133777	1.300050	1.444860
3.5	0.987662	1.159927	1.332835	1.484935
4.0	0.992356	1.181688	1.360598	1.517908
4.5	0.998427	1.199469	1.383430	1.543896
5.0	1.004651	1.213701	1.401602	1.563438

But it is different in the forced convection dominated region. On the other hand, the average fluid temperature (θ_{av}) in the cavity and the temperature (θ_c) at the cylinder center increases smoothly for higher values of Re (Re = 100, 150, 200) and increases gradually for the lowest value of Re (Re = 50) with increasing Ri. In addition, the values of θ_{av} and θ_c are found minimum for Re = 200 at the pure forced convection (Ri = 0.0) and for Re = 50 at the pure mixed convection (Ri = 1.0) and free convection dominated region. But in the forced convection dominated region the variation of θ_{av} and θ_c are found irregular.

However, a visual examination of the figure 4.18 show qualitatively similar plots for both of the cases at different values of Re and Ri. Lastly, the quantitative differences of the values of Nu at different values of Re are indicated in Tables 4.8 (a) and 4.8 (b) between the two mentioned cases.

4.4.6 Effect of Prandtl Number

The effect of Prandtl number on the flow fields as streamlines in the cavity for the case 1 and case 2 at three different values of Ri is shown in figure 4.19, while AR = 1.0, Re = 100, D = 0.2, Ha = 10.0, J = 1.0, $L_x = L_y$ = 0.5 and K = 5.0. The flow fields for all values of Pr (Pr = 0.071, 0.71, 1.0 and 3.0) and low Ri (Ri = 0.0) are found to be established due to the shear induced force by the moving lid only. Next at Ri = 1.0, the balance between the shear and buoyancy effect is manifested in the formation of two vortices inside the cavity. It is also seen that the shear effect produces the clockwise vortex, which is comparatively small than that of the two-cellular counter clockwise vortex produced by the buoyant force. As the Richardson number increases further to 5.0, the heat transfer is mostly by convection in the cavity, as a result the two-cellular counter clockwise vortex become uni-cellular and large enough and the clockwise vortex becomes shrink in size at each values of Pr considered. Besides, the flows represented by the streamlines are almost independent of the Prandtl number at each Ri. It is also notable that cylinder shape has unimportant effect on streamline plots for various values of Prandtl number.
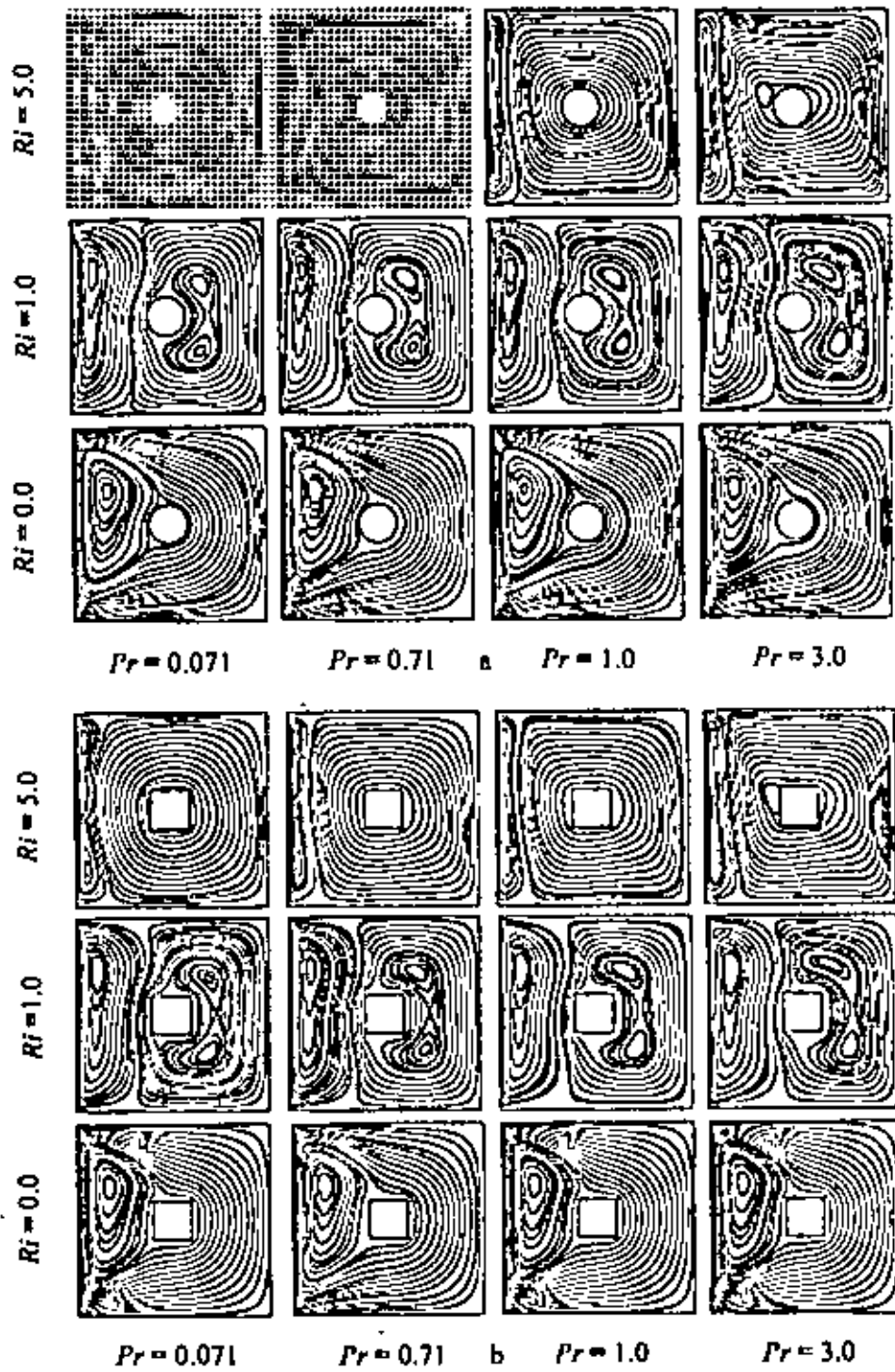
Figure 4.19: Streamlines for the (a) case 1 and (b) case 2 at different values of Prandtl number Pr and Richardson number Ri, while $AR = 1.0$, $Re = 100$, $Ha = 10.0$, $J = 1.0$, $L_x = L_y = 0.5$, $K = 5.0$, and $D = 0.2$.
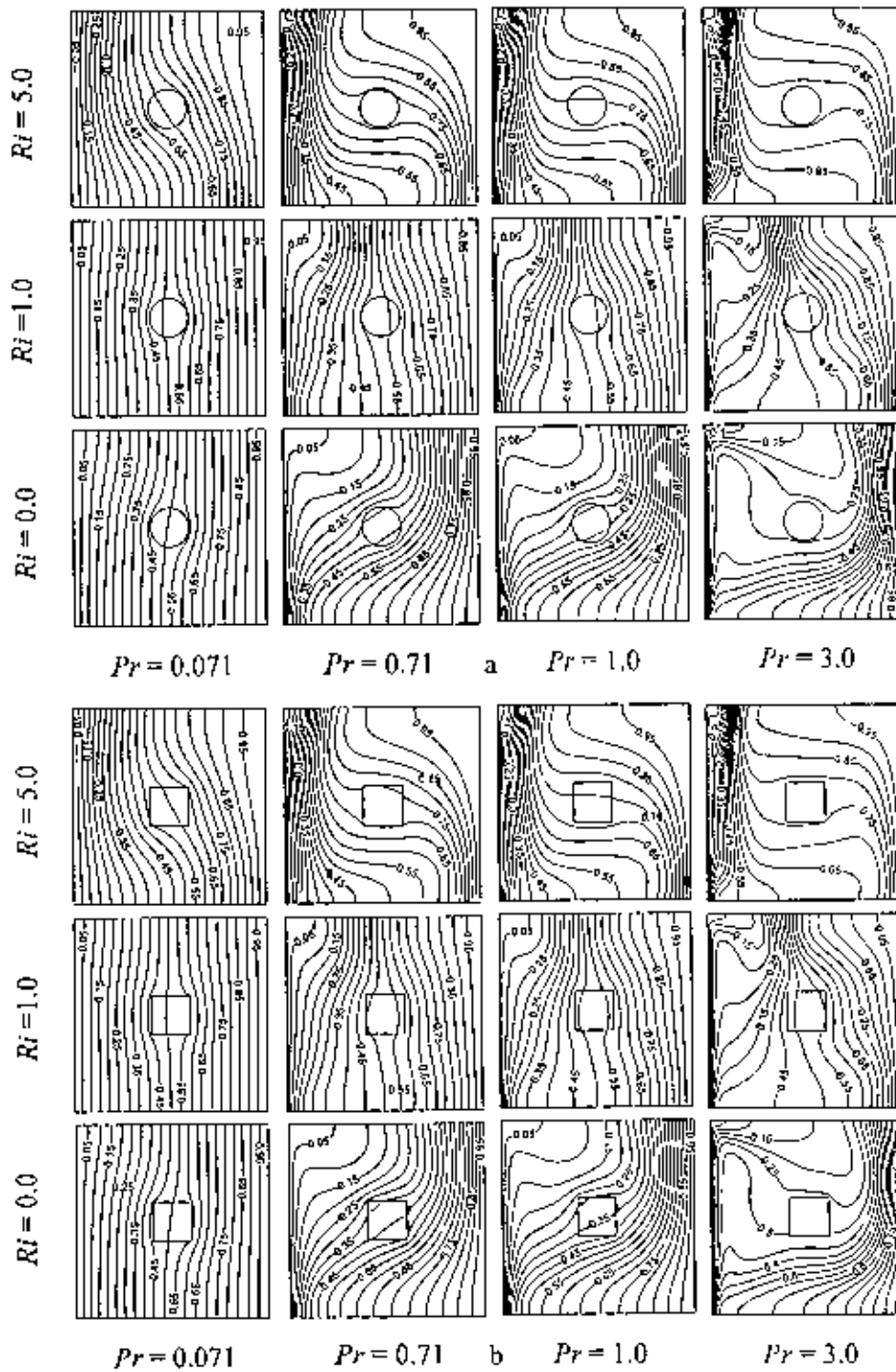
Figure 4.20: Isotherms for the (a) case 1 and (b) case 2 at different values of Prandtl number *Pr* and Richardson number *Ri*, while *AR* = 1.0, *Re* = 100, *Ha* = 10.0, *J* = 1.0, $L_x = L_y$ = 0.5, *K* = 5.0 and *D* = 0.2.

The effect of Prandtl number on thermal characteristics as isotherms in the cavity for the case 1 and case 2 at three different values of Ri are shown in figure 4.20, while $AR = 1.0$, $Re = 100$, $D = 0.2$, $Ha = 10.0$, $J = 1.0$, $L_x = L_y = 0.5$ and $K = 5.0$. The isotherms at very low Pr ($Pr = 0.071$) and lower Ri ($Ri = 0.0, 1.0$) become almost parallel to the vertical walls, resembling the conduction like heat transfer in the cavity. A closer examinations also show the isothermal lines are symmetric about the line $Y = 0.5$. As Ri increases to 5.0, the symmetry in isotherms become disappears in the cavity. But in this folder the degree of distortion from the conduction heat transfer is very noticeable and the isotherms become more packed near the left top surface in the cavity at each values of Ri and the higher Prandtl numbers ($Pr = 0.71$, 1.0 and 3.0). The bend in isothermal lines appears due to the high convective current inside the cavity.

Figures 4.21 depict the variations of average Nusselt number (Nu) at the heated wall, average temperature (θ_{av}) of the fluid in the cavity and temperature (θ_c) at the cylinder center at various values of Pr and Ri for the case1 and case 2. It is shown that, for the lowest Pr the average Nusselt number decreases gradually with increasing Ri and for the higher Pr ($Pr = 0.71$ and 1.0) the values of Nu decreases with increasing Ri in the forced convection dominated region and increases gradually with Ri in the free convection dominated region. But for the highest Pr ($Pr = 3.0$), it is seen that the values of Nu decreases sharply with increasing Ri in the forced convection dominated region and increases smoothly up to $Ri \leq 1.8$, after then Nu is independent of Ri. In addition, maximum values of Nu are found for the highest value of Pr at all values of Ri. Moreover, the average fluid temperature (θ_{av}) in the cavity and the temperature (θ_c) at the cylinder center increase smoothly for higher values of Pr ($Pr = 0.71$, 1.0 and 3.0) and increases gradually for the lowest value of Pr ($Pr = 0.071$) with increasing Ri. On the other hand, minimum values of θ_{av} and θ_c are found at the highest Pr ($Pr = 3.0$) in the forced convection dominated region and at the lowest value of Pr ($Pr = 0.071$) in the free convection dominated region. Finally Tables 4.9 (a) and 4.9 (b) compares the values of average Nusselt number between the two-abovementioned cases considered. From these tables it is also seen that the variation of the values of Nu are unsystematic with cylinder shapes.
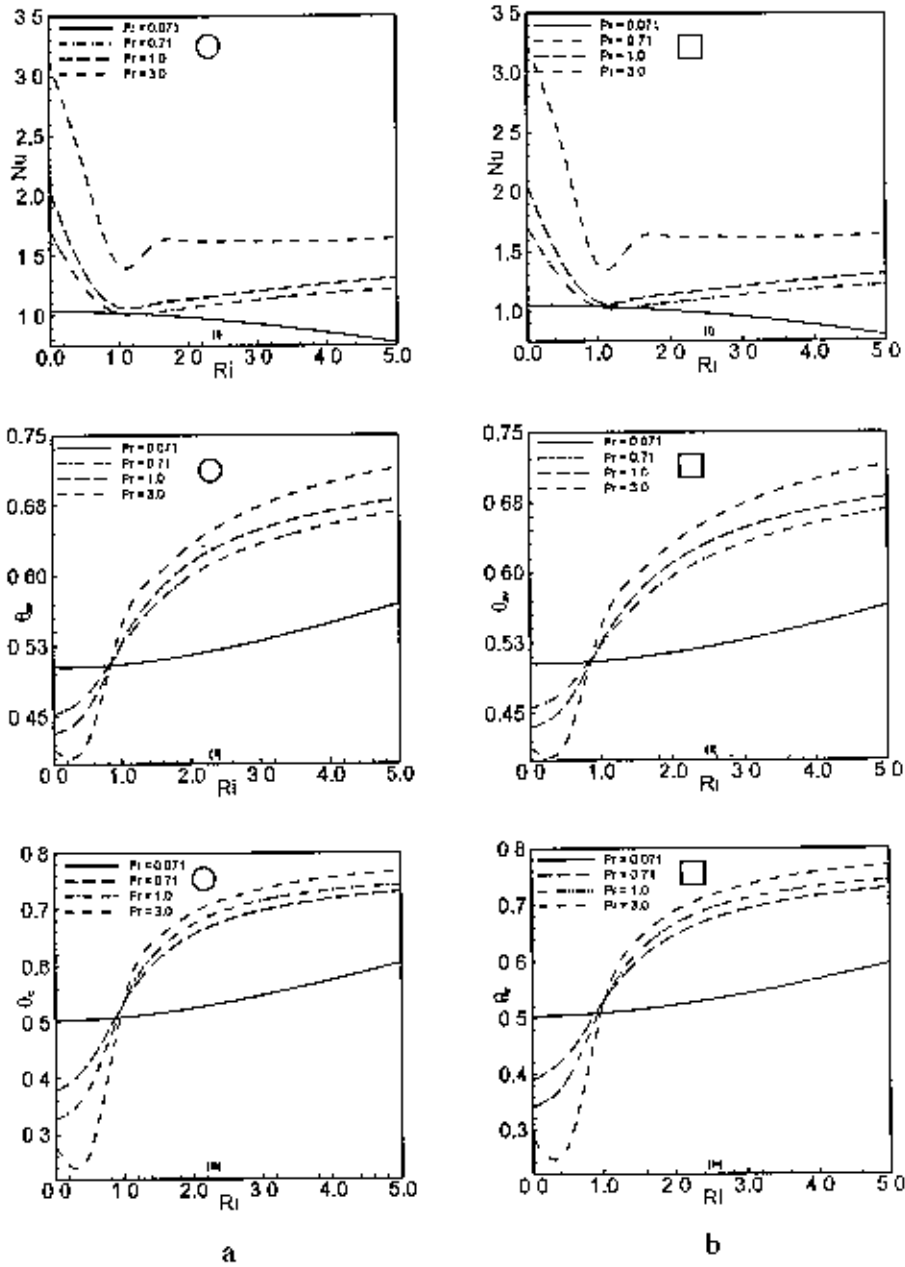
Figure 4.21: Effect of Prandtl number Pr on (i) average Nusselt number, (ii) average fluid temperature and (iii) temperature at the cylinder center for the (a) case 1 and (b) case 2, while $AR = 1.0$, $Re = 100$, $Ha = 10.0$, $J = 1.0$, $L_x = L_y = 0.5$, $K = 5.0$ and $D = 0.2$.

Table 4.9 (a): Variation of average Nusselt number with Prandtl number for the case 1

Ri	Nu			
	$Pr = 0.071$	$Pr = 0.71$	$Pr = 1.0$	$Pr = 3.0$
0.0	1.039148	1.710726	2.041835	3.136956
0.5	1.034628	1.239607	1.369445	2.235250
1.0	1.024186	1.022651	1.071852	1.422283
1.5	1.008087	1.028463	1.098935	1.590875
2.0	0.986682	1.064352	1.136079	1.623106
2.5	0.960397	1.100379	1.170740	1.621783
3.0	0.929720	1.132416	1.203577	1.616093
3.5	0.895172	1.159872	1.234383	1.616437
4.0	0.857280	1.182924	1.262789	1.619037
4.5	0 816544	1 201949	1.288545	1.628686
5.0	0.773427	1.217358	1.311545	1.642432

Table 4.9 (b): Variation of average Nusselt number with Prandtl number for the case 2

Ri	Nu			
	$Pr = 0.071$	$Pr = 0.71$	$Pr = 1.0$	$Pr = 3.0$
0.0	1.052335	1.712326	2.056506	3.234548
0.5	1 048895	1.260904	1.404421	2.394429
1.0	1.039677	1.034922	1.076873	1.383427
1.5	1.024919	1.034097	1.100272	1.582687
2.0	1.004946	1.068257	1.138322	1.624153
2.5	0.980141	1.103024	1.172607	1.623493
3.0	0.950926	1.133777	1.204383	1.616298
3.5	0.917758	1.159927	1.233887	1.612982
4.0	0.881106	1.181688	1.260961	1.615782
4.5	0.841431	1.199469	1.285453	1.624225
5.0	0.799172	1.213701	1.307299	1.637122

4.4.7 Effect of Inner Cylinder Locations

The dependence of flow fields on the locations of the inner cylinder can be observed in the plots of streamlines for the case 1 and the case 2 at various values of the Richardson number are shown in the figure 4.22, while $AR = 1.0$, $Re = 100$, $Ha = 10.0$, $J = 1.0$, $D = 0.2$, $Pr = 0.71$ and $K = 5.0$. From the bottom row of this figure, it is seen that in the pure forced convection region ($Ri = 0.0$) the flow patterns inside the cavity remain unchanged at the different locations of the cylinder, except the shape of the core of the circulatory flow. As Ri increases to 1.0, the effect of buoyant force and the shear force are of the same order of magnitude, a shear cell is formed adjacent to the moving wall and a vortex cell caused due to buoyant force is seen near the hot wall at different locations of the cylinder. However, in the mixed convection region it is also seen that, when the inner cylinder moves closer to the left cold wall along the mid-horizontal plane, the shear driven vortex becomes two cellular and buoyancy induced vortex becomes uni-cellular for both of the cases. If the cylinder moves further closer to the heat source along the mid-horizontal plane an opposite result is observed as compared to the previous position. Furthermore when the cylinder moves near the top and bottom insulated wall of the cavity along the mid vertical plane, then two counter rotating vortices are formed in the cavity for the both cases. It is also seen that the size of the vortices are almost identical. Finally, when the Richardson number Ri increases to 5.0, the magnitude of the velocity circulating in the cavity increases, the size of the buoyancy induced vortex becomes larger than the share induced vortex at all values of the cylinder locations considered, because of the stronger convection effects of the increased Richardson number.

The dependence of the thermal fields on locations of the inner cylinder in the cavity can be obtained in the plots of the isotherms for the case1 and case 2 at various values of the cylinder locations are shown in figure 4.23, while $AR = 1.0$, $Re = 100$, $Ha = 10.0$, $J = 1.0$, $D = 0.2$, $Pr = 0.71$ and $K = 5.0$. At $Ri = 0.0$ and different locations of the inner cylinder, the isothermal lines near the heat source are parallel to the right vertical wall and become skewed near the left top corner of the cavity, due to the dominating influence of the conduction and mixed convection heat transfer.

Figure 4.22: Streamlines for the (a) case 1 and (b) case 2 at different values of cylinder locations (L_x, L_y) and Richardson number Ri, while $AR = 1.0$, $Re = 100$, $Ha = 10.0$, $J = 1.0$, $K = 5.0$, $D = 0.2$ and $Pr = 0.71$.

133
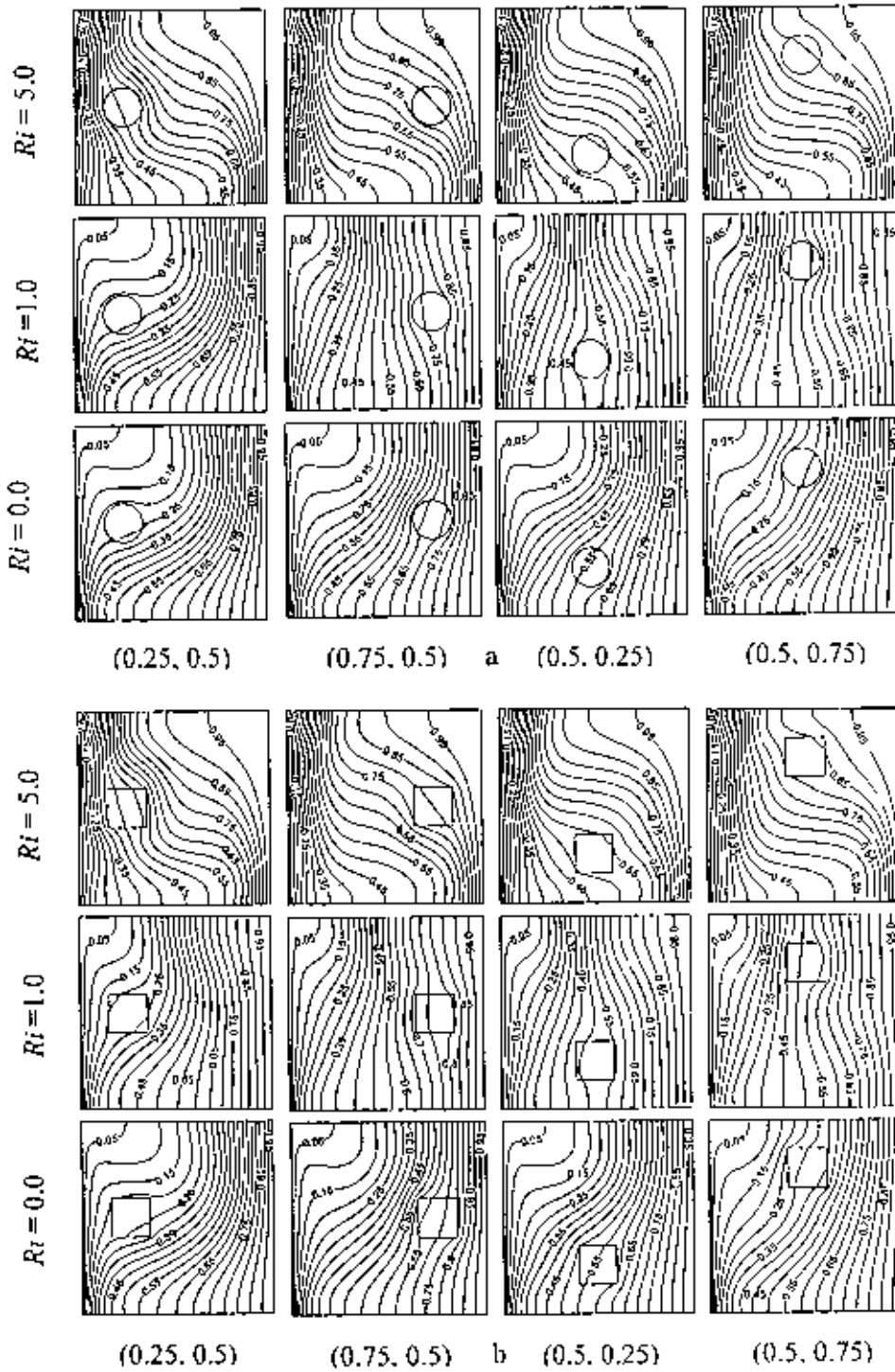
Figure 4.23: Isotherms for the (a) case 1 and (b) case 2 at different values of cylinder locations (L_x, L_y) and Richardson number R_i, while $AR = 1.0$, $Re = 100$, $Ha = 10.0$, $J = 1.0$, $K = 5.0$, $D = 0.2$ and $Pr = 0.71$.
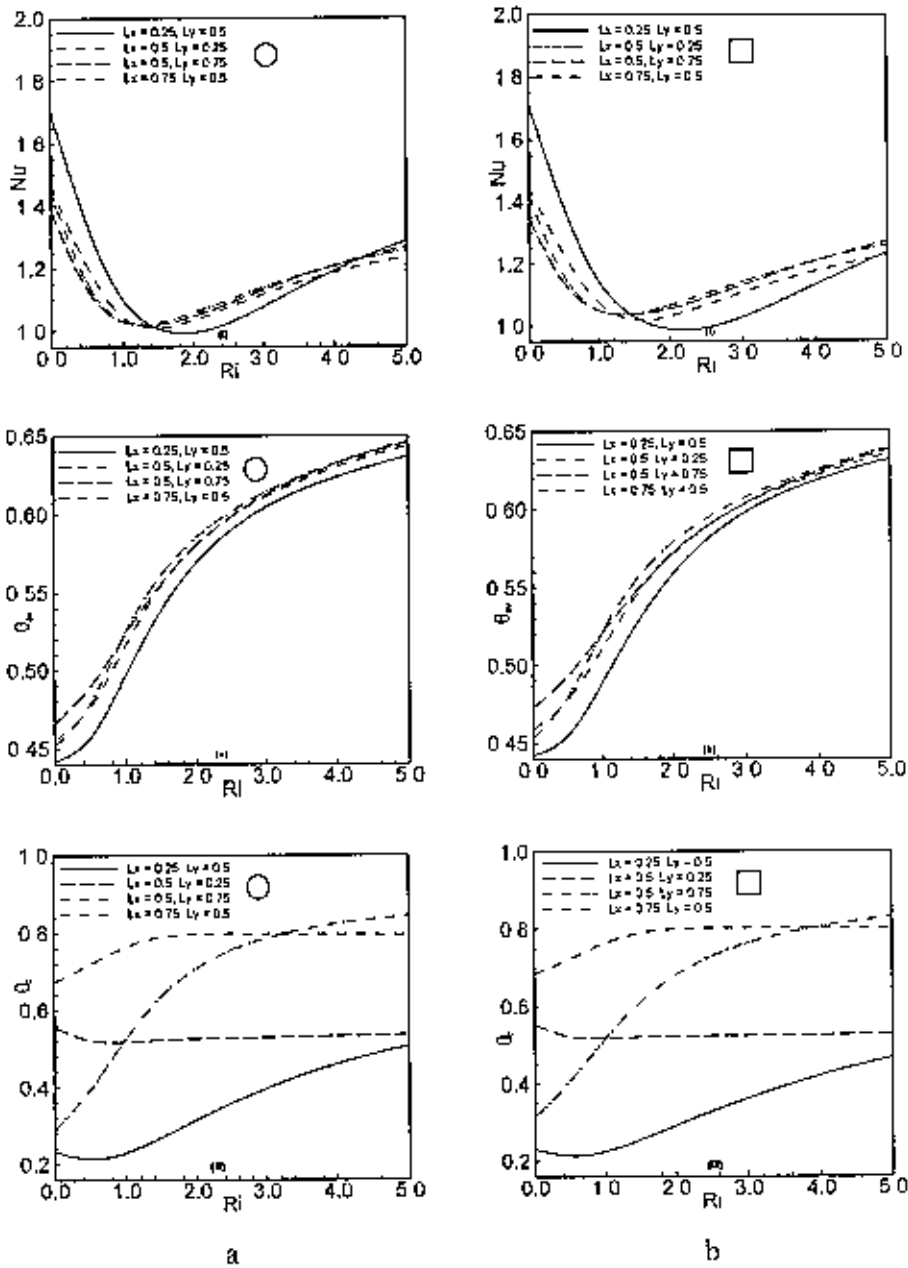
Figure 4.24: Effect of cylinder locations (L_x, L_y) on (i) average Nusselt number, (ii) average fluid temperature and (iii) temperature at the cylinder center for (a) case 1 and (b) case 2, while $AR = 1.0$, $Re = 100$, $Ha = 10.0$, $J = 1.0$, $Pr = 0.71$, $K = 5.0$ and $D = 0.2$.

Table 4.10 (a): Variation of average Nusselt number with cylinder locations for the case 1

Ri	Nu			
	(0.25, 0.5)	(0.5, 0.25)	(0.5, 0.75)	(0.75, 0.5)
0.0	1.702954	1.449321	1.389233	1.468700
0.5	1.342464	1.154362	1.134795	1.208068
1.0	1.100091	1.033496	1.030037	1.044595
1.5	1.008073	1.028374	1.020831	1.009662
2.0	0.995173	1.059638	1.048289	1.035423
2.5	1.026419	1.099846	1.088562	1.076644
3.0	1.078620	1.139807	1.131534	1.118232
3.5	1.136758	1.176249	1.172479	1.155607
4.0	1.192977	1.208107	1.209340	1.187580
4.5	1.243755	1.235211	1.241419	1.214121
5.0	1.287813	1.257767	1.268685	1.235600

Table 4.10 (b): Variation of average Nusselt number with cylinder locations for the case 2

Ri	Nu			
	(0.25, 0.5)	(0.5, 0.25)	(0 5, 0.75)	(0.75, 0.5)
0.0	1.714455	1.419111	1.348573	1.448793
0.5	1.380974	1.159858	1.137167	1.229474
1.0	1.140098	1.049525	1.048052	1.072343
1.5	1.028226	1.040029	1.035186	1.018390
2 0	0.988133	1.065955	1.055393	1.031070
2.5	0.993000	1.102441	1.089870	1.066217
3.0	1.026872	1.140287	1.129556	1.105324
3.5	1.075883	1.175815	1.169421	1.142018
4.0	1.130156	1.207575	1.206751	1.174241
4.5	1.183827	1.235106	1.240259	1.201523
5.0	1.233794	1.258404	1.269486	1.223990

Further increase of Ri to 1.0, the isothermal lines become almost parallel to the vertical walls for all the locations of the cylinder owing to the conjugate effect of conduction and mixed convection. Lastly, at $Ri = 5.0$, convective distortion of the isothermal lines occurred throughout the cavity due to the strong influence of the convective current and a thermal boundary layer is developed near the cold wall at all values of the cylinder locations considered. In this folder it is also seen that no significant difference is found due to cylinder shape.

The average Nusselt number (Nu) at the heated surface, average fluid temperature (θ_{av}) in the cavity and the temperature (θ_c) at the cylinder center are plotted against Richardson numbers in figures 4.24 (a) and 4.24 (b) for the aforementioned cases at the four different locations of the cylinder respectively. For each locations of the cylinder, the Nu-Ri profile is parabolic shape shows two distinct zones depending on Richardson number. Up to a certain value of Ri the distribution of Nu smoothly decreases with increasing Ri and beyond these values of Ri it is increases with Ri. Furthermore, the values of Nu are found maximum, when the inner cylinder moves closer to the left wall along the mid-horizontal plane at the values of $Ri < 1.5$, and beyond these values of Ri it is the highest when the cylinder moves near the bottom insulated wall of the cavity along the mid vertical plane. This is also supported from the numerical values obtained for the aforementioned cases shown in the Tables 4.10 (a) and 4.10 (b). On the other hand, average fluid temperature (θ_{av}) in the cavity increases monotonically with Ri at each locations of the cylinder. But the temperature (θ_c) at the cylinder center is not monotonic with Ri at the different locations of the cylinder. Besides, the values of θ_{av} and θ_c are always lower, when the cylinder center is at (0.25, 0.5) for both of the abovementioned cases

4.4.8 Effect of Cavity Aspect Ratio

The influence of the cavity aspect ratio on the flow field in the cavity is shown in the figure 4.25 at three convective regime for the abovementioned two cases, while $Re = 100$, $D = 0.2$, $K = 5.0$, $Ha = 10.0$, $J = 1.0$, $L_x = L_y = 0.5$ and $Pr = 0.71$. The aspect ratio is the ratio of the length L and height H. The results presented in the preceding subsections are for a square cavity in which the aspect ratio AR is 1.0.
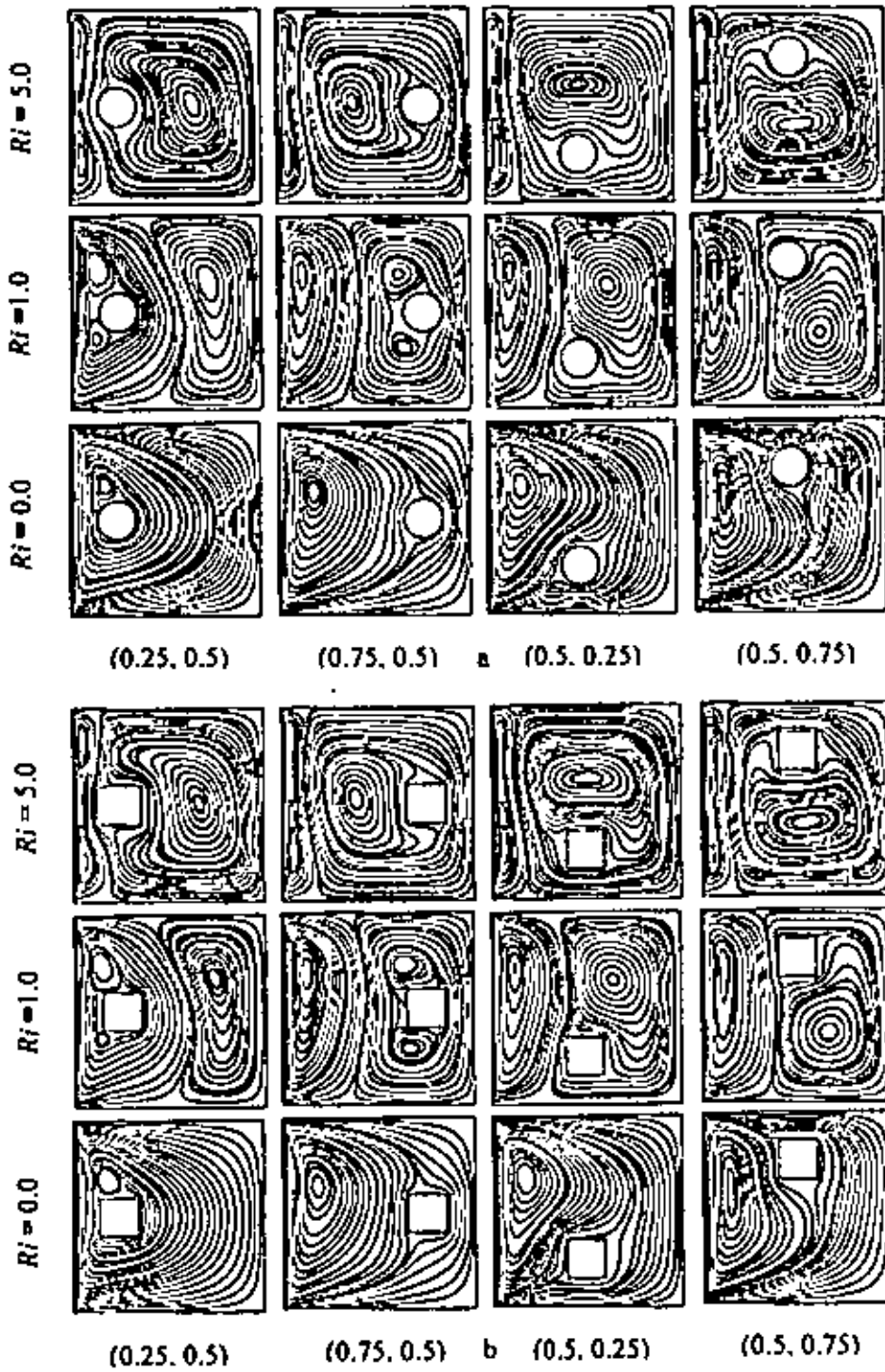
Figure 4.25: Streamlines for the (a) case 1 and (b) case 2 at different values of cavity aspect ratio AR and Richardson number Ri, while $Re = 100$, $Ha = 10.0$, $J = 1.0$, $L_x = L_y = 0.5$, $K = 5.0$, $D = 0.2$ and $Pr = 0.71$.

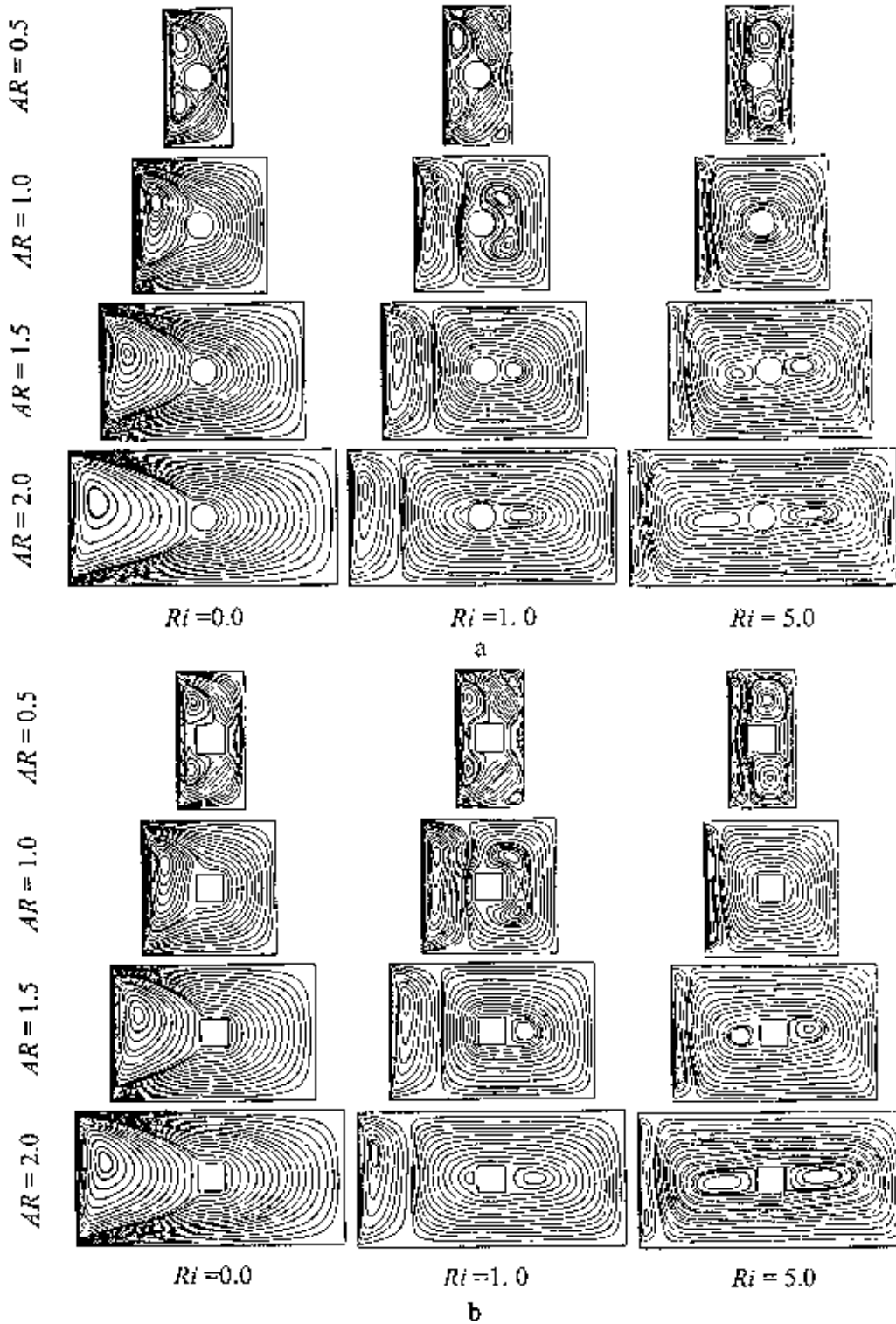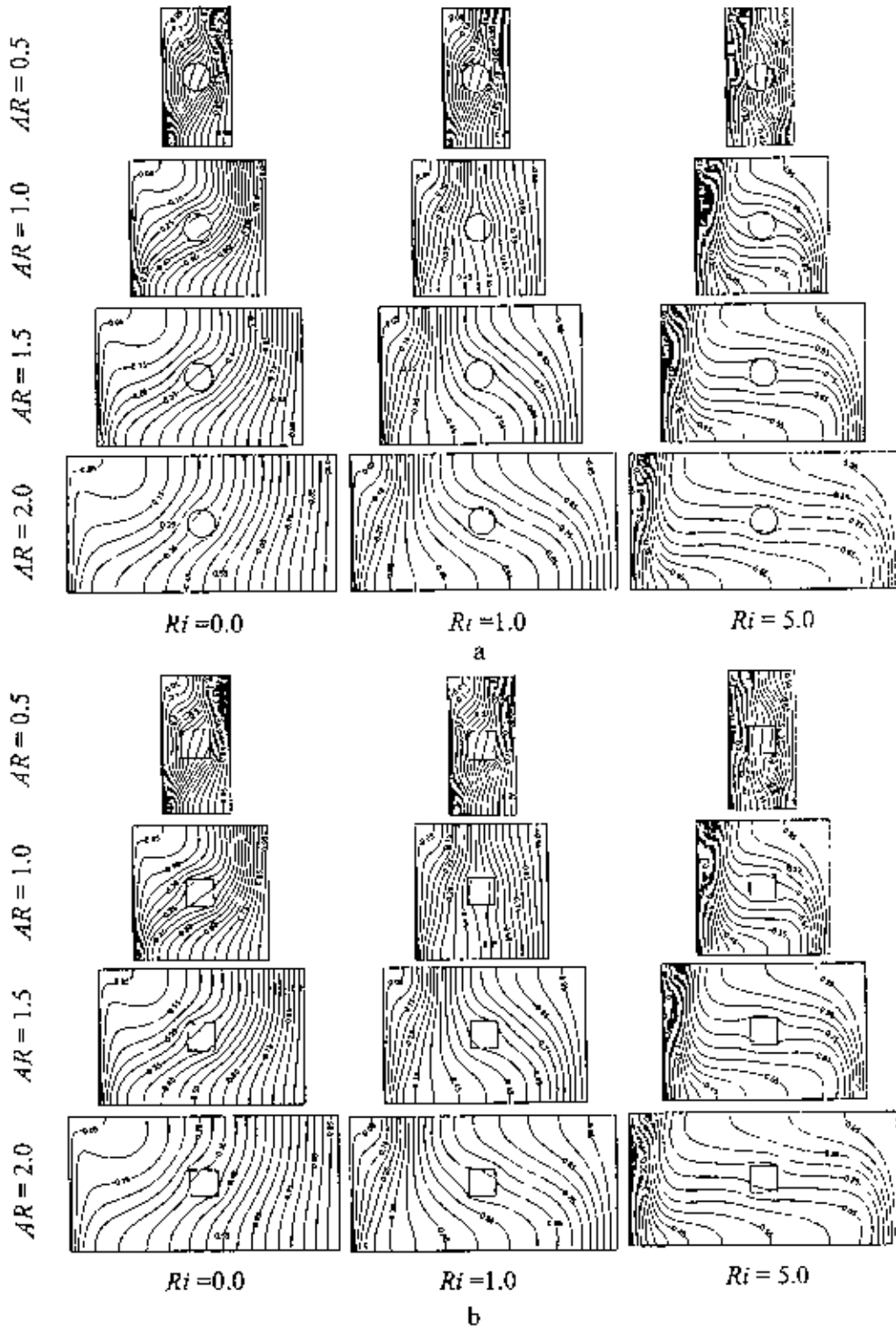Figure 4.26: Isotherms for the (a) case 1 and (b) case 2 at different values of cavity aspect ratio AR and Richardson number Ri, while $Re = 100$, $Ha = 10.0$, $J = 1.0$, $L_x = L_y = 0.5$, $K = 5.0$, $D = 0.2$ and $Pr = 0.71$

In order to investigate the convective heat transfer behavior at other aspect ratios, computations are also done for cavities at three additional aspect ratios of 0.5, 1.5 and 2.0. Now at $Ri = 0.0$ and $AR = 0.5$, it is seen that a two cellular vortex which we called primary vortex is generated due to the motion of the left wall. It is also seen from these figures that the vortex become uni-cellular and large in size with increasing AR at fixed $Ri = 0.0$. Next at $Ri = 1.0$ and $AR = 0.5$ it is observed that the primary vortex remain unchanged and two secondary vortices are developed at the top and bottom corner near the right wall due to the natural convection effect. With the increase of AR at $Ri = 1.0$, it is seen that the size of the secondary vortex increases rapidly as a result the size of the primary vortex decreases rapidly. Further, at $Ri = 5.0$ and all values of AR ($AR = 0.5, 1.0, 1.5$ and 2.0), it is seen that the secondary vortex spreads and thereby squeezes the primary vortex. indicating a sign of supremacy of natural convection in the cavity. However, it is also seen that the streamlines are independent of cylinder shape at all values of AR and Ri.

The effects of the cavity aspect ratio on the thermal field in the cavity is revealed in the figures 4.26 (a) and 4.26 (b) at three convective regime for the case1 and case 2 respectively, while $Re = 100$, $D = 0.2$, $K = 5.0$, $Ha = 10.0$, $J = 1.0$, $L_x = L_y = 0.5$ and $Pr = 0.71$. For the low $Ri = 0.0$ and the four cavity aspect ratios ($AR = 0.5, 1.0, 1.5$ and 2.0), the isothermal lines nearly follow the geometry of the right vertical surface and start to turn back towards the hot wall at the left top corner of the cavity due to the dominating influence of conduction and forced convection heat transfer. Now making a comparison of the isothermal lines for $Ri = 1.0$ and different AR that of for $Ri = 0.0$ and different AR no significant difference is found at lower AR, but for higher AR the isothermal lines start to turn back towards the cold wall in the upper part of the cavity. Further at $Ri = 5.0$ and low $AR = 0.5$ the isothermal lines are almost parallel to the left vertical and start to turn back towards the cold wall at the right top corner of the cavity due to the dominating influence of convective heat transfer. On the other hand, at $Ri = 5.0$ and higher values of AR ($1.0, 1.5$ and 2.0) a significant convective distortion in the isothermal lines occurs due to the strong influence of the convective current as a result a concentrated thermal layer near the cold wall is developed.
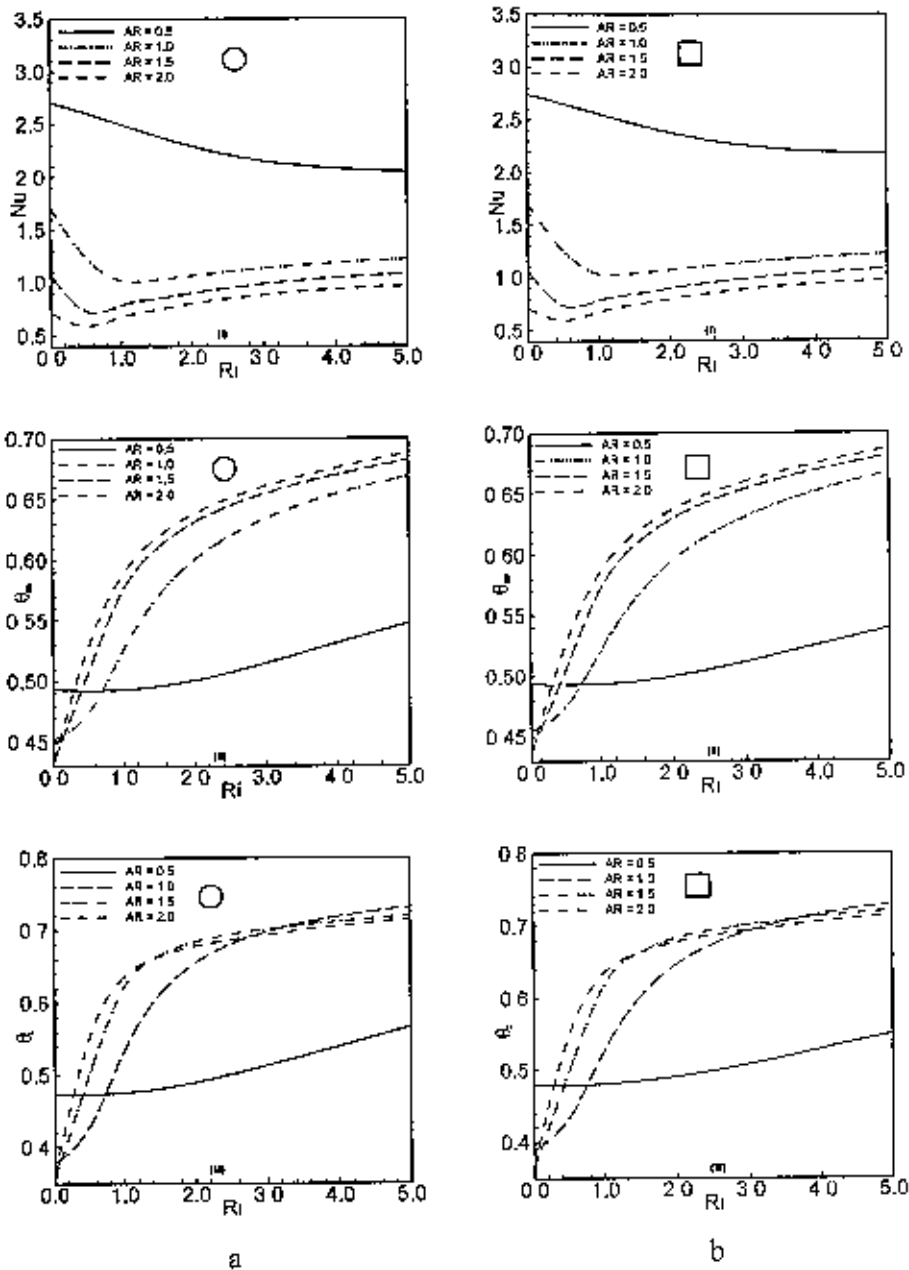
Figure 4.27: Effect of cavity aspect ratio AR on (i) average Nusselt number, (ii) average fluid temperature and (iii) temperature at the cylinder center for (a) case 1 and (b) case 2, while $Re = 100$, $Ha = 10.0$, $J = 1.0$, $Pr = 0.71$, $L_x = L_y = 0.5$, $K = 5.0$ and $D = 0.2$.

Table 4.11 (a): Variation of average Nusselt number with cavity aspect ratio for the case 1

Ri	Nu			
	AR = 0.5	AR = 1.0	AR = 1.5	AR = 2.0
0.0	2.709510	1.710726	1.078983	0.715308
0.5	2.608611	1.239607	0.733203	0.596536
1.0	2.500252	1.022651	0.785437	0.677311
1.5	2.391729	1.028463	0.847057	0.745028
2.0	2.292422	1.064352	0.901585	0.800972
2.5	2.210390	1.100379	0.948050	0.846863
3.0	2.148919	1.132416	0.986563	0.883972
3.5	2.106212	1.159872	1.017821	0.913439
4.0	2.077815	1.182924	1.042681	0.936301
4.5	2.059003	1.201949	1.061977	0.953475
5.0	2.045923	1.217358	1.076461	0.965751

Table 4.11 (b): Variation of average Nusselt number with cavity aspect ratio for the case 2

Ri	Nu			
	AR = 0.5	AR = 1.0	AR = 1.5	AR = 2.0
0.0	2.743597	1.712326	1.072806	0.712698
0.5	2.654432	1.260904	0.734511	0.594594
1.0	2.559823	1.034922	0.782060	0.672767
1.5	2.465723	1.034097	0.842509	0.739944
2.0	2.379547	1.068257	0.896581	0.795811
2.5	2.307770	1.103024	0.942911	0.841777
3.0	2.253429	1.133777	0.981407	0.879035
3.5	2.215600	1.159927	1.012687	0.908695
4.0	2.190931	1.181688	1.037582	0.931776
4.5	2.175474	1.199469	1.056918	0.949180
5.0	2.165766	1.213701	1.071448	0.961692

The average Nusselt number (Nu) at the heat source, average temperature (θ_{av}) of the fluid in the cavity and the temperature (θ_c) at the cylinder center are plotted as a function of Richardson number in figures 4.27 (a) and 4.27 (b) for the two cases at $AR = 0.5, 1.0\ 1.5$ and 2.0. For each higher AR, the Nu-Ri profile shows two distinct zones depending on the Richardson number. The distribution of the average Nusselt number goes down sharply in the forced convection dominated region, and goes up gradually in the free convection dominated region with increasing Ri. On the other hand, for the lowest value of AR ($AR = 0.5$), the average Nusselt number decreases monotonically with increasing Ri. However, maximum average Nusselt number is found for the low $AR = 0.5$ at each Ri owing to the shortest distance between the hot and cold wall. From the figures 4.27 (a) and 4.27 (b), it is also seen that average temperature of the fluid in the cavity and the temperature at the cylinder center goes up sharply for the higher values of AR (1.0, 1.5 and 2 0) and gradually for lowest AR with increasing Ri. In addition, the values of the average temperature of the fluid in the cavity and the temperature at the cylinder center are lower for the higher values of AR in the forced convection dominated region, also for the lowest value of AR in the free convection dominated region.

However, a visual examination of the streamline and isotherms plots does not reveal any significant difference between the two cases considered. On the other hand, Tables 4.11 (a) and 4.11 (b) compare the values of average Nusselt number between the case 1 and case 2 respectively. It is clearly seen from the Tables 4.11 (a) and 4.11 (b) that the values of average Nusselt number, for the case 1 are considerably lower than those obtained for the case 2 only at the lowest value of AR.

4.5 Concluding Remarks

Steady mixed convection flow and heat transfer in a rectangular lid-driven cavity with the presence of a joule heating, magnetic field and heat-conducting horizontal cylinder operating under laminar regime were numerically investigated. An external excitation was imposed on the lid motion. A detailed analysis for the distribution of streamlines, isotherms, average Nusselt number at the hot wall, average fluid temperature in the cavity and temperature at the cylinder center were carried out to investigate the effect of the dimensionless parameters. The investigation was carried

out for a number of relevant dimensionless groups, namely the Reynolds number Re, Richardson number Ri, Prandtl number Pr, Hartmann number Ha, Joule heating parameter J, as well as various configurations of the cylinder, thermal property of the cylinder, various location of the cylinder in the cavity and cavity aspect ratio. From an examination of the heat transfer and fluid flow phenomena revealed by the numerical experiments, the following major conclusion have been drawn as follows:

- Cylinder diameter has significant influence on the flow field in the pure forced convection dominated region and on the thermal fields in the free convection dominated region in the cavity. On the other hand there are noticeable changes in the flow and thermal fields as the Richardson number increases for particular values of cylinder diameter. Higher average Nusselt number is always found for the largest value of D for both of the abovementioned cases. The average temperature of the fluid and temperature at the cylinder center in the cavity are lesser for $D = 0.0$ in the forced convection dominated region, but for $D = 0.6$ in the free convection dominated region.

- The thermal conductivity ratio of the solid to that of the fluid, K affects the isotherm distribution in the inner body, thus it affects also isotherms in the entire cavity, whereas the distribution of streamlines are independent on the thermal conductivity ratio K. The effect of K on the average Nusselt number Nu depends upon the cylinder size. Relatively large effect on thermal phenomenon is observed for a big size cylinder. A deficiency in the heat transfer rate is obtained when the cylinder size is decreased. A similar trend is also observed on the average temperature of the fluid and temperature at the cylinder center in the cavity.

- It is found that the flow behavior and the heat transfer characteristics inside the cavity are strongly depending upon the strength of the magnetic field. In the absence of the magnetic force, the convection-dominated zone is extended in the forced convection dominated region resulting better convective heat transfer performance. Increasing Hartmann number retards the fluid circulation causing the lower temperature gradients throughout the cavity in the forced convection dominated region. Therefore, major portion of the heat is transferred mainly by conduction. The inverse phenomena are observed in the free convection

dominated area. However, lesser average fluid temperature and cylinder center temperature are observed for lower values of Ha ($Ha = 10.0, 20.0$) at the forced convection dominated area and for $Ha = 50.0$ at the free convection dominated area.

- The Joule heating parameter has insignificant on streamlines in the pure forced convection region, but have significant effect in the pure mixed convection and free convection dominated region. An increase in the value of the Joule heating parameter leads to increase in the flow rates in the shear induced recirculation cell. Further increase in the value of Joule heating parameter causes for development of more cells in the cavity. On the other hand, the Joule heating parameter has noteworthy effect on isotherm plots The temperature of the fluid in the cavity and the temperature at the cylinder center increase due to the increases of J and hence that negates the heat transfer from the heated surface.

- The effect of Reynolds number Re on streamlines are not significant in the pure forced convection region, but in the pure mixed convection and free convection dominated area these effects are significant. On the other hand, Reynolds number Re affects strongly on isotherm structures in the cavity at all convective regime However, the values of average Nusselt number is the maximum for the highest value of Re at the pure forced convection, pure mixed convection and free convection dominated area, but some unexpected behavior is seen in the forced convection dominated region. Moreover, average temperature of the fluid in the cavity and temperature at the cylinder center become smaller for the higher values of Re at the forced convection dominated region, but beyond these region that are smaller for $Re = 50$.

- The influence of Prandtl number on the streamlines in the cavity is found to similar for all the cases, whereas the influence of Pr on the isotherms is remarkable for different values of Pr. For low values of Pr the heat transfer is dominated by conduction and it become reduces with increasing Pr. Furthermore, clearly different flow behaviors and heat transfer characteristics are observed among the three different flow regimes. The average Nusselt number is always superior for the large value of Pr. The average temperature of the fluid in the cavity and the temperature at the cylinder center are inferior for $Pr = 3.0$ in the

forced convection dominated region, also for $Pr = 0.071$ in the free convection dominated region.

- It is observed that the location of the inner cylinder is one of the most important parameter on fluid flow, temperature fields and heat transfer characteristics. Moreover, noticeably different flow behaviors and heat transfer characteristics are observed among the three different flow regimes. The value of the average Nusselt number is greater if the solid cylinder is placed near the cold wall along the mid-horizontal plane at $Ri < 1.5$ and beyond these values of Ri it is the highest when the cylinder moves near the bottom insulated wall of the cavity along the mid vertical plane. On the other hand, the average fluid temperature and temperature at the cylinder center are always lesser when the solid cylinder is placed near the cold wall along the mid-horizontal plane.

- Cavity aspect ratio has significant effects on the streamlines and isotherms distributions. Buoyancy-induced vortex in the streamlines and convective current in the isotherms increases with increasing aspect ratio of the cavity. Moreover, markedly different flow behaviors and heat transfer characteristics are observed among the three different flow regimes. On the other hand, average Nusselt number is always higher for lowest value of the cavity aspect ratio AR ($AR = 0.5$). The values of average temperature of the fluid in the cavity and temperature at the cylinder center are lower in the forced convection dominated region for the higher values of AR and in the free convection dominated region for the lowest value of AR.

- The difference of the values of average Nusselt number between the case 1 and case 2 are not significant from the engineering point of view.

Chapter 5

Conclusions

A numerical study on the conjugate effect of conduction and mixed convection in obstructed cavity has been studied by solving steady state two-dimensional Navier-Stokes equations, energy equations and continuity equation. The work reported in this thesis are basically dependent on two types of cavity configurations namely (i) vented cavity and (ii) lid-driven cavity. The various ideas and results have been discussed in individual detail at the relevant chapter of the thesis. In the present chapter an attempt is made to summaries the concepts presented and results obtained in the work reported already. A section on the scope of further work on associated fields of investigation is also included.

5.1 Summary of the Major Outcomes

The analysis has been confined to cases of vented as well as lid-driven obstructed cavities. In cases of vented cavity the nature of flow and thermal fields as well as characteristics of heat transfer process particularly its augmentation due to the introduction of solid material has been evaluated in chapter 3. On the basis of the analysis the following conclusions have been drawn:

(i) The inlet and outlet locations have significant effect on the flow and thermal distributions at the three convective regimes. The average Nusselt number (Nu) at the hot wall is the highest for the BT configuration, whereas the BB configuration has the lowest heat transfer rate at the three convective regimes. Moreover, the average Nusselt number, when circular cylinder is considered is slightly lower than those obtained with square cylinder for the BT configuration whereas the inverse scenario is found for the BB configuration.

(ii) Flow and thermal field's modifications are observed due to the blockage effect of the solid cylinder. Moreover by introducing the cylinder, the heat transfer capacity on the hot wall is always increased. However, the average Nusselt number (Nu) for the case of square cylinder (case 2) is slightly higher than those obtained for the case of circular cylinder (case 1) only at $D = 0.2$.

(iii) Although the thermal conductivity ratio K is not an effective parameter on the flow field, it has an important effect on the thermal field. The variation of average Nusselt number (Nu) with the values of K is not significant at all values of Ri for the smallest value of D. On the other hand, the average Nusselt number (Nu) with the values of K is more significant at all values of Ri for the largest value of D. Moreover the average Nusselt number (Nu) for the case of square cylinder (case 2) is slightly higher than those obtained for the case of circular cylinder (case 1) at all values of K considered.

(iv) In general the Reynolds number Re has a stronger influence on flow and thermal fields. The average Nusselt number (Nu) is always upper for the largest value of Re. Moreover the average Nusselt number (Nu) for the case of square cylinder (case 2) is higher than those obtained for the case of circular cylinder (case 1) at the higher values of Reynolds number Re (Re = 100, 150 and 200).

(v) Fluids with a smaller Prandtl number Pr are more sensitive to changes in the buoyancy force than fluids with a higher Prandtl number. Increasing the Prandtl number increases the average Nusselt number (Nu). In addition, the heat transfer rate at the hot wall for the case of square cylinder (case 2) is higher than those obtained for the case of circular cylinder (case 1) at all values of Pr considered.

(vi) Locations of the inner cylinder are one of the most important parameter on flow and temperature fields as well as heat transfer at the hot surface. Maximum value of Nu is found when the cylinder center is at (0.25, 0.5) and (0.5, 0.75) Moreover, the average Nusselt number (Nu) for the case of square cylinder (case 2) is higher than those obtained for the case of circular cylinder (case 1) when the cylinder center is at (0.25, 0.5). On the other hand, the inverse results are found when the cylinder center is at (0.25, 0.5) and (0.75, 0.5).

(vii) The influence of cavity aspect ratio on fluid flow and temperature field is found to be pronounced. The heat transfer rate for lower cavity aspect ratio is higher than for higher aspect ratio. Moreover the average Nusselt number (Nu) for the case of square cylinder (case 2) is higher than those obtained for the case of circular cylinder (case 1) at all values of AR considered.

The effect of joule heating in the coupling of conduction with MHD mixed convection flow in a rectangular lid-driven cavity along with a heat conducting horizontal cylinder has been investigated numerically in chapter 4. From the investigation the following conclusions have been drawn:

(i)   Cylinder diameter has significant influence on the flow in the forced convection dominated region and on the thermal fields in the free convection dominated region in both of the cases. Higher average Nusselt number is always found for the largest value of D for both of the abovementioned cases. The average temperature of the fluid and temperature at the cylinder center in the cavity are not linear. Moreover, the average Nusselt number (Nu) for the case of square cylinder (case 2) is slightly higher than those obtained for the case of circular cylinder (case 1) at the higher values of D ($D = 0.4$ and 0.6)

(ii) Thermal conductivity ratio K has a negligible effect on the velocity field and has significant effect on the thermal field at the three convective regimes. The effect of K on the average Nusselt number Nu depends upon the cylinder size. In addition, the heat transfer coefficient is influenced significantly by the thermal conductivity ratio for a big size cylinder. Moreover the heat transfer coefficient is not monotonic with the values of K for the abovementioned two cases.

(iii) Magnetic field affects the flow and temperature fields and it retards the heat transfer from the heated surface. However, the average Nusselt number (Nu) for the case of square cylinder (case 2) is slightly higher than those obtained for the case of circular cylinder (case 1) at $Ha = 0.0$ and 50.0.

(iv) Joule heating parameter J has insignificant on flow field at the pure forced convection region, but have significant effect at the pure mixed convection and free convection dominated region. On the other hand, Joule heating parameter has significant effect on thermal field at the three convective regimes. The temperature of the fluid in the cavity and the temperature at the cylinder center increase due to the increases of J and hence that negates the heat transfer from the heated surface. Moreover, the average Nusselt number (Nu) for the case of square cylinder (case 2) is higher than those obtained for the case of circular cylinder (case 1) only at the value of $J = 1.0$.

(v)   Reynolds number Re has significant effects on the flow field at the pure mixed convection and free convection dominated region. On the other hand, Re has significant effect on temperature field at the three convective regimes. However, the values of average Nusselt number with Ri are not linear for the higher values of Re. Moreover, the average Nusselt number (Nu) for the case of square cylinder (case 2) is higher than those obtained for the case of circular cylinder (case 1) only at the value of $Re = 50$.

(vi) Prandtl number Pr does not have significant contribution on flow field, whereas there are noticeable changes in the thermal field as Pr changes for a particular Ri. The variation of the average Nusselt number Nu is nonlinear with higher Pr and linear with the lowest values of Pr. In addition the values of Nu is always superior for the large value of Pr. Moreover the heat transfer coefficient is not monotonic with the values of Pr for the abovementioned two cases

(vii) Location of the inner cylinder is an effective parameter on fluid flow; temperature fields and heat transfer characteristics. Moreover, the variation the average Nusselt number is nonlinear with the location of the inner cylinder. In addition the heat transfer coefficient is not monotonic with the values of cylinder location for the abovementioned two cases.

(viii) The influence of cavity aspect ratio on fluid flow and temperature distribution is found to be pronounced. The average Nusselt number is always higher for lowest value of the cavity aspect ratio AR ($AR = 0.5$). Moreover, the average Nusselt number (Nu) for the case of square cylinder (case 2) is higher than those obtained for the case of circular cylinder (case 1) only at the value of $AR = 0.5$.

(ix) The difference of the values of average Nusselt number between the case 1 and case 2 are not significant from the engineering point of view.

(x) Moreover, markedly different flow and heat transfer behavior are observed among the three different flow regimes.

5.2 Further Works

The following can be put forward for the further works as follow-ups of the present research as.

❖ In the future, the study can be extended by incorporating different physics like radiation effects, internal heat generation / absorption, capillary effects.

❖ Double diffusive mixed convection can be analyzed through including the governing equation of concentration conservation.

❖ Investigation can be performed by using magnetic fluid instead of electrically conducting fluid within the porous medium and changing the boundary conditions of the cavity's walls.

❖ The study can be extended for turbulent flow using different fluids, different thermal boundary conditions such as constant heat flux or radiation and unsteady flow.

❖ Only two-dimensional fluid flow and heat transfer has been analyzed in this thesis. So this deliberation may be extended to three-dimensional analyses to investigate the effects of parameters on flow fields and heat transfer in cavities. In addition, the problem of fluid flow and heat transfer along with heat generating cylinder may be studied in three-dimensional cases.

References

Angirasa, D., "Mixed convection in a vented enclosure with isothermal vertical surface", Fluid Dyn. Res. Vol. 26, pp. 219-233, 2000.

Anderson, J. D., "Computational fluid dynamics", International Ed., McGraw-Hill, 1995.

Aydin, O., "Aiding and opposing mechanisms of mixed convection in a shear-buoyancy driven cavity", Int. Commun. Heat Mass Transfer. Vol. 26, pp. 1019-1028, 1999.

Aydin, O., and Yang, W. J., "Mixed convection in cavities with a locally heated lower wall and moving side walls", Numer. Heat Transfer, Part A, Vol. 37, pp. 695-710, 2000.

Bhave, P., Narasimhan, A., and Ress, D. A. S., "Natural convection heat transfer enhancement using adiabatic block: Optimal block size and Prandtl number effect", Int. J. of Heat and Mass Transfer, Vol. 49, pp. 3807-3818, 2006.

Bhoite, M. T., Narasimham, G. S. V. L., and Murthy, M. V. K., "Mixed convection in a shallow enclosure with a series of heat generating components", Int. J. of Thermal Sciences, Vol. 44, pp. 125-135, 2005.

Bilgen, E., "Natural convection in cavities with a thin fin on the hat wall", Int. J. of Heat and Mass Transfer, Vol. 48, pp. 3493-3505, 2005.

Bilgen, E., and Yamane, T., "Conjugate heat transfer in enclosures with openings for ventilation", Heat and Mass Transfer, Vol. 40, pp. 401-411, 2004.

Biswas, G., Laschefski, H., Mitra, N. K. and Fiebig, M., "Numerical investigation of mixed convection heat transfer in a horizontal channel with a built in square cylinder", Numer. Heat Transfer, Vol. 18, pp. 173-188, 1990.

Braga, E. J., and de Lemos, M. J. S., "Laminar natural convection in cavities filed with circular and square rods", Int. Commun. in Heat and Mass Transfer, Vol. 32, pp. 1289-1297, 2005.

Calmidi, V. V., and Mahajan, R. L., "Mixed convection over a heated horizontal surface in a partial enclosure", Int. J. of Heat and Fluid Flow, Vol. 19, pp. 358-367, 1998.

Cengel, Y. A., "Heat and mass transfer", Third Ed., Tata McGraw-Hill, 2007.

Chamkha, A. J., "Hydromagnetic combined convection flow in a vertical lid-driven cavity with internal heat generation or absorption", Numer. Heat Transfer, Part A, Vol. 41, pp. 529-546, 2002.

Chang, T. S., and Shiau, Y. H., "Flow pulsation and baffle's effects on the opposing mixed convection in a vertical channel", Int. J. of Heat and Mass Transfer, Vol. 48, pp. 4190-4204, 2005.

Chung, T. J., "Computational fluid dynamics", First Ed., Cambridge University Press, 2002.

Das, M. K., and Reddy, K. S. K., "Conjugate natural convection heat transfer in an inclined square cavity containing a conducting block", Int. J of Heat and Mass Transfer, Vol. 49, pp. 4987-5000, 2006.

Deng, Q. H., and Tang, G. F., "Numerical visualization of mass and heat transport for conjugate natural convection/ heat conduction by streamline and heatline", Int. J. of Heat Mass Transfer, Vol. 45, pp. 2373-2385, 2002.

Dechaumphai, P., "Finite Element Method in Engineering", second Ed., Chulalongkorn University Press, Bangkok, 1999.

Dong, S. F., and Li, Y.T., "Conjugate of natural convection and conduction in a complicated enclosure", Int. J. of Heat and Mass Transfer, Vol. 47, pp. 2233-2239, 2004.

Ferziger, J. H. and Perić, M., "Computational methods for fluid dynamics", Second Ed., Springer Verlag, Berlin Hedelberg, 1997.

Fletcher, C. A. J., "Computational techniques for fluid dynamics 1", Second Ed., Springer Verlag, Berlin Hedelberg, 1991.

Garandet, J. P., Alboussiere, T., and Moreau, R., "Buoyancy driven convection in a rectangular enclosure with a transverse magnetic field", Int. J. of Heat Mass Transfer, Vol. 35, pp. 741-748, 1992.

Gau, C., Jeng, Y.C., and Liu, C.G., "An experimental study on mixed convection in a horizontal rectangular channel heated from a side", ASME J. Heat Transfer, Vol. 122, pp. 701–707, 2000.

Gowda, Y. T. K., Narayana, P. A. A., and Seetharamu, K. N., "Mixed convection heat transfer past in-line cylinders in a vertical duct", Numer. Heat Transfer, Part A, Vol. 31, pp. 551-562, 1997.

Gau, G., Sharif, M. A. R., "Mixed convection in rectangular cavities at various aspect ratios with moving isothermal side walls and constant flux heat source on the bottom wall", Int. J. of Thermal Sciences, Vol. 43, pp. 465-475, 2004.

Ha, M. Y., and Jung, M. J., "A numerical study on three-dimensional conjugate heat transfer of natural convection and conduction in a differentially heated cubic

enclosure with a heat-generating cubic conducting body", Int. J. of Heat and Mass Transfer, Vol. 43, pp. 4229-4248, 2000.

Ha, M. Y., Jung, M. J., and Kim, Y.S., "Numerical study on transient heat transfer and fluid flow of natural convection in an enclosure with a heat-generating conducting body", Numer. Heat Transfer, Part A, Vol. 35, pp. 415-434, 1999.

Hagen, K. D., "Heat transfer with applications", First Ed., Prentice-Hall International, 1999.

Hossain, M. A., and Gorla, R. S. R., "Effect of viscous dissipation on mixed convection flow of water near its density maximum in a rectangular enclosure with isothermal wall", Int. J. of Numer. Methods for Heat and Fluid Flow, Vol. 16, No. 1, pp. 5-17, 2006.

House, J. M., Beckermann, C. and Smith, T. F., "Effect of a centered conducting body on natural convection heat transfer in an enclosure", Numer. Heat Transfer, Part A, Vol. 18, pp. 213-225, 1990.

How, S.P. and Hsu, T.H., "Transient mixed convection in a partially divided enclosure", Comput. Math. Appl. Vol. 36, pp. 95-115, 1998.

Hsu, T.H., and How, S. P., "Mixed convection in an enclosure with a heat-conducting body", Acta Mechanica, Vol. 133, pp. 87-104, 1999.

Hsu, T.H., and Wang, S. G., "Mixed convection in a rectangular enclosure with discrete heat sources", Numer. Heat Transfer, Part A, Vol. 38, pp. 627-652, 2000.

Hsu, T.H., Hsu, P.T., How, S.P., "Mixed convection in a partially divided rectangular enclosure", Numer. Heat Transfer, Part A, Vol. 31, pp. 655-683, 1997.

Hung, T. C., and Fu, C. S., "Conjugate heat transfer analysis for the passive enhancement of electronic cooling through geometric modification in a mixed convection domain", Numer. Heat Transfer, Part A, Vol. 35, pp. 519-535, 1999.

Jami, M., Mezrhab, A. Bouzidi, M and Lallemand, P , "Lattice boltzmann method applied to the laminar natural convection conduction in an enclosure with a heat generating cylinder conducting body", Int. J. of Thermal Sciences, Vol. 46, pp. 38-47, 2007.

Kumar De, A., and Dalal, A., "A numerical study of natural convection around a square, horizontal, heated cylinder placed in an enclosure", Int. J of Heat and Mass Transfer, Vol. 49, pp. 4608-4623, 2006.

Khanafer, K., Vafai, K., and Lightstone, M., "Mixed convection heat transfer in two-dimensional open-ended enclosure", Int. J. of Heat and Mass Transfer, Vol. 45, pp. 5171-5190, 2002.

Kimura, T., Takeuchi, M., Nagai, N., and Yoshida, T., "Heat transfer in an inclined enclosure with an inner rotating plate", Heat Transfer-Asian Research, Vol. 30, No. 4, pp. 331-340, 2001.

Lacroix, M., "Natural convection heat transfer around two heated horizontal cylinders inside a rectangular cavity cooled from above", Numer. Heat Transfer, Part A, Vol. 21, pp. 37-54, 1992.

Lacroix, M., and Joyeux, A., "Natural convection heat transfer around heated cylinders inside a cavity with conducting walls", Numer. Heat Transfer, Part A, Vol. 27, pp. 335-349, 1995.

Lee, J. R., and Ha, M. Y., "A numerical study of natural convection in a horizontal enclosure with a conducting body", Int J. of Heat and Mass Transfer, Vol. 48, pp. 3308-3318, 2005.

Lee, J. R., and Ha, M. Y., "Numerical simulation of natural convection in a horizontal enclosure with a heat-generating conducting body", Int. J. of Heat and Mass Transfer, Vol. 49, pp. 2684-2702, 2006.

Lin, J., and Sharif, M. A. R., "Numerical study of fluid flow and heat transfer in a channel with heated normal plates", Numer. Heat Transfer, Part A, Vol. 31, pp. 853-865, 1997.

Luo, W. J., and Yang, R. J., "Multiple fluid flow and heat transfer solutions in a two-sided lid-driven cavity", Int. J. of Heat and Mass Transfer, Vol. 50, pp. 2394-2405, 2007.

Mahmud, S., Tasnim, S. H, and Mamun, M. A. H., "Thermodynamic analysis of mixed convection in a channel with transverse hydromagnetic effect", Int. J. of Thermal Sciences, Vol. 42, pp. 731-740, 2003.

Manca, O., Nardini, S., Khanafer, K., and Vafai, K., "Effect of heated wall position on mixed convection in a channel with an open cavity", Numer. Heat Transfer, Part A, Vol. 43, pp. 259–282, 2003.

Manca, O., Nardini, S., and Vafai, K., "Experimental investigation mixed convection in a channel with an open cavity", Experimental Heat Transfer, Vol. 19, pp. 53–68, 2006.

Merrikh, A. A., and Lage, J. L., "Natural convection in an enclosure with disconnected and conducting solid blocks", Int. J. Heat Mass Transfer, Vol. 48, No. 7, pp. 1361-1372, 2005.

Misra, D., and Sarkar, A., "Finite element analysis of conjugate natural convection in a square enclosure with a conducting vertical wall", Comput. Methods Appl. Mech. Engg., Vol. 141, pp. 205-219, 1997.

Najam, M., Amahmid, A., Hasnaoui, M., and Alami, M. E., "Unsteady mixed convection in a horizontal channel with rectangular blocks periodically distributed on its lower wall", Int. J. of Heat and Fluid Flow, Vol.24, pp. 726-735, 2003.

Nakhi, A. B., and Chamkha, A. J., "Natural convection in inclined partitioned enclosures", Heat Mass Transfer, Vol. 42, pp. 311-321, 2006.

Nakhi, A. B., and Chamkha, A. J., "Conjugate natural convection around a finned pipe in a square enclosure with internal heat generation", Int. J. of Heat and Mass Transfer, Vol. 50, pp. 2260-2271, 2007.

Oh, J. Y., Ha, M. Y., and Kim, K. C., "Numerical study of heat transfer and flow of natural convection in an enclosure with a heat generating conducting body", Numer. Heat Transfer, Part A, Vol. 31, pp. 289-304, 1997.

Omri, A., and Nasrallah, S. B., "Control volume finite element numerical simulation of mixed convection in an air-cooled cavity", Numer. Heat Transfer, Part A, Vol. 36, pp. 615–637, 1999.

Oreper, G. M., Szekely, J., "The effect of an externally imposed magnetic field on buoyancy driven flow in a rectangular cavity", J. of Crystal Growth, Vol. 64, pp 505-515, 1983.

Ozoe, H., and Maruo, M., "Magnetic and gravitational natural convection of melted silicon-two dimensional numerical computations for the rate of heat transfer", JSME, Vol. 30, pp. 774-784, 1987.

Oztop, H. F., and Dagtekin, I., "Comparison of position of heated thin plate located in a cavity for natural convection", Int. Commun. Heat Mass Transfer, Vol. 31, No. 1, pp. 121-132, 2004a.

Oztop, H. F., and Dagtekin, I., "Mixed convection in two-sided lid-driven differentially heated square cavity", Int. J. of Heat and Mass Transfer, Vol. 47, pp. 1761-1769, 2004b.

Oztop, H., and Bilgen, E., "Natural convection in differentially heated and partially divided square cavities with internal heat generation", Int. J. of Heat and Fluid Flow, Vol. 27, pp. 466-475, 2006.

Papanicolaou, E., and Jaluria, Y., "Mixed convection from an isolated heat source in a rectangular enclosure", Numer. Heat Transfer, Part A, Vol. 18, pp. 427–461, 1990.

Papanicolaou, E., and Jaluria, Y., "Transition to a periodic regime in mixed convection in a square cavity", J. Fluid Mech., Vol. 239, pp. 489–509, 1992.

Papanicolaou, E., and Jaluria, Y., "Mixed convection from a localized heat source in a cavity with conducting walls: A numerical study", Numer. Heat Transfer, Part A, Vol. 23, pp. 463–484, 1993.

Papanicolaou, E., and Jaluria, Y., "Mixed convection from simulated electronic components at varying relative positions in a cavity", J. Heat Transfer, Vol. 116, pp. 960–970, 1994.

Patankar, S. V., "Numerical heat transfer and fluid flow", Second Ed., Washington, D. C. Homisphere, 1980.

Rahman, M. M., Alim, M. A., Mamun, M. A. H., Chowdhury, M.K. and Islam, A.K.M.S., "Numerical Study of Opposing Mixed Convection in a Vented Enclosure", ARPN J. of Engineering and Applied Sciences, Vol. 2, No. 2, pp 25-36, 2007.

Rahman, M. M., Alim, M. A., Saha, S. and Chowdhury, M. K., "A Numerical Study of Mixed Convection in A Square Cavity with A Heat Conducting Square Cylinder at Different Locations", J. of Mechanical Engineering, The Institution of Engineers, Bangladesh, Vol. ME 39, No. 2, pp. 78 - 85, 2008a.

Rahman, M. M., Alim, M. A., Saha, S. and Chowdhury, M. K., "Mixed Convection in a vented Square Cavity with a Heat Conducting Horizontal Solid Circular Cylinder", *Journal of Naval Architecture and Marine Engineering*, Vol. 5, No. 2, pp.37 - 46, 2008b.

Rahman, M. M., Alim, M. A. and Mamun, M. A. H. "Finite element analysis of mixed convection in a rectangular cavity with a heat-conducting horizontal circular cylinder", Nonlinear analysis: Modeling and Control, Vol.14, No. 2, pp 217-247, 2009.

Raji, A., and Hasnaoui, M., "Mixed convection heat transfer in a rectangular cavity ventilated and heated from the side", Numer. Heat Transfer, Part A, Vol. 33, pp. 533–548, 1998a.

Raji, A., and Hasnaoui, M., "Correlations on mixed convection in ventilated cavities", Revue Ge´ne´rale de Thermique, Vol. 37, pp 874–884, 1998b.

Raji, A., and Hasnaoui, M., "Mixed convection heat transfer in ventilated cavities with opposing and assisting flows", Int. J. Computer-Aided Eng. Software, Vol. 17(5), pp 556–572, 2000.

Reddy, J. N. and Gartling, D. K., "The Finite Element Method in Heat Transfer and Fluid Dynamics", CRC Press, Inc., Boca Raton, Florida, 1994.

Roychowdhury, D.G, Das, S.K. and Sundararajan, T.S., "Numerical simulation of natural convection heat transfer and fluid flow around a heated cylinder inside an enclosure", Heat and Mass Transfer, Vol. 38, pp. 565-576, 2002.

Rudraiah, N., Venkatachalappa, M., and Subbaraya, C. K., "Combined surface tension and buoyancy-driven convection in a rectangular open cavity in the presence of magnetic field", Int. J. Non-linear Mech., Vol. 30(5), pp. 759-770, 1995a.

Rudraiah, N., Barron, R. M., Venkatachalappa, M., and Subbaraya, C. K., "Effect of magnetic field on free convection in a rectangular enclosure", Int. J. Engng. Sci., Vol. 33, pp. 1075-1084, 1995b.

Saeidi, S. M., and Khodadadi, J. M., "Forced convection in a square cavity with inlet and outlet ports", Int. J. of Heat and Mass Transfer, Vol. 49, pp. 1896-1906, 2006.

Sahoo, D., and Sharif, M. A. R., "Mixed-convective cooling of an isothermal hot surface by confined slot jet impingement", Numer. Heat Transfer, Part A, Vol. 45, pp. 887-909, 2004.

Sarris, I. E., Kakarantzas, S. C., Grecos, A. P., and Vlachos, N. S., "MHD natural convection in a laterally and volumetrically heated square cavity", Int. J. of Heat and Mass Transfer, Vol. 48, pp. 3443-3453, 2005.

Sasaguchi, K., Kuwabara, K., Kusano, K., and Kitagawa, H., "Transient cooling of water around a cylinder in a rectangular cavity- a numerical analysis of the effect of the position of the cylinder", Int. J. of Heat and Mass Transfer, Vol. 41, pp. 3149-3156, 1998.

Shuja, S.Z., Yilbas, B.S. and Budair, M.O., "Natural convection in a square cavity with heat generating body: Entropy consideration", Heat and Mass Transfer, Vol. 36, pp. 343-350, 2000.

Shuja, S.Z., Yilbas, B.S. and Iqbal, M.O., "Mixed convection in a square cavity due to heat generating rectangular body", Int. J. of Numer. Methods for Heat & Fluid Flow, Vol. 10, No. 8, pp. 824-841, 2000a.

Shuja, S.Z., Yilbas, B.S. and Iqbal, M.O., "Heat transfer characteristics of flow past a rectangular protruding body", Numer. Heat Transfer, Part A, Vol. 37, pp. 307-321, 2000b.

Shercliff, J. A., A Textbook of Magnetohydrodynamics, First Ed., Pergamon Press, UK, 1965.

Singh, S., and Sharif, M. A. R., "Mixed convective cooling of a rectangular cavity with inlet and exit openings on differentially heated side walls", Numer. Heat Transfer, Part A Vol. 44, pp. 233–253, 2003.

Singh, S., Biswas, G. and Mukhopadhyay, A., "Effect of thermal buoyancy on the flow through a vertical channel with a built-in circular cylinder", Numer. Heat Transfer, Part A, Vol. 34, pp. 769-789, 1998.

Sun, Y.S. and Emery, A. F., "Effect of wall conduction, internal heat sources and an internal baffle on natural convection heat transfer in a rectangular enclosure", Int. J. Heat and Mass Transfer, Vol. 40 (4), pp. 915-929, 1997

Tasnim, S. H., and Collins, M. R., "Numerical analysis of heat transfer in a square cavity with a baffle on the hot wall", Int. Commun Heat Transfer, Vol. 31, No. 5, pp. 639-650, 2004.

Tasnim, S. H., and Collins, M. R., "Suppressing natural convection in a differentially heated square cavity with an arc shaped baffle", Int. Commun. in Heat and Mass Transfer, Vol. 32, pp. 94-106, 2005.

Tsay, Y. L., Cheng, J. C., and Chang, T. S., "Enhancement of heat transfer from surface-mounted block heat sources in a duct with baffles ", Numer Heat Transfer, Part A, Vol. 43, pp. 827-841, 2003.

Turki, S., Abbassi, H. and Nasrallah, S.B., "Two-dimensional laminar fluid flow and heat transfer in a channel with a built-in heated square cylinder", Int. J of Thermal Sciences, Vol. 42, pp. 1105-1113, 2003.

Wang, Q., and Jaluria, Y., "Instability and heat transfer in mixed convection flow in a horizontal duct with discrete heat sources", Numer. Heat Transfer, Part A, Vol. 42, pp. 445-463, 2002.

Xu, F., Patterson, J. C., and Lei, C., "Experimental observations of the thermal flow around a square obstruction on a vertical wall in a differentially heated cavity", Experiments in Fluids, Vol. 40, pp. 364-371, 2006.

Yedder, R.B. and Bilgen, E., "Laminar natural convection in inclined enclosures bounded by a solid wall", Heat and Mass Transfer", Vol. 32, pp 455-462, 1997.

Yilbas, B. S., Shuja, S. Z., and Iqbal, M. O., "Energy and entropy analysis in a square cavity with protruding body: effects of protruding body aspect ratio", Int J. Energy Res., Vol. 26, pp. 851-866, 2002.

Yucel, N. and Turkoglu, H., "Numerical analysis of laminar natural convection in enclosures with fins attached to an active wall", Heat and Mass Transfer, Vol. 33, pp. 307-314, 1998.

Zienkiewicz, O. C. and Taylor, R. L., "The finite element method", Fourth Ed., McGraw-Hill, 1991.